NBER WORKING PAPER SERIES

ANTICIPATING CLIMATE CHANGE ACROSS THE UNITED STATES

Adrien Bilal
Esteban Rossi-Hansberg

Working Paper 31323
http://www.nber.org/papers/w31323

NATIONAL BUREAU OF ECONOMIC RESEARCH
1050 Massachusetts Avenue
Cambridge, MA 02138
June 2023

We thank Leonardo D'Amico, Bin Cheng, Santiago Franco, and Sreyas Mahadevan for outstanding research assistance. We also thank Dave Donaldson, Stephie Fried, and two anonymous referees for helpful comments. Support from the Chae Family Economics Research Fund is gratefully acknowledged. The views expressed herein are those of the authors and do not necessarily reflect the views of the National Bureau of Economic Research.

Anticipating Climate Change Across the United States
Adrien Bilal and Esteban Rossi-Hansberg
NBER Working Paper No. 31323
June 2023
JEL No. C6, E3, Q54, R11

ABSTRACT

We evaluate how anticipation and adaptation shape the aggregate and local costs of climate change. We develop a dynamic spatial model of the U.S. economy and its 3,143 counties that features costly forward-looking migration and capital investment decisions. We leverage the 'Master Equation' representation of the economy to make the model tractable. We propose reduced-form estimates of the county-level impact of severe storms and heat waves over the 20th century on local income, employment, and investment. We match these effects in the model by estimating migration and investment elasticities, capital depreciation shocks for storms, and a combination of productivity and amenity shocks for heat waves. Our counterfactuals show, first, that the impact of climate on capital depreciation magnifies the U.S. aggregate welfare costs of climate change twofold to 2.8% in 2025 under a business-as-usual warming scenario. Second, anticipation of future climate damages amplifies climate-induced worker and investment mobility, thereby significantly reducing the losses of workers in the most affected locations. Third, migration offsets 25-40% of aggregate losses and reduces substantially the spatial variance in the welfare impact of climate change.

Adrien Bilal
Stanford University
Department of Economics
and NBER
adrienbilal@stanford.edu

Esteban Rossi-Hansberg
University of Chicago
and CEPR
and also NBER
rossihansberg@uchicago.edu

Anticipating Climate Change Across the United States*

Adrien Bilal — *Stanford University*

Esteban Rossi-Hansberg — *University of Chicago*

October 29, 2025

Abstract

We evaluate how anticipation and adaptation shape the aggregate and local costs of climate change. We develop a dynamic spatial model of the U.S. economy and its 3,143 counties that features costly forward-looking migration and capital investment decisions. We leverage the 'Master Equation' representation of the economy to make the model tractable. We propose reduced-form estimates of the county-level impact of severe storms and heat waves over the 20^{th} century on local income, employment, and investment. We match these effects in the model by estimating migration and investment elasticities, capital depreciation shocks for storms, and a combination of productivity and amenity shocks for heat waves. Our counterfactuals show, first, that the impact of climate on capital depreciation magnifies the U.S. aggregate welfare costs of climate change twofold to 2.8% in 2025 under a business-as-usual warming scenario. Second, anticipation of future climate damages amplifies climate-induced worker and investment mobility, thereby significantly reducing the losses of workers in the most affected locations. Third, migration offsets 25-40% of aggregate losses and reduces substantially the spatial variance in the welfare impact of climate change.

1 Introduction

The accumulation of CO_2 in the atmosphere is affecting the climate of our planet. Some of these effects are evident today, but many others, including the increased frequency and intensity of storms and heat waves (IPCC, 2022), are expected over the next century as the Earth's average temperature increases further. The ability of humans to anticipate these future climate effects can have profound implications on their adaptation efforts to reduce the worst consequences. What is the importance of these anticipatory

*Adrien Bilal: adrienbilal@stanford.edu. Esteban Rossi-Hansberg: rossihansberg@uchicago.edu. We thank Leonardo D'Amico, Bin Cheng, Santiago Franco, and Sreyas Mahadevan for outstanding research assistance. We also thank Dave Donaldson, Stephie Fried, and two anonymous referees for helpful comments. Support from the Chae Family Economics Research Fund is gratefully acknowledged.

and adaptive responses in determining the aggregate and local costs of climate change? In this paper, we answer this question using a general equilibrium dynamic quantitative spatial model of the 3,143 counties in the U.S. economy. In our framework, agents anticipate the effect of climate change on productivity and capital depreciation and make forward-looking migration and local capital investment decisions. We quantify climate damages using novel empirical estimates of the local impact of storms and heat waves on economic activity.

The analysis of anticipatory and adaptation responses to climate change at this level of spatial resolution has previously been hindered by the dimensionality of the resulting state space. In a dynamic model with costly forward-looking migration and local capital investment decisions, the whole distribution of employment and capital are state variables in the dynamic problem of individual workers and local capital investors. Connecting such a framework with micro-level estimates of the impact of storms and heat waves requires a fine level of spatial disaggregation. To make progress, we use analytic first-order perturbations around a long-run steady-state that allow us to solve for quantitative general equilibrium counterfactuals in heterogeneous agent models with aggregate shocks (Bilal, 2023). With this technique in hand, we develop a framework to evaluate the impact of climate change on the U.S. economy.

Our starting point is a standard forward-looking dynamic migration model as in Caliendo et al. (2019). Forward-looking workers decide where to live and work. They earn an equilibrium wage in their location that they use to consume and lease housing at equilibrium rents. They receive random preference shocks for locations that motivate them to migrate subject to bilateral migration costs. We enrich this environment along several dimensions. First, as in Kleinman et al. (2023), we introduce local capitalists who own the capital stock in the location where they live. They face a dynamic consumption-investment decision subject to adjustment costs that accounts for the future expected path of the economy and its climate. The evolution of the local paths of capital depreciation rates, productivities, and amenities depends on climate change through its effect on storms and heat waves. Capitalists rent out their capital stock to developers who use it to produce housing and commercial structures, and can trade bonds with capitalists across locations. Local firms produce consumption goods using labor and commercial structures with productivity that is heterogeneous across locations and varies with global temperatures.

An essential part of the quantification of this model is our estimation of damage functions that map global temperature changes into local changes in capital depreciation rates, productivity, and amenities. We collect daily data on mean and extreme temperature, precipitation, and windspeed for every county in the U.S. since 1900. We use these data to construct county-level indicators of 1-in-50-years storms, and 1-in-20-years heat waves. We document that the probability of storms in coastal counties, and heat waves in warm (above-median) counties in the U.S. has risen fourfold and twofold, respectively, with the 1°C of global warming the planet experienced in the last century. We confirm these trends in storm count information from the National Oceanic and Atmospheric Administration (NOAA).

We then estimate the impact of these extreme events on economic activity from the year 1990 onwards

using an event study design. Specifically, we use a distributed lag specification to estimate how income per capita, employment, and investment respond to extreme events conditional on a rich set of controls. We find that storms reduce income per capita by over 2.5% and employment by 5%, while investment rises to peak at a 20% increase. These effects are concentrated in coastal counties, precisely where storms are becoming more frequent. Together, these patterns are consistent with a capital depreciation shock in the model. Heat waves reduce income per capita and population by 1.5%, while investment declines modestly, in counties with temperatures above the median where their frequency is rising. These results are consistent with a combination of negative productivity and amenity shocks in the model.

We use these reduced-form estimates to quantify our framework. We first estimate the migration and investment elasticities. Given a guess for these elasticities, and a standard calibration of the rest of the model parameters, we can invert the model in steady-state, and obtain all the local characteristics, including local productivities, amenities, and the level of local capital investment costs. To estimate the two elasticities, we leverage a key property of the first-order approximation of changes in our economy around the steady state, namely, that the *relative* response of economic outcomes to shocks is independent of the magnitude of the shock. Hence, we estimate these elasticities by matching the estimated reduced-form response of employment, relative to income per capita and investment, to storms and heat waves. We leverage the computational efficiency of our solution method to propose global identification guarantees.

To estimate the damage functions, we first recover the magnitude of the capital depreciation, productivity, and amenity shocks corresponding to a 1-in-50-years storm and a 1-in-20 years heat wave by matching the *level* of the cumulative impulse response of employment and income in the model to the one we estimated in the data over a 25-year period. We then interact damages from a given event with changes in the empirical probability of that event for each location in response to changes in temperature.

Storms and heat waves have large effects on capital depreciation, productivity, and amenities. Through the lens of our model, storms generate a 30% capital depreciation shock, while heat waves generate a 2% productivity shock together with a 0.6% amenity shock. The resulting structural damage functions imply that the South-Eastern Atlantic coast should expect a 2 to 6 p.p. increase in the annual capital depreciation rate for every 1°C increase in global mean temperatures because of rising storm activity. Southern Florida should expect a 5% reduction in productivity, and a 1.6% reduction in amenities, for every 1°C increase in global mean temperature.

We use the quantified model to evaluate the social cost of climate change in the U.S. economy. Our central scenario is a gradual increase of global mean temperature from 1°C to 4°C above pre-industrial levels by 2100, consistent with the IPCC's business-as-usual scenario. In our baseline counterfactual, the consumption-equivalent present discounted welfare of workers falls by 2.8% on average in 2025 ($1,717 per year per worker). Our solution method enables us to construct standard errors efficiently. The 95% confidence interval for the aggregate worker welfare loss in 2025 ranges from 1.1% to 4.6%, after accounting for standard errors around our estimated damage functions.

Despite the ability of workers to migrate away from affected areas, there is substantial dispersion across counties. The spatial standard deviation of welfare losses for workers is 0.8 p.p. Capitalists lose 1.2% on average but face much larger inequality: a spatial standard deviation of losses of 10.1 p.p in 2025 and of 24.3 p.p. by 2100. Losses to capitalists are more dispersed because physical capital cannot be moved directly: it is left to depreciate in impacted areas such as southern Florida and accumulate through investments in less affected areas such as inland Maine. By 2100, average welfare losses reach 4.2% for workers ($2,575 per year per worker) and 3.7% for capitalists. These welfare losses occur despite sizable population and capital flows. By 2100, the population has changed by 28% on average across all counties due to climate change; the aggregate capital stock of the U.S. economy has declined by 7.9%.

Given the magnitude of the changes in capital depreciation, productivity, and amenities that we consider and the substantial population and capital reallocation that ensues, it is important to assess the accuracy of our first-order perturbation approach. We do so using standard methods for checking value function and distributional errors (Haan and Marcet, 1994; Santos, 2000) across multiple model specifications. To do so, we hold either decisions or allocations fixed along a transition, and compare the perturbation of the other to their fully nonlinear counterpart. We find that expanding the law of motion of capital in logs rather than in levels improves accuracy because it is already log-linear. Most importantly, expanding around the final steady-state is much more accurate because it constrains the perturbation and the nonlinear solution to coincide at the initial and final periods for allocations, and at the final time for decisions. By contrast, perturbation around the initial steady-state only constrains initial allocations to coincide. Intuitively, expanding around the final steady-state allows agents' decisions to adapt properly to the long-run consequences of climate change on the economy.

Having established the accuracy of our approach, our main goal is to gauge the importance of anticipation and adaptation responses in determining the impact of climate change. To do so, we perform three distinct exercises in which we shut down particular channels in the model. First, we shut down the effect of storms on capital depreciation. This allows us to assess the relevance of incorporating capital in a climate assessment model. The effect of changes in global temperature on capital depreciation alone accounts for 60% of welfare losses to workers, 66% of welfare losses to capitalists, and 83% of the aggregate reduction in capital by 2100. The destruction created by storms through changes in local capital depreciation rates at a high degree of spatial granularity is a novel feature of our analysis, and this channel turns out to be quantitatively critical to account accurately for expected losses from climate change.

In a second exercise, we shut down climate change anticipation by workers and capitalists. In this counterfactual, agents experience the effect of the current and past changes in temperatures but they believe that in the future temperatures will remain as in the current period for a prolonged period. Hence, their actions incorporate no anticipation effects: their behavior reacts neither to short-run changes in the climate (by shutting down expectations of future increases in temperature) nor to long-run changes in the climate (by using the initial steady-state as a point of expansion). Our results indicate that anticipation

plays a crucial role for mobility and investment. Without anticipation, mobility drops by 41% by 2050. There are two main reasons. First, workers fail to out-migrate enough from locations that will become less attractive as the climate worsens. Second, capitalists keep investing in these same locations, raising the incentives for workers to stay there. Without anticipation, local losses for workers are 38% more dispersed across locations. For example, workers in Florida lose an additional 1% of consumption equivalent welfare. Nevertheless, gains in some locations offset losses in others, yielding similar aggregate welfare losses.

In the third and final exercise, we measure the importance of adaptation through migration for the spatial distribution of county losses from climate change. To do so, we simply prevent people from moving in response to climate change, while capital can adjust as in the baseline. Without migration, aggregate welfare losses rise to 4%. Excess losses take place despite our first-order perturbation approach because we use the final steady-state as a point of expansion, thereby capturing long-run behavioral changes to permanent climate change. Thus, the envelope theorem does not apply with respect to private migration decisions and migration delivers sizable benefits. When we use an expansion around the initial steady-state instead, we cannot capture these benefits by construction.[1]

The distribution of welfare losses for workers spreads out from 9.4 p.p to 16.3 p.p in 2100. Workers in particularly adversely affected areas, such as coastal counties in Florida and Louisiana, experience losses ranging from 25% to 50% in 2025 instead of 5% to 9%, corresponding to an additional loss of $26,375 per year per capita. In contrast, since capital stocks are not mobile, the lack of mobility of workers insures local capitalists in affected areas. Hence, the dispersion in capitalist welfare declines more than threefold in 2025 and by half in 2100. Our results point to a dynamic complementarity between migration and investment decisions that shapes the spatial distribution of winners and losers of climate change.

The methodology that allows us to reach these conclusions is related to the literature on mean-field games. Together, the elements of our framework represent a heterogeneous agent environment with aggregate shocks in which the full distribution of workers and capital stocks across counties matters for the evolution of the economy. Standard solution methods are not well-suited for the dimensionality of this framework. To make progress, we leverage the 'Master Equation' representation of the economy (Bilal, 2023), itself introduced in the mathematics mean field games literature (Cardaliaguet et al., 2019). It coincides with the state space representation of our framework in which the distribution is a state variable (Reiter, 2009). We take analytic first-order perturbations of the Master Equation in aggregate temperature shocks and in the underlying distribution around the final deterministic steady-state to obtain low-dimensional Bellman equations for the directional derivatives of individual value functions with respect to the underlying distribution and aggregate shocks.

Our paper is also related to the literature on dynamic spatial models. Relative to Desmet et al. (2018), our methodology allows us to introduce forward-looking decisions in migration and capital investments,

[1] In previous drafts, where we used the initial steady-state as a point of expansion, migration had only negligible effects on the aggregate cost of climate change. The difference illustrates how allowing agents to consider the long-run consequences of climate change in their decisions is crucial for an accurate description of the role of migration as an adaptation mechanism.

although we abstract from agglomeration effects in productivity and technology innovations, and focus our analysis on the U.S. Caliendo et al. (2019) introduces forward-looking migration decisions and Kleinman et al. (2023) adds local capital investments. Both of them also introduce costly trade, which we abstract from. Relative to these papers, we compute counterfactuals for a much larger number of locations (all counties in the U.S. v.s. 50 states). Perhaps more important, our computation method allows us to estimate the two key elasticities, the climate damage functions, and the associated confidence intervals around counterfactuals by precisely matching the model results with the reduced-form local responses that we estimate in the data.

Of course, the main contribution of our paper is to evaluate the economic losses due to the capital depreciation generated by storms, together with the productivity and amenity losses due to heat waves. We aim to analyze the role of anticipation and adaptation in determining aggregate and local losses as well as the resulting migration flows and geography of investments. In doing so, we also contribute to the reduced-form literature that estimates the impact of storms (Deryugina, 2013, Hsiang and Jina, 2014, Roth Tran and Wilson, 2023, Phan and Schwartzman, 2023, Bakkensen and Barrage, 2025) and extreme heat (Deschênes and Greenstone, 2011, Dell et al., 2012, Dell et al., 2014, Leduc and Wilson, 2023) by providing comprehensive county-level estimates for the U.S. of the effect of storms on coastal counties and heat waves in warm counties.

We use our reduced-form estimates to quantify a general equilibrium dynamic spatial climate assessment model. A recent literature has proposed related frameworks. Many of those papers focus on other issues and abstract completely from capital investments or anticipation effects (Desmet and Rossi-Hansberg, 2015, Desmet et al., 2021, Cruz and Rossi-Hansberg, 2023, and Conte et al., 2022). Cruz (2021) and Balboni (2021) study the effect of temperature changes and flooding, respectively, in models with forward-looking migration but abstract from local capital accumulation.[2] Rudik et al. (2022) also incorporates forward-looking migration and trade and calculates the impact of climate change in the U.S. on productivity and welfare using trade and migration flows, but also abstract from capital investments and capital depreciation shocks. In contrast, Krusell and Smith (2022) propose a model of the effect of climate change on local capital investments for the entire world but abstract from migration or the capital destruction shocks generated by floods and storms. Fried (2022) evaluates the impact of storms in an incomplete credit market model with adaptation across two regions. Relative to this literature, we are the first to quantify the effect of climate-change-induced storms and heat waves by proposing a spatially disaggregated dynamic model with forward-looking migration and capital investments, and use it to gauge the role of anticipation and adaptation in determining the size and spatial distribution of these losses.

The rest of this paper is organized as follows. Section 2 lays out the model. Section 3 characterizes our solution method. Section 4 describes our reduced-form results. Section 5 details our quantification

[2]We abstract from local industry specialization, unlike Costinot et al. (2016), Nath (2022), Cruz (2021), and Conte et al. (2022).

procedure. Section 6 presents our three main results. Section 7 concludes.

2 A model of location and investment choices in a warming world

This section presents the setup of our dynamic spatial model. We model an economy with many locations and two types of agents: workers and capitalists. Workers can move subject to mobility costs and earn a wage that they consume each period. Capitalists are fixed in a location, earn the returns on their capital investments, and face a dynamic consumption-savings decision.

2.1 Agents and preferences

There is a unit mass of infinitely-lived workers who choose in which location $i \in \{1, ..., \mathcal{I}\}$ to live. Workers living in location i have CRRA preferences $A_{it} + u(C) = A_{it} + \frac{C^{1-\gamma}-1}{1-\gamma}$ over amenities A_{it} in the location where they live at time t and a Cobb-Douglas aggregator C of a freely traded final good, used as the numeraire, and housing. Namely, $C = \left(\frac{c}{1-\beta}\right)^{1-\beta}\left(\frac{h}{\beta}\right)^{\beta}$, where β denotes the share of housing in expenditure. Workers discount the future at rate ρ. Workers are allowed to move at rate μ, in which case they draw type-I generalized extreme value distributed idiosyncratic preference shocks for potential destinations, with dispersion parameter ν. ν governs the migration elasticity with respect to changes in a location's value. If they move, they pay a bilateral moving cost τ_{ij}. We define the long-run (A_i) and time-varying (a_{it}) components of amenities in location i as $A_{it} = A_i + a_{it}$.

Each location is populated by a unit measure of capitalists. They are immobile and have risk-neutral preferences $u^{\text{cap}}(C) = C$ over the final consumption good. They do not consume housing.

2.2 Technology

Workers in location i are employed by a representative final good firm that produces using commercial structures and labor and faces constant returns to scale. Locations are endowed with a local productivity Z_{it} and a local stock of land L_i. A representative firm is endowed with a production function for the final good given by $Y_{it} = Z_{it}S_{it}^{\alpha}(N_{it}^{P})^{1-\alpha}$, where S_{it} denotes local commercial structures and N_{it}^{P} the local number of workers employed in final good production. We denote by N_{it} the total number of workers in i at time t. We define the long-run, Z_i, and time-varying, χ_{it}, components of productivity as $Z_{it} = Z_i e^{\chi_{it}}$.

In every location, there is an equilibrium capital stock K_{it}. Capital can be combined with land L_i and construction labor N_{it}^{B} to produce buildings B_{it} according to the production function $B_{it} = L_i^{\omega}(N_{it}^{B})^{\varpi}K_{it}^{1-\omega-\varpi}$. Buildings B_{it} can be costlessly repurposed between residential housing and commercial structures, so that $B_{it} = S_{it} + H_{it}$. Denote by r_{it} the common rental rate of buildings to firms and workers.

Capitalists decide how much to invest in every location subject to constant returns to scale investment costs, convex in I, $c_i(I/K)K = \frac{c_{i0}^{-1/\zeta}}{1+1/\zeta}\left(\frac{I}{K}\right)^{1+1/\zeta}K$. ζ represents the investment elasticity with respect to changes in the value of capital. These costs are paid in the final good whose price is normalized to

1. To finance investment, capitalists borrow or save in a risk-free national bond market which carries an equilibrium interest rate $\overline{R}_t$. Capital is not mobile across locations. We denote by $R_{K,it}$ the return on a unit of capital. The local capital stock depreciates at rate Δ_{it}. We define the long-run (Δ_i) and time-varying (δ_{it}) components of capital depreciation rates as $\Delta_{it} = \Delta_i + \delta_{it}$.

Capitalists are endowed with an equal number of non-traded shares of a national mutual fund. This mutual fund owns all the land in the economy. Denote by π_{it} the payment from the mutual fund to capitalists in location i at time t.

2.3 Climate change

The path of global mean temperature T_t is exogenous. Going forward, the vast majority of carbon emissions is expected to stem from developing economies and is thus largely exogenous to U.S. economic activity. Global mean temperatures relative to reference—for instance, pre-industrial—levels T^P satisfy: $T_t - T^P = \epsilon\big(z_t + T_t^D\big)$. T_t^D is a deterministic path corresponding to a central climate scenario. z_t is a mean-zero shock that captures natural climate variability. ϵ is a scaling parameter that clarifies notation for our solution method.[3]

Local productivity χ_{it}, amenities a_{it}, and capital depreciation δ_{it} depend on time only through the path of global mean temperatures. We parameterize these shifters through the following functions:

$$\chi_{it} = \chi_i\left(T_t - T^P\right), \qquad a_{it} = a_i\left(T_t - T^P\right), \qquad \delta_{it} = \delta_i\left(T_t - T^P\right), \tag{1}$$

where $\chi_i(0) = a_i(0) = \delta_i(0) = 0$. Even though these damages functions take global temperature as an argument, they capture flexibly the possible dependence of damages on local temperature through their location index i.[4]

2.4 Static equilibrium

The maximization problem of firms implies that the wage w_{it} in location i satisfies the firm's first-order condition $w_{it} = (1-\alpha)Z_{it}(S_{it}/N_{it}^P)^{\alpha}$. Similarly, the rental rate for structures satisfies $r_{it} = \alpha Z_{it}(S_{it}/N_{it}^P)^{-(1-\alpha)}$, since depreciation is not covered by the users of buildings. The optimal choice of labor in building production implies $\varpi r_{it}B_{it}/N_{it}^B = w_{it}$. Furthermore, the local demand for housing by workers implies that an equilibrium in the housing market satisfies $\beta w_{it}N_{it} = r_{it}H_{it}$.

We determine equilibrium prices and quantities as functions of the local capital stock K_{it} and local number of workers N_{it}. We show that labor is allocated to goods and buildings production in constant shares: $N_{it}^P = xN_{it}$ and $H_{it} = yB_{it}$, where x, y are combinations of parameters described in equation (18),

[3] We could introduce uncertainty in the long-run path of temperatures by writing $T_t - T^P = \epsilon\big(z_t + \tilde{z}_t T_t^D\big)$ for some process $\tilde{z}_t$. Since our solution method relies on a first-order perturbation of the economy, such uncertainty would be immaterial for our results. Uncertainty matters for higher-order perturbations.

[4] For instance, they are equivalent to positing that damages are a function of local temperature deviations (e.g. $\chi_{it} = F(T_{it} - \overline{T}_i)$) and that local temperature is related to global temperature according to $T_{it} = \overline{T}_i + \overline{\tau}_i(T_t - T^P)$.

Appendix A.1. Using these shares and the production function of buildings, the wage and the rental rate of buildings become: $w_{it} = w_{i0} Z_{it} L_i^{\omega\alpha} (K_{it}^{1-\omega-\varpi} N_{it}^{\varpi-1})^{\alpha}$ and $r_{it} = r_{i0} Z_{it} L_i^{-\omega(1-\alpha)} (K_{it}^{1-\omega-\varpi} N_{it}^{\varpi-1})^{-(1-\alpha)}$, where w_{i0}, r_{i0} are combinations of parameters and local fundamentals expressed in Appendix A.1.

The rental rate of capital depends on the rental rate of buildings. Profit maximization by developers implies that it satisfies: $R_{K,it} = R_{0i} e^{\chi_{it}} K_{it}^{-\phi} N_{it}^{\psi} \equiv R_i(\chi_{it}, K_{it}, N_{it})$, where R_{0i} is a location-specific constant that depends on the permanent component of productivity and available land, and ϕ and ψ are combinations of parameters detailed in Appendix A.1.

We can now solve for consumption given prices. Consumption by workers in location i is equal to the real wage. It satisfies $C_{it} = w_{it}/r_{it}^{\beta} = C_{0i} e^{(1-\beta)\chi_{it}} \left(K_{it}^{1-\omega-\varpi}/N_{it}^{1-\varpi}\right)^{\xi}$, where C_{0i} is a location-specific constant, and ξ a combination of parameters detailed in Appendix A.1. Finally, flow utility of workers in location i at time t is: $A_{it} + u\left(w_{it}/r_{it}^{\beta}\right) = A_i + a_{it} + u\left(C_{0i} e^{(1-\beta)\chi_{it}} \left(K_{it}^{1-\omega-\varpi}/N_{it}^{1-\varpi}\right)^{\xi}\right) \equiv U_i(a_{it}, \chi_{it}, K_{it}, N_{it})$.

2.5 Migration decisions

Workers solve a forward-looking dynamic migration decision problem. We denote by V_{it} the value of being located in i at time t. V_{it} satisfies the Hamilton-Jacobi-Bellman (HJB) equation given by:

$$\rho V_{it} = U_i(a_{it}, \chi_{it}, K_{it}, N_{it}) + \mathcal{M}_i[V] + \frac{\mathbb{E}[d_t V_{it}]}{dt}, \qquad \mathcal{M}_i[V] \equiv \mu \left\{ \frac{1}{\nu} \log \left(\sum_j e^{\nu(V_{jt} - \tau_{ij})} \right) - V_{it} \right\}, \tag{2}$$

where we used standard discrete choice results and denoted $\mathcal{M}_i[V]$ the continuation value from migration. The last term in the worker's HJB equation represents the continuation value from changes in the aggregate state, where the notation d_t denotes the time increment due to changes in aggregates only and not due to individual migration. Standard discrete choice results then imply migration shares as a function of the vector of values V given by:

$$m_{ij}(V) = \frac{e^{\nu(V_j - \tau_{ij})}}{\sum_k e^{\nu(V_k - \tau_{ik})}}. \tag{3}$$

The population distribution evolves according to the Kolmogorov Forward (KF) equation:

$$\frac{dN_{it}}{dt} = \mu \left(\sum_k m_{ki}(V_t) N_{kt} - N_{it} \right) \equiv \mu \Big(\big(m^*(V_t) - \mathrm{Id}\big) N_t \Big)_i. \tag{4}$$

In equation (4), m denotes the matrix of migration shares $m_{ij}(V_t)$. m^* denotes the matrix transpose of the matrix m. We also denote by $M^*(V) = \mu\big(m^*(V) - \mathrm{Id}\big)$ a matrix that collects migration shares and the identity matrix, so that (4) becomes, in matrix notation, $\frac{dN_t}{dt} = M^*(V) N_t$. We denote $M(V) = \mu(m(V) - \mathrm{Id}))$ the transpose of $M^*(V)$ for future reference.

2.6 Investment decisions

Capitalists solve a forward-looking dynamic investment decision problem. We denote $\mathcal{P}_{it}(K,b)$ the value of being located in i at time t and holding K units of local capital together with b units of bonds. $\mathcal{P}_{it}(K,b)$ satisfies the HJB equation:

$$\rho\mathcal{P}_{it}(K,b) = \max_{I,C} C + \Big(\overline{R}_t b + R_{K,it}K + \pi_{it} - c_i(I/K)K - C\Big)\frac{\partial \mathcal{P}_{it}}{\partial b} + \big(I - \Delta_{it}K\big)\frac{\partial \mathcal{P}_{it}}{\partial K} + \frac{\mathbb{E}_t[d_t\mathcal{P}_{it}]}{dt}. \tag{5}$$

The first term in the capitalist HJB is the flow utility from consumption. The second term is the continuation value from net savings. Net savings are given by returns on bonds and capital, proceeds from the land-holding mutual fund, minus expenditures on investment adjustment costs and consumption. Net savings are valued at the marginal value $\frac{\partial \mathcal{P}_{it}}{\partial b}$. The third term represents the continuation value from net investment, namely, gross investment minus depreciation multiplied by the marginal value of capital $\frac{\partial \mathcal{P}_{it}}{\partial K}$. The final term in the capitalists' HJB is the continuation value from changes in the aggregate state.

We show in Appendix A.2 that $\mathcal{P}_{it}(K,b) = Q_{it}K + b + \Pi_{it}$, where Π_{it} is the present value of transfers from the mutual fund, and Q_{it} satisfies:

$$\rho Q_{it} = R_i(\chi_{it}, K_{it}, N_{it}) + \frac{c_{i0}Q_{it}^{1+\zeta}}{1+\zeta} - \Delta_{it}Q_{it} + \frac{\mathbb{E}_t[d_tQ_{it}]}{dt}. \tag{6}$$

The investment policy of capitalists then satisfies $I_{it}^* = c_{i0}Q_{it}^{\zeta}K_{it}$. The law of motion of capital in every location becomes:

$$\frac{dK_{it}}{dt} = (c_{i0}Q_{it}^{\zeta} - \Delta_{it})K_{it}. \tag{7}$$

2.7 Steady-state

In steady-state at baseline temperatures, $\epsilon = 0$. All time derivatives are equal to zero. The HJB equation of workers (2) and capitalists (6) become:

$$\rho V_i^{ss} = U_i(0,0,K_i^{ss},N_i^{ss}) + \mathcal{M}_i[V^{ss}], \qquad \rho Q_i^{ss} = R_i(0,K_i^{ss},N_i^{ss}) - \frac{\zeta c_{i0}(Q_i^{ss})^{1+\zeta}}{1+\zeta}. \tag{8}$$

The steady-state population distribution $N^{ss} = \{N_i^{ss}\}_i$ and capital distribution $K^{ss} = \{K_i^{ss}\}_i$ satisfy:

$$0 = M^*(V^{ss})N^{ss}, \qquad \Delta_i = c_{i0}(Q_i^{ss})^{\zeta}. \tag{9}$$

Appendix B describes a simple algorithm to solve for the steady-state that leverages equations (8)-(9).

3 The Master Equation, the FAME, and transitional dynamics

3.1 Strategy

Our economy is a dynamic general equilibrium economy in which the distributions of workers $N_t = \{N_{it}\}_i$ and capital $K_t = \{K_{it}\}_i$ are aggregate state variables that determine local prices. The distribution of

workers and capital evolves slowly according to the laws of motions (4) and (7). These laws of motion in turn depend on the values of workers given by the HJB equations (2) and (6).

Solving for this dynamic fixed point is challenging in our high-dimensional environment with over 3,000 counties. We make progress by leveraging the 'Master Equation' representation of the economy developed in Bilal (2023).

The Master Equation approach is structured in two steps. First, we merge the individual decision problems with the laws of motion of the population and capital distributions into a single Bellman equation: the Master Equation. The Master Equation is a state-space representation of the equilibrium. Second, we take a local perturbation of the Master Equation in the scale parameter ϵ around a steady-state of the economy. The key insight from the local perturbation is to simplify the dynamic fixed point to a set of simple and standard Bellman equations that we solve rapidly with entirely standard techniques. This approach delivers an analytic counterpart to the approach in Reiter (2009). For clarity, we present a self-contained description of our approach that closely follows the steps in Bilal (2023).

3.2 The Master Equation

We start with the Master Equation for workers. We combine the HJB equation (2) with the laws of motion (4) and (7) with a simple change of variables. We index value functions by the population and capital distributions instead of calendar time alone. The core idea is that the population and capital distributions are no more than large-dimensional state variables from the perspective of any given worker. Of course, we need to keep calendar time as a separate index because of climate change embedded in global mean temperatures T_t^D.

Specifically, we change variables by writing $V_{it} = V_{it}(z_t, N_t, K_t)$ and $Q_{it} = Q_{it}(z_t, N_t, K_t)$, where now the time subscript t only captures dependence on deterministic temperature.[5] Recall that $N_t = \{N_{it}\}_i$ denotes the vector of population across locations at time t, and $K_t = \{K_{it}\}_i$ similarly denotes the capital distribution. Leveraging this change of variables, we use the chain rule to express the continuation value from changes in aggregate states as:

$$\mathbb{E}_t\left[\frac{d_t V_{it}}{dt}\right] = \underbrace{\frac{\partial V_{it}}{\partial t}}_{\substack{\text{change in } T_t^D}} + \underbrace{\mathcal{A}_\epsilon(z)[V_{it}]}_{\substack{\text{change in } z_t: \\ \text{continuation value}}} + \underbrace{\sum_j \frac{\partial V_{it}}{\partial N_j}\frac{dN_{jt}}{dt}}_{\substack{\text{change in } N_t: \\ \text{chain rule}}} + \underbrace{\sum_j \frac{\partial V_{it}}{\partial K_j}\frac{dK_{jt}}{dt}}_{\substack{\text{change in } K_t: \\ \text{chain rule}}}, \tag{10}$$

where $\mathcal{A}_\epsilon(z)$ is an operator that embeds the continuation value arising from natural climate variability. For instance, if z_t follows a continuous-time AR(1) process $dz_t = -\iota z_t + \sigma dW_t$, the operator $\mathcal{A}_\epsilon(z)$ is given by $\mathcal{A}_\epsilon(z)[V] = -\iota z \epsilon \frac{\partial V}{\partial z} + \frac{\sigma^2\epsilon^2}{2}\frac{\partial^2 V}{\partial z^2}$.

[5] If the evolution of temperature was determined by current temperature and the evolution of the economy through its emissions, as in a integrated assessment models of the world economy, we would simply add temperature as a state variable and eliminate time dependence in the value function altogether.

The last two components encode how the value of workers changes with the population and capital distributions across locations. When workers reallocate across locations in equilibrium, or when the distribution of capital shifts in equilibrium, the distribution of local wages, building rental rates, and capital rental rates change. Changes in these three distributions of prices affect residents of location i.

We then use the laws of motion of the population and capital distributions (4) and (7) to express the time change of population and capital in (10). After this substitution into the continuation value (10) and into the HJB (2), we obtain the Master Equation for workers:[6]

$$\begin{aligned}\rho V_{it}(z,N,K) &= \underbrace{U_i\Big(a_i(\epsilon(z+T_t^D)),\chi_i(\epsilon(z+T_t^D)),K_i,N_i\Big)}_{\text{flow payoff}} + \underbrace{\mathcal{M}_i[V]}_{\substack{\text{continuation value}\\ \text{from own migration}}} \\ &+ \underbrace{\sum_j \frac{\partial V_{it}}{\partial N_j}\left(M^*(V)N_t\right)_j + \sum_j \frac{\partial V_{it}}{\partial K_j}\left(c_{j0}Q_{jt}^{\zeta} - \Delta_j - \delta_j(\epsilon(z+T_t^D))\right)K_j + \mathcal{A}_\epsilon(z)[V_{it}] + \frac{\partial V_i}{\partial t}}_{\text{continuation values from aggregate changes}}.\end{aligned} \tag{11}$$

The Master Equation for workers depends on the value of capitalists Q because the latter affects investment, capital accumulation, prices, and, ultimately, worker welfare.

A similar logic delivers the Master Equation for capitalists, which is given by:

$$\begin{aligned}\rho Q_{it}(z,N,K) &= \underbrace{R_i\left(\chi_i(\epsilon(z+T_t^D)),K_i,N_i\right)}_{\text{flow payoff}} + \underbrace{\frac{c_{i0}Q_i^{1+\zeta}}{1+\zeta} - \left(\Delta_i + \delta_i(\epsilon(z+T_t^D))\right)Q_{it}}_{\text{continuation values from own investment}} \\ &+ \underbrace{\sum_j \frac{\partial Q_{it}}{\partial N_j}\left(M^*(V)N_t\right)_j + \sum_j \frac{\partial Q_{it}}{\partial K_j}\left(c_{j0}Q_{jt}^{\zeta} - \Delta_j - \delta_j(\epsilon(z+T_t^D))\right)K_j + \mathcal{A}_\epsilon(z)[Q_{it}] + \frac{\partial Q_{it}}{\partial t}}_{\text{continuation values from aggregate changes}}.\end{aligned} \tag{12}$$

Our equilibrium definition is standard and therefore omitted. The main advantage of the Master Equations (11)-(12) is that they provide a parsimonious representation of the general equilibrium of the economy. The derivations above prove our first result.

Proposition 1. *(Equilibrium)*
A solution (V,Q) to the Master Equations (11)-(12) together with a solution to the population and capital distributions $\{N_t,K_t\}_t$ to the KF equations (3) and (7) is an equilibrium of our economy.

3.3 The FAME

Despite providing a parsimonious representation of the equilibrium, the nonlinear Master Equations (11)-(12) are challenging to solve numerically because they depend on large-dimensional distributions. Traditional global numerical techniques would rapidly run into the curse of dimensionality. Instead, we use an analytic approach to gain economic insights and substantially simplify the computational burden. We

[6] We omit the full dependence of the value function and its derivatives on (K,N,t,ϵ) on the right-hand-side for brevity.

seek a local solution to the Master Equations (11)-(12) when the scale parameter ϵ is small enough. That is, we solve the First-order Approximation to the Master Equations (FAME).

The FAME is a first-order Taylor expansion of the Master Equations (11)-(12) in ϵ around the initial steady-state. We consider distributions and shocks that are close enough to steady-state. Namely, denote $N = N^{ss} + \epsilon n$ and $K = K^{ss} + \epsilon k$, where the vectors n, k denote scaled deviations of the population and capital distributions from steady-state.

We then seek a solution of the form:

$$\begin{aligned} V_{it}(z, N^{ss} + \epsilon n, K^{ss} + \epsilon k) &= V_i^{ss} + \epsilon \left\{ \sum_j v_{ij}^N n_j + \sum_j v_{ij}^K k_j + v_i^Z z + v_{it}^T \right\} + \mathcal{O}(\epsilon^2), \\ Q_{it}(z, N^{ss} + \epsilon n, K^{ss} + \epsilon k) &= Q_i^{ss} + \epsilon \left\{ \sum_j q_{ij}^N n_j + \sum_j q_{ij}^K k_j + q_i^Z z + q_{it}^T \right\} + \mathcal{O}(\epsilon^2). \end{aligned} \tag{13}$$

The additive separability follows from the first-order Taylor expansion in ϵ.

Thus, instead of seeking full functions V, Q as solutions to the Master Equations, the first-order approach lets us seek a restricted number of coefficients: the directional derivatives $v_{ij}^N, v_{ij}^K, v_i^Z, v_{it}^T$ of the value function with respect to the population and capital distributions, temperature shocks and temperature trends, called 'impulse values'. We substitute the first-order Taylor expansions (13) into the Master Equations (11)-(12) and obtain a set of restrictions on these directional derivatives: the FAME. These restrictions constitute our second key set of results, proven in Appendix C.

Proposition 2. *(Deterministic and trend FAME)*
The matrices $v^N, v^K, q^N, q^K, v_t^T, q_t^T$ satisfy the generalized Sylvester matrix equation in $\mathrm{v}^d = \begin{pmatrix} v^N & v^K \\ q^N & q^K \end{pmatrix}$ and the Ordinary Differential Equation systems in $\mathrm{v}_t^T = \begin{pmatrix} v_t^T \\ q_t^T \end{pmatrix}$ and $p_t = \begin{pmatrix} n_t \\ k_t \end{pmatrix}$:

$$\begin{aligned} \rho \mathrm{v}^d &= \mathrm{D}^d + \mathrm{M}\mathrm{v}^d + \mathrm{v}^d \mathrm{M}^* + \mathrm{v}^d \mathrm{P} \mathrm{v}^d, \\ \rho \mathrm{v}_t^T &= D_t^T + (\mathrm{M} + \mathrm{v}^d \mathrm{P}) \mathrm{v}_t^T + \frac{\partial \mathrm{v}_t^T}{\partial t}, \\ \frac{dp_t}{dt} &= D_t^p + \mathrm{P}(\mathrm{v}_t^T + z_t \mathrm{v}^Z) + (\mathrm{M}^* + \mathrm{P}\mathrm{v}^d) p_t, \end{aligned}$$

where the matrices $\mathrm{D}^d, \mathrm{M}, \mathrm{P}$ and vectors D_t^T, D_t^p only depend on parameters, steady-state objects, and T_t^D. They are specified in Appendix C together with the stochastic FAME for v^Z and q^Z.

The deterministic FAME for v^d in Proposition 2 is a Bellman equation that is satisfied by the deterministic impulse values v^N, v^K, q^N, q^K. This Bellman equation takes the form of a nonlinear Sylvester matrix equation.[7] The right-hand-side of the deterministic FAME has four components. Each one encodes a particular force that affects how the value of workers and capitalists in location i changes in equilibrium when an additional worker enters location j or an additional unit of capital is added in location j.

[7] A standard Sylvester matrix equation is a matrix equation in an unknown matrix X such that $AX + XB + C = 0$.

The first component in the deterministic FAME is the direct price impact matrix D^d. When population and capital distributions change, prices and thus flow payoffs also change. The upper left block of the price impact matrix D^d, $D_{UN} = -\xi(1-\varpi)\mathbf{diag}\Big(u'(C_i^{ss})C_i^{ss}/N_i^{ss}\Big)$, encapsulates how changes in the population distribution affect workers in location i. The combination of parameters $\xi(1-\varpi)$ summarize the effect on real wages. The diagonal marginal utility matrix converts real wage changes into utility changes. Similarly, the upper right block of the impact matrix D^d encapsulates how changes in the capital distribution affect workers in location i through their effect on real wages. The lower half of the price impact matrix D^d reflects how changes in the population and capital distributions affect the return on capital.

The second component in the deterministic FAME, Mv^d, encodes the partial equilibrium option value of migration. The FAME reveals that workers only need to evaluate this option value using their steady-state migration matrix M included in M. This property arises because of the envelope condition: migration decisions are already optimal before the economy moves out of steady-state.

The third component in the deterministic FAME, $\mathrm{v}^d\mathrm{M}^*$, represents a first general equilibrium force. When contemplating the effect of an additional worker in location j, workers and capitalists in location i expect this additional worker in location j to migrate going forward, which they need to keep track of. The FAME shows that this expectation is summarized by the steady-state migration matrix M.[8]

The fourth component in the deterministic FAME, $\mathrm{v}^d\mathrm{Pv}^d$, encodes a second general equilibrium force. It represents how workers and capitalists in location i value changes in the law of motion of the population and capital distributions that arise because of an additional worker or capital unit in location j.

The structure of the trend FAME in Proposition 2 is similar to the deterministic FAME. The first component D_t^T in the trend FAME is the direct climate impact and depends linearly on the product of damage coefficients $a_i \equiv a_i'(0)$, $\chi_i \equiv \chi_i'(0), \delta_i \equiv \delta_i'(0)$ and global mean temperature T_t^D. The remaining components in the trend FAME represent partial and general equilibrium forces analogous to the ones in the deterministic FAME.

Proposition 2 highlights the three key properties of the deterministic FAME that are direct consequences of the analytic local perturbation. First, the deterministic FAME is a standard Bellman equation in finite dimension. The dimensionality of the impulse value v^d is $(2\mathcal{I})^2$, instead of being infinite-dimensional like the nonlinear Master Equations (11)-(12). Second, all the objects entering in the FAME are steady-state objects with closed form expressions. Third, the FAME is block-recursive. The deterministic FAME does not depend on the trend or stochastic FAMEs. The trend and stochastic FAMEs do not depend on allocations. Hence, one can solve for the deterministic FAME in a first step. In a second step, given the deterministic impulse value v^d, one solves for the trend and stochastic impulse values v^T and v^Z. In a third step, one can solve for the equilibrium path of allocations p_t from a single

[8]The corresponding component for capital drops out because there is no gross capital growth in steady-state in any location.

time iteration given the deterministic, trend and stochastic impulse values.

Proposition 2 indicates a straightforward algorithm to compute the deterministic impulse value. Indeed, all the known inputs into the deterministic FAME can be directly constructed given steady-state objects. Thus, given steady-state objects, we directly construct the $2\mathcal{I} \times 2\mathcal{I}$ matrices D_d, M and P. We then seek a $2\mathcal{I} \times 2\mathcal{I}$ matrix v^d that satisfies the nonlinear Sylvester matrix equation: $0 = \mathrm{D}_d + (\mathrm{M} - \rho \mathrm{Id})\mathrm{v}^d + \mathrm{v}^d \mathrm{M}^* + \mathrm{v}^d \mathrm{P} \mathrm{v}^d$.

Two methods are available to solve this equation. The first one is a simple iterative algorithm that leverages standard numerical packages solving standard Sylvester equations of the form. The second method is to recast this nonlinear Sylvester equation as a larger $4\mathcal{I} \times 4\mathcal{I}$ linear rational expectation system (Blanchard and Kahn, 1980; Reiter, 2009) and use standard rational expectations solution methods. Both methods exhibit comparable performance in our setting. We provide more details for both approaches in Appendix C.6.

Once we have solved for the deterministic impulse value v^d, we solve for the trend impulse value with a simple backward iteration leveraging Proposition 2. Once we have solved for the deterministic and trend impulse values, we compute any impulse response to a shock or initial conditions with a simple forward iteration as per Proposition 2.

3.4 Accuracy

To operationalize the FAME, we must make two additional choices. First, we must choose whether to expand around the initial steady-state—prior to climate change—or around the final steady-state—after climate change materializes.

Using the final steady-state offers two advantages. The first one is that it captures how the sensitivity of migration and investment decisions to changes in the economy depends on long-run climate change. By contrast, using the initial steady-state fixes this sensitivity. Thus, expanding around the final steady-state let us capture the benefits from adaptation more comprehensively.

The second advantage of using the final steady-state is that it improves accuracy. Expanding around the final steady-state constrains allocations—population and capital—to coincide with their exact, non-linear counterparts at dates $t = 0$ and $t = +\infty$. In addition, decisions and welfare also coincide with their exact, nonlinear counterparts at $t = +\infty$. By contrast, using the initial steady-state only constrains allocation at date $t = 0$. Therefore, expanding around the final steady-state imposes substantially more discipline on the FAME.

The second choice we must make is whether to consider perturbations in population and capital levels—as we did so far—or whether to consider perturbation in log population and log capital. The capital law of motion is log-linear, and thus a perturbation in log capital is likely to be more accurate. Similarly, utility and the interest rate are log-linear in capital and population. Thus, a perturbation in log population may further improve accuracy. In those cases, we only need to appropriately rescale the

Figure 1: Accuracy in the FAME.

(a) Aggregate worker welfare in 2050

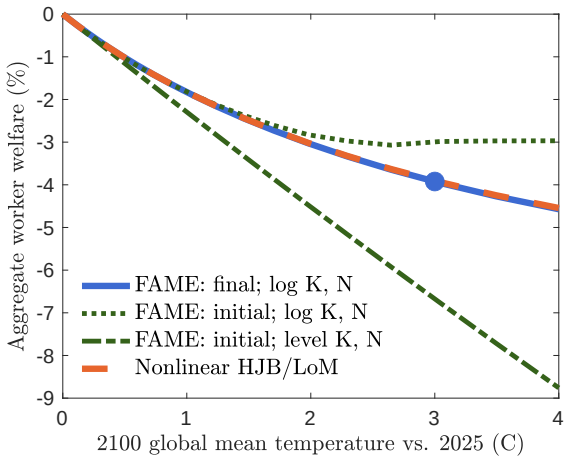

(b) Aggregate capital in 2050

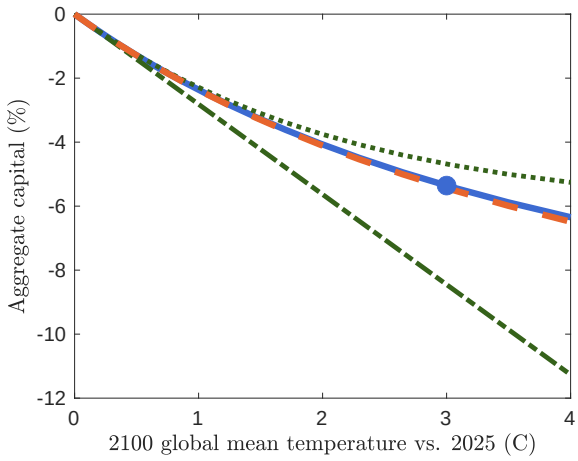

Note: Panel (a): aggregate worker welfare. Panel (b): aggregate capital. Both panels shown as a function of global mean temperature in 2100 relative to global mean temperature in 2025 in degrees Celsius. Green dash-dot line: using the FAME expanded around the initial steady-state, with capital and population in level deviations. Green dotted line: using the FAME expanded around the initial steady-state, with capital and population in log deviations. Solid blue line: using the FAME expanded around the final steady-state, with capital and population in log deviations. Dashed orange line: using the nonlinear value function (in panel a) or the nonlinear law of motion (in panel b) given allocations (in panel a) or decisions (in panel b) from the FAME.

matrices $\mathrm{D}^d, \mathrm{M}, \mathrm{P}$ and the vectors D_t^T, D_t^p by K_i^{ss} and N_i^{ss}.

To assess accuracy of our perturbation approach under these choices, we draw on standard tools developed in Haan and Marcet (1994) and Santos (2000). Given the allocations computed in the FAME, we solve for decisions and welfare with the exact, nonlinear HJB equation and compare it to the FAME solution. Conversely, given the decisions computed in the FAME, we can solve for the path of allocations with the exact, nonlinear KF equation and compare it to the path of allocations from the FAME.

Figure 1 illustrates this comparison for various ways of specifying the FAME. Figure 15 in Appendix C.6.1 displays additional statistics. Anticipating on our estimation in Section 5, Panel 15(a) displays 2050 aggregate worker welfare in our estimated model as a function of long-run warming. Panel 15(c) displays 2050 aggregate capital as a function of long-run warming. Using the initial steady-state incurs a larger approximation error relative to the nonlinear solution for warming scenarios above 1°C, in particular when specifying allocations in levels rather than in logs.

When we expand around the final steady-state and specify allocations in logs, the FAME and the nonlinear solution nearly coincide for warming scenarios up to 4°C. Crucially, using the final steady-state as the point of expansion captures nonlinearities in welfare and aggregate capital. This feature arises despite our solution method being a first-order perturbation because we compute the final steady-state nonlinearly. This property is central to our ability to capture the benefits from adaptation in Section 6. Hence, in what follows, we use perturbations in log population and capital and the final steady-state as a point of expansion in all our exercises, except when considering cases with limited anticipation.

3.5 Confidence intervals

In addition to counterfactuals, the FAME offers a practical approach to constructing confidence intervals around them. Consider uncertainty in the damage functions χ_i, a_i, δ_i. Inspecting the equations in Proposition 2 reveals three observations. First, the deterministic FAME is independent from damage functions conditional on the steady-state. Second, the trend FAME and the path of allocations are linear functions of damage functions through D_t^T and D_t^p.

We thus leverage the Delta method to construct confidence intervals around counterfactuals given uncertainty around damage functions. Holding the steady-state fixed for now, we only need to calculate the derivatives of the trend impulse values v_t^T and allocations p_t with respect to damage functions. We collect them as $\mathcal{V}_t = \left(\{\partial_{\chi_i}\mathrm{v}_t^T\}_i, \{\partial_{a_i}\mathrm{v}_t^T\}_i, \{\partial_{\delta_i}\mathrm{v}_t^T\}_i\right)$ and $\mathcal{P}_t = (\{\partial_{\chi_i}p_t\}_i, \{\partial_{a_i}p_t\}_i, \{\partial_{\delta_i}p_t\}_i)$, which are a $2\mathcal{I} \times 3\mathcal{I}$ matrices for each t. Proposition 2 implies that these derivatives satisfy standard differential equations that we solve with a similar algorithm to the one described in Section 3. We present this result for a path $z_t = 0$ for simplicity, but our results immediately generalize to $z_t \neq 0$.

Proposition 3. *(Confidence intervals)*
When $z_t = 0$, $\mathcal{V}_t$ and $\mathcal{P}_t$ satisfy the Ordinary Differential Equation system:

$$\rho\mathcal{V}_t = \mathcal{D}_t + \mathrm{M}\mathcal{V}_t + \mathrm{v}^d\mathrm{P}\mathcal{V}_t + \frac{\partial\mathcal{V}_t}{\partial t}, \qquad \frac{d\mathcal{P}_t}{dt} = \mathcal{D}_t^p + (\mathrm{M}^* + \mathrm{P}\mathrm{v}^d)\mathcal{P}_t + \mathrm{P}\mathcal{V}_t,$$

where the matrices $\mathcal{D}_t, \mathcal{D}_t^p$ only depend on the parameters and steady-state objects given in Appendix C.

Proposition 3 allows us to obtain the derivatives of counterfactuals with respect to damage functions necessary for the Delta method, conditional on the steady-state. When we expand around the initial steady-state, these derivatives are sufficient for the Delta method because the initial steady-state does not depend on the damage functions. When we expand around the final steady-state, the Delta method additionally requires the derivative of the final steady-state with respect to damage functions. In that case, we leverage our efficient steady-state calculation together with parallelization to obtain these derivatives numerically.[9] Having established an efficient and accurate solution method for counterfactuals and confidence intervals, we turn to our reduced-form estimates and estimation strategy.

4 Reduced-form trends in natural disasters and their impact

In order to quantify our model in a way that accounts well for the economic impact of climate change, we start by estimating the reduced-form impact that climate change has had on economic outcomes. In the next section we use these results to estimate the climate damage functions, as well as the mobility and investment elasticities.

[9] We do not need to consider the derivative of the deterministic FAME with respect to damage functions even when using the final steady-state because the resulting terms would be second order and thus irrelevant for the Delta method.

4.1 Data

We combine data of two types. First, we use economic data from several sources by county and year. We collect data on employment, wages and related statistics from the Bureau of Economic Analysis. We obtain investment data at 5-year intervals from the Census of Manufactures. These data span the years 1960 to 2019. We provide more details in Appendix E.1.

Second, we use weather data. We obtain daily information on surface temperature, windspeed, and precipitation for a raster at the 0.5° by 0.5° since 1901 from the inputs to the Inter-Sectoral Impact Model Intercomparison Project (ISMIP). This information consists of reanalysis data: it combines historical station-level weather measurements with a climate model to produce high-resolution weather information. We convert this information into a dataset that tracks annual extremes for every county and year in the U.S. We provide details in Appendix E.2.

We seek to capture the impact of extreme weather events. To that end, we construct indicator variables that capture whether local weather realizations are above a pre-specified threshold. Specifically, we first consider weather variables X_{it} for county i at time t in the following list: (i) maximum daily windspeed in the year, (ii) maximum daily precipitation in the year, and (iii) fraction of days with temperature above the 95^{th} percentile of the national annual mean temperature distribution in 1901-1910. We provide more details in Appendix E.3.

Our weather variables are designed to capture salient features of (i-ii) storms and flooding, which we combine into 'storms' and (iii) heat waves. Of course, the physical processes leading to and defining such events are necessarily more complex than the specific metrics available in large-scale datasets covering the entire U.S. for over a century. For our purposes, it only matters that these variables correlate strongly enough with actual storms, floods, and heat waves. Ultimately, the impact of our weather-related variables on economic activity determines climate damages regardless of their specific interpretation. We refer to our variables as storms and heat waves for expositional simplicity but acknowledge that our variables necessarily are a stylized measurement of the underlying phenomena.[10]

Different locations may be differentially adapted to natural disasters. To capture this adaptation and not overstate damages, we residualize our three weather variables X_{it} before constructing the indicator of extreme realizations. Therefore, we capture storm and heat wave realizations that are particularly severe relative to county-specific and annual conditions. Specifically, we strip out county and year fixed effects by estimating the linear regression: $X_{it} = \alpha_i + \beta_t + \hat{X}_{it}, \;\; \mathbb{E}_i[\hat{X}_{it}] = \mathbb{E}_t[\hat{X}_{it}] = 0$. We then use the estimated residual $\hat{X}_{it}$ to construct our indicator of extreme value for $\hat{X}_{it}$: $D_{it} = \mathbf{1}[\hat{X}_{it} \geq \text{p}(\hat{X})]$, where $\text{p}(\hat{X})$ denotes a given percentile of $\hat{X}_{it}$ across all counties i and years t. We choose realizations above the 99^{th} percentile for windspeed and precipitation. This choice is guided by meteorological estimates of wind and concentrated precipitation measures that lead to property damages. It also coincides with the

[10] Our measures also have the advantage of being objective physical measures, rather than human-made reports of storms or floods that are likely to be endogenous to economic activity or population density.

Figure 2: Global mean temperature and natural disasters: ISIMIP.

(a) Global temperature over time (b) 1-in-50-years storm (c) 1-in-20-years heat wave

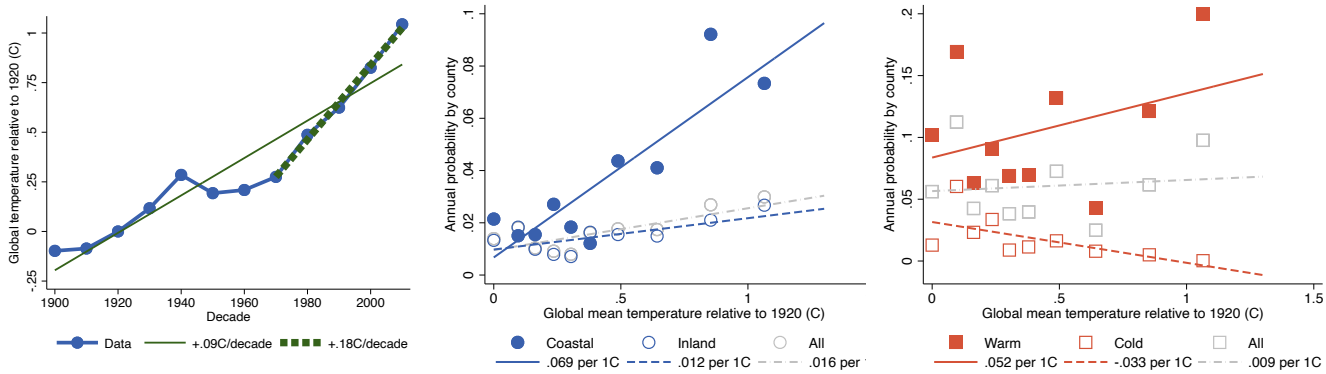

Note: Panel (a): global mean temperature by decade relative to 1920, in Celsius. Linear regression lines for 1900-2019 and 1970-2019. Panel (b): annual probability that a county experiences a storm event. For coastal counties, inland counties, and all counties in the U.S. Linear regression slopes of probability on global mean temperature. Panel (c): annual probability that a county experiences a heat wave event. For warm (above-median annual average temperature) counties, cold (below-median annual average temperature) counties, and all counties in the U.S. Linear regression slopes of probability on global mean temperature.

threshold at which we detect significant economic damages. We define our storm indicator as $D_{it}^{\text{storm}} = \max\{D_{it}^{\text{windspeed}}, D_{it}^{\text{precipitation}}\}$. A similar logic leads us to choose realizations above the 95$^{\text{th}}$ percentile for heat waves. Finally, we also construct event indicators that do not account for local adaptation and instead use the raw, unresidualized variables X to define D. We provide details in Appendix E.3.[11]

4.2 Trends in natural disasters

We start by documenting salient trends in natural disasters over the course of the 20$^{\text{th}}$ century for the U.S. Figure 2(a) first shows the well-known fact that global mean temperatures have risen by over 1°C since 1900. The rate of warming has accelerated in the last decades, reaching nearly 0.2°C by decade.

Figure 2(b) presents a binned scatterplot of the relationship between global mean temperature and the annual probability of a 1-in-50-years storm and a 1-in-20-years heat wave.[12] We start with severe storms, which occur every 50 years on average in the middle of the century according to our definition. The frequency of severe storms, presented in panel (b), rises substantially and approximately linearly with global mean temperatures across the U.S., consistently with the conclusions of the IPCC (2022).

Figure 2(b) reveals that the frequency of severe storms rises particularly fast in coastal counties—counties that have a coast along the Atlantic or Pacific oceans. A warming of 1°C over the course of the 20th century implies that the frequency of severe storms more than quadruples in coastal counties, from less than 2% to nearly 8%. These probabilities imply that severe storms used to occur less than every 50 years at pre-industrial temperatures in coastal counties. They now occur every 12 years. If global mean temperatures increase by 4°C by 2100 as in the business-as-usual scenario, severe storms would occur

[11] We also choose realizations below the 5$^{\text{th}}$ percentile for cold waves when we introduce them in Appendix F.6.
[12] We focus on observations post-1920 to have precisely one century of data.

every 3 years in coastal counties. In contrast, the frequency of severe storms rises only modestly in inland areas—which we define as any county that does not have a coast along the Atlantic or Pacific oceans.

We present the frequency of heat waves in Figure 2(c). We split our analysis between warm counties that have above-median average annual temperatures, and cold counties that have below-median average annual temperatures. Consistent with the conclusions of the IPCC (2022), we find that a heat wave that occurred every 20 years on average at 1920 global temperatures occurs every 5 years on average in 2025 in warm counties.[13] If global mean temperatures increase by 4°C by 2100 as in the business-as-usual scenario, a heat wave that happened only every 20 years in 1920 would happen every 2 years by 2100. By contrast, the frequency of heat waves in cold counties remains largely constant and close to zero.[14]

The marked increase in the frequency of coastal storms may be surprising in light of the lack of scientific consensus on changes in storm activity due to climate change. We reconcile these views with two arguments. First, we underscore changes in coastal storm activity in the U.S., while scientific studies often study worldwide or country-wide storm activity. Consistent with scientific consensus, Figure 2 shows only a modest increase in storm activity across the U.S. as a whole, but a concentrated rise in the coastal U.S. In fact, the trends in our data are similar to those documented in Klink (1999) for maximum windspeed in coastal and inland locations in the U.S.

Second, we validate our measure against direct storm counts from NOAA in Figure 3. Panel (a) shows that occurrences of tropical storms and hurricanes have been steadily rising with global mean temperature in the North Atlantic. Of course, not all NOAA storms make landfall, and those that do affect multiple counties. Thus, we estimate the number of counties affected by the average NOAA storm based either on presidential disaster declarations or on average storm size.[15]

Figure 3(b) displays how the (estimated) probability that a county experiences a NOAA storm evolves with global mean temperature. This probability changes virtually identically to our measure of 1-in-50 year storms in Figure 2(b) for coastal, inland, and all counties. This result supports the view that our definition of storms is highly correlated with occurrences of tropical storms and hurricanes, and displays similar trends over time.

Which locations experience more natural disasters? Figure 2 illustrates the extent to which coastal and warm counties have been more exposed in the last decades. We map out the detailed geography of exposure in Figure 4. The South-East Atlantic coast is particularly exposed to storms. For instance, counties in Texas, Louisiana, Florida, Georgia, North Carolina, and Virginia have experienced over 4 severe storms since 1990. However, inland counties in states such as Nebraska and New York have also

[13] The prevalence of extreme heat is subject to important natural variability. For instance, the second square from the left corresponds to Dust Bowl years.

[14] We also show that the frequency of cold waves declines markedly with global temperature in Figure 21, Appendix F.6.

[15] In either case, we find that the typical NOAA storm affects 50 counties on average conditional on landfall. Out of those 50 counties, about 7 are coastal. 10 to 20% of NOAA storms make landfall. Using the upper bound for coastal counties that are more likely to be affected, and the lower bound for inland counties that are less likely to be affected, we obtain that the typical NOAA storm affects 2 coastal counties and 4 inland counties on average, which we use to convert NOAA storm counts into the number of affected counties.

Figure 3: Global mean temperature and natural disasters: NOAA.

(a) NOAA raw storm counts

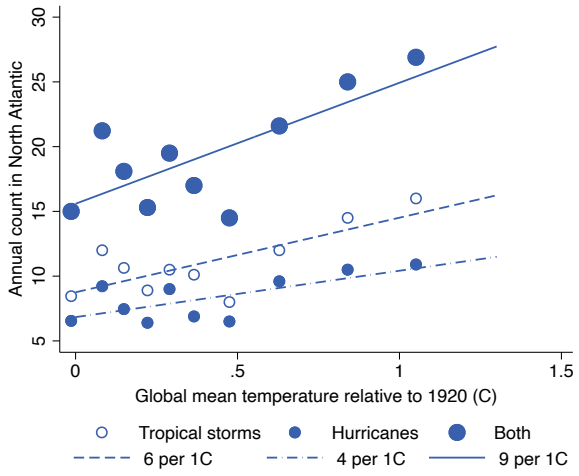

(b) NOAA storms

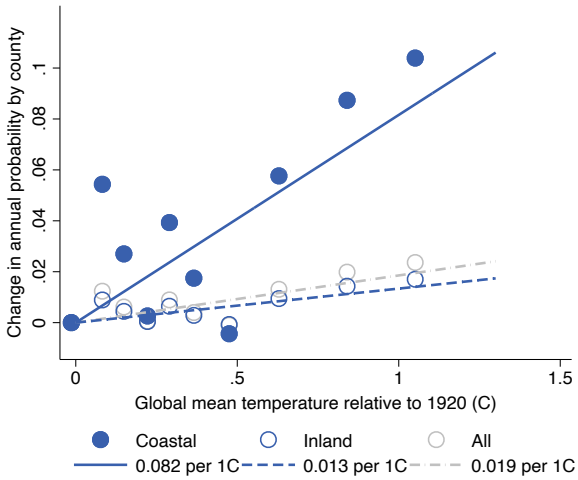

Note: Panel (a): number of North Atlantic tropical storms and hurricanes per year from NOAA, and linear regression slopes. Panel (b): change in estimated probability of a given county experiencing a NOAA tropical storm or hurricane per year. Every tropical storm or hurricane estimated to affect 2 coastal counties and 4 inland counties on average after taking storm size and landfall rate into account. Linear regression slopes.

experienced several severe storms. Heat waves are prevalent across the South of the U.S. Many counties in Florida, Louisiana, Texas, Kansas, New Mexico, and Arizona are among the most exposed, with over 5 heat waves since 1990.[16]

4.3 Event study design

The next step is to estimate the effect of a given natural disaster on economic activity. We use a standard distributed lag specification given by:

$$y_{it} = \alpha_i + \beta_t + \sum_{h=-A}^{B} \gamma_h D_{i,t-h} + \gamma_{-A-1}\bar{D}_{i,t,-A-1} + \gamma_{B+1}\bar{D}_{i,t,B+1} + \delta_{S(i),t} + W_{it}\eta' + \varepsilon_{it}, \quad (14)$$

where i denotes counties and t denotes calendar years. y_{it} denotes the logged outcome of interest: income per capita, employment, or investment. α_i is a county fixed effect, β_t is a year fixed effect. $D_{i,t-h}$ is our indicator that an extreme event occurred h years before calendar year t in county i. We include individual horizons h up to $A = 5$ years prior to and $B = 10$ years after the event. We also control for the average effect before A and after B: $\bar{D}_{i,t,-A-1} = \sum_{h \leq -A-1} D_{i,t-h}$, and $\bar{D}_{i,t,B+1} = \sum_{h \leq B+1} D_{i,t-h}$. $\delta_{S(i),t}$ denotes a set of trends by state, local mean temperature decile, local maximum daily windspeed and maximum precipitation deciles, population and income per capita deciles. W_{it} denotes a time-varying county-specific controls that includes local government expenditures lagged by 5 years.[17] ε_{it} is a mean-zero residual. Our coefficients of interest are γ_h, the effect of an event h periods ago on outcomes today.

[16] Figure 16, Appendix F.1, depicts the spatial distribution of natural disasters defined without residualizing.
[17] Including or excluding government expenditures does not affect our conclusions.

Figure 4: Natural disasters across counties.

(a) Storm counts since 1990

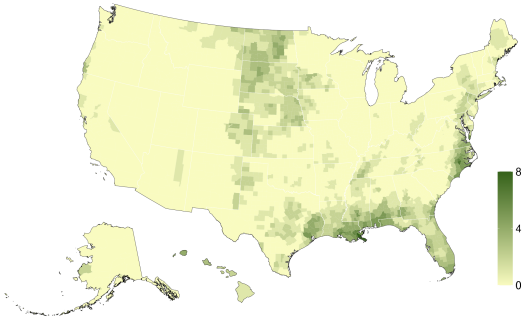

(b) Heat wave counts since 1990

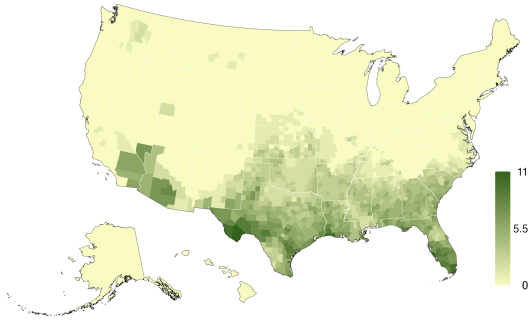

Note: Panel (a): total count of 1-in-50-years storms summed over 1990-2015 for each county in the U.S. Panel (b): total count of 1-in-20-years heat waves summed over 1990-2015 for each county in the U.S. White: missing data. Natural disasters based on our definition after residualizing.

We focus on years after 1990. Given that we include $B = 10$ lags and $A = 5$ leads, we use calendar years t after 2000. Restricting the data to focus on the post-1990 period lets us capture the most recent severity of extreme events in case it is time-varying. To the extent that not only the frequency but also the intensity of extreme events is projected to grow over time, our estimates represent a lower bound on expected damages going forward.

We allow the effect of storms and temperature to differ depending on the characteristics of locations. Namely, we allow the impact of storms to differ in coastal counties and inland counties. This split is natural given that severe storms on the coast may concur with coastal storm surges that worsen damages. In line with the literature that has found nonlinear effects of temperature on mortality and productivity (e.g. Deschênes and Greenstone, 2011 and Cruz and Rossi-Hansberg, 2023, respectively), we allow the effect of temperature to differ depending on the average temperature of a given location. We operationalize these ideas by running our analysis separately for coastal, inland, warm and cold counties as defined in Section 4.2.

Our identification condition is that treatment is randomly assigned conditional on our controls. Crucially, we include rich controls for location-specific trends $\delta_{S(i),t}$. These state-specific and county-group-specific trends absorb potentially important confounds to our exercise. For instance, demographic and income shifts have pushed high-income households to move to states such as Florida over the last 20 years. Florida also happens to be more exposed to severe storms and heat waves. As a result, omitting an adjustment to these background trends may lead to inferring that storms and heat waves increase income and employment.

Another concern for identification is whether the Stable Unit Treatment Value Assumption (SUTVA) is satisfied, namely that the control group remains unaffected by the treatment. This concern is valid given that in our model, untreated locations may respond to shocks in other regions because of general

Figure 5: The impact of 1-in-50-years-storms on economic activity in coastal counties.

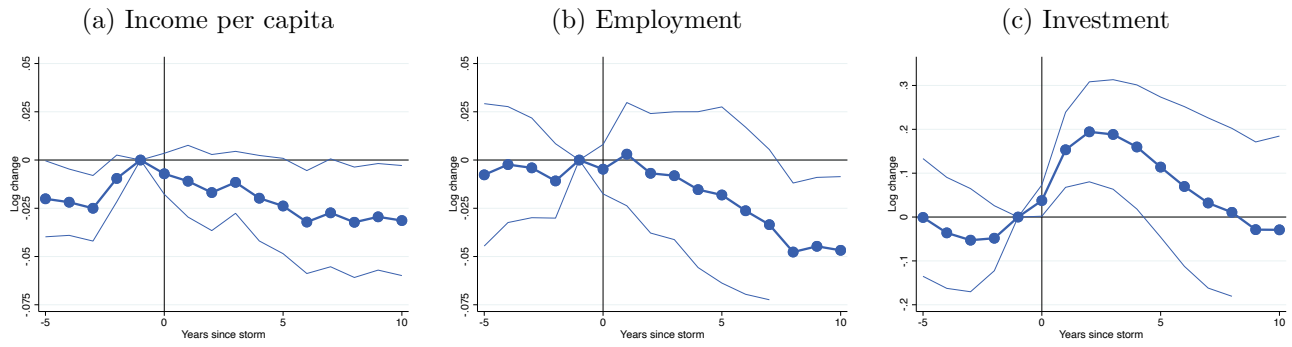

Note: Point estimates of coefficients γ_h from distributed lag regressions (14) for 1-in-50-years storms, and 95% confidence bands clustered by county. Coastal counties only. Panel (a): log income per capita. Panel (b): log employment. Panel (c): log investment. Years 1990-2015. Controls: county and year fixed effects; nonparametric trends by state, local annual mean temperature decile, local maximum daily windspeed and maximum precipitation deciles, population decile, and income per capita decile; 5-year lag of local government expenditures. Weighted by average county population in 1960-1980. Standard errors clustered by county.

equilibrium effects. Thus, our empirical estimates may be biased by these general equilibrium effects. Our structural approach addresses this concern since we estimate our model by indirect inference. Namely, we replicate the same regression in the model accounting for the spatial correlation pattern of storms and heat waves, and match the empirical coefficient—thus accounting for general equilibrium effects and the spatial distribution of extreme events directly.

4.4 Results

Storms. We find that severe storms have a significant impact on economic activity in coastal counties. Figure 5 displays the impact of 1-in-50-year storms on three indicators of economic activity. Each panel shows year-by-year point estimates together with 95% confidence intervals.

Panel 5(a) shows that a 1-in-50-years storm lowers income per capita of employed workers by about 2.5% over 10 years. Despite our rich set of controls, our estimated effects for income per capita display somewhat of an upward pre-trend. If we accounted for this differential trend, the estimated effect would be even larger. Panel 5(b) shows that employment drops by 5% after 10 years in coastal counties that experience a severe storm. Panel 5(c) reveals that investment booms after a severe storm, with a peak at 20% in the third year after the storm. To the extent that storms destroy capital, this positive investment response is natural given the need for reconstruction.

Taken together, these results indicate that severe storms in coastal counties are well captured by a capital depreciation shock. Indeed, in our model—as in a standard Real Business Cycle model—a capital depreciation shock lowers wages and employment but increases investment, as the local economy rebuilds its capital stock. Key to this interpretation is the positive sign of the investment response. A negative investment response would, instead, suggest a negative productivity shock.

We gauge the robustness of our results with four additional exercises. First, since our measure of

Figure 6: The impact of 1-in-20-years heat waves on economic activity in warm counties.

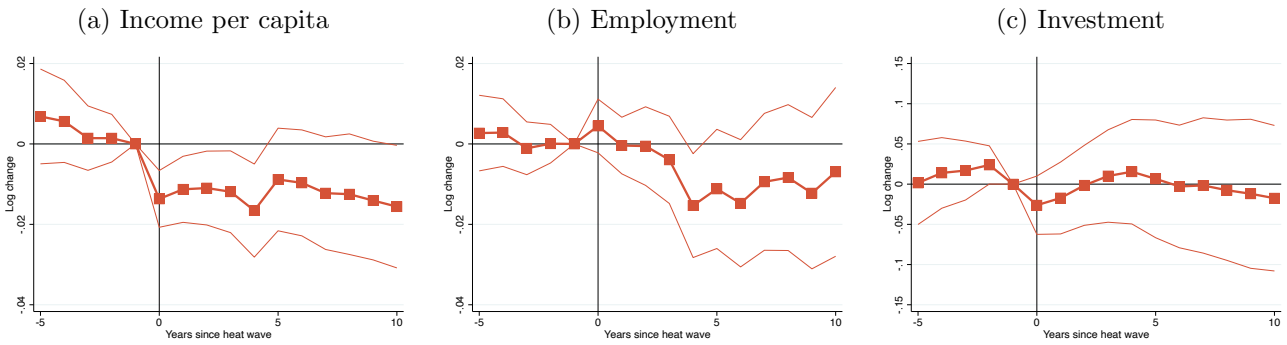

Note: Point estimates of coefficients γ_h from distributed lag regressions (14) for 1-in-20-years heat waves, and 95% confidence bands clustered by county. Warm (above-median average annual temperature) counties only. Panel (a): log income per capita. Panel (b): log employment. Panel (c): log investment. Years 1990-2015. Controls: county and year fixed effects; nonparametric trends by state, local annual mean temperature decile, local quantile of fraction of hot days, population decile, and income per capita decile; 5-year lag of local government expenditures. Weighted by average county population in 1960-1980.

investment only accounts for manufacturing investment, we reproduce our main result in Figure 17, Appendix F.2, rescaling the manufacturing investment by the manufacturing employment share in the same year. This adjustment has virtually no effect on our results. Second, since we interpolated our investment measure to trace out annual impulse response functions, we reproduce our main results in Figure 18, Appendix F.2, where we use investment aggregated at 5-year intervals to account for infrequent Census years. We find similar, or even somewhat more pronounced, effects. Third, we verify whether accounting for adaptation using residualized maximum windspeed and precipitation affects our results. We reproduce our results using raw maximum windspeed and precipitation to define storm events in Figure 19, Appendix F.3. We find virtually identical results, suggesting that adaptation to severe storms is weak. Fourth, we investigate the impact of severe storms on inland counties in Figure 19, Appendix F.3. We find no statistically significant or economically meaningful effect.

Heat. Having established the effect of severe storms on economic activity, we turn to the impact of temperature. We start with the effect of heat waves on counties with temperatures above the median (warm counties). Figure 6 displays the impact of heat waves on the same three indicators of economic activity as for storms. Panel 6(a) shows that income per capita drops by 1.5% and remains persistently low. Employment falls by 1.5% over the course of 10 years following a 1-in-20-years heat wave. Investment shows a moderate and negative response following a heat wave.

Together, these results suggest that heat waves in warm counties are well captured by a negative productivity shock. Crucially, the moderate negative investment response allows us to differentiate the effect of a heat wave from the effect of a storm. Given the sizable employment response, heat waves may also be associated with a negative local amenity shock. Our structural estimation in Section 5 allows for both.

As for storms, we gauge the robustness of our results with four additional exercises. First, we reproduce our main result in Figure 17, Appendix F.2, where we rescale manufacturing investment by the manufacturing employment share in the same year. We find virtually identical results. Second, we reproduce our main result in Figure 18, Appendix F.2, where we use investment aggregated at 5-year intervals to account for infrequent Census years. We find similar, although more pronouncedly negative, effects. Third, we verify whether accounting for adaptation using the residualized fraction of days above a temperature threshold affects our results. We reproduce our results using the raw fraction of days above a temperature threshold to define heat wave events in Figure 20, Appendix F.4. We find attenuated statistically insignificant results, suggesting that adaptation to heat is important. Since climate change is likely to bring about stronger heat waves in the future than in the past, we view our residualized estimates as most relevant for climate change counterfactuals. Nevertheless, in Section 6, we report how our counterfactuals change when we estimate our model using raw storms and heat waves. Fourth, we investigate the impact of heat waves in cold counties in Figure 20, Appendix F.4. We find statistically insignificant and economically inconclusive effects there, and thus do not attempt to use these estimates in the rest of our analysis.

Cold. We also estimate the impact of cold waves on economic activity in Figure 22, Appendix F.6. We do not detect statistically significant or economically consistent effects of cold waves in cold counties. Thus, we exclude cold waves from our main structural analysis in Sections 5 and 6. We report sensitivity analysis when we include cold waves, but their effect is quantitatively small relative to storms and heat.

With these reduced-form estimates of the impact of extreme events on economic activity in hand, we now turn to estimating the underlying damage functions and quantifying our model.

5 Model Quantification

5.1 Baseline parameters

We start by determining baseline preference and technology parameters. Importantly, we estimate the two key migration and investment elasticities in Section 5.3 below. Throughout the rest of the paper, we interpret an interval $[t, t+1)$ as one year.

Preference parameters are determined as follows. We use a pure rate of time preference $\rho = 0.02$, a value that is standard in the climate change literature (Rennert et al., 2022). We analyze the impact of different choices of the discount rate on our results in Section 6. We set the housing expenditure share for workers to the common value of $\beta = 0.3$ (Davis and Ortalo-Magné, 2011). We set the risk-aversion parameter to $\gamma = 1$ since we do not analyze the role played by climate risk.

The next step is to determine the parameters governing migration decisions. We set $\mu = 2.30$ so that 90% of workers have the option to migrate within a year. We estimate bilateral migration costs

τ_{ij} consistent with the empirical migration rate at baseline, as described in more detail below. Local amenities are estimated using the model inversion as described in the next section.

The parameters in the production function of goods and buildings are set to standard values. The share of commercial structures in goods production in the model includes both capital and physical structures in the data. Typical estimates put the first share at 0.3, and the second at 0.1, so $\alpha = 0.4$. To obtain the share of labor ϖ in the production function of buildings, we measure the fraction of labor in the structures production sector x from the BEA input-output data. We obtain $x = 0.95$. Thus, we recover $\varpi = \frac{(1-\alpha)(1-x)}{\alpha x+(1-\alpha)\beta} = 0.05$. To obtain the share of land in the building production function ω, we use common estimates from the real estate literature. For a typical urban property, the value of land represents around 50% of the property value, while the building value represents the other 50% (Davis et al., 2021). Hence, we set $\omega = 0.5$. Local productivities are the result of the model inversion, as described below.

The final set of parameters is related to investment choices. We impose a common capital depreciation rate of $\Delta_i = \Delta = 0.08$ for all counties at baseline. Of course, climate change affects the depreciation rate heterogeneously across locations. We estimate the investment elasticity and the local investment costs as described below.

5.2 Inversion of fundamentals

Our second step is to estimate time-invariant fundamentals for every location. Suppose for now that we have estimates of the migration elasticity ν and the investment elasticity ζ.

We use 2012 data for wages w_i, employment N_i, investment I_i, and migration flows $\mathtt{m}_{ij}$ for every pair of counties i, j. We interpret 2012 as the initial stead-state of the economy. We use a recursive scheme to recover the time-invariant fundamentals in every location, Z_i, A_i, c_{i0}, and τ_{ij}. The following proposition, proven in Appendix D, shows that given the observed data we can uniquely recover these fundamentals.

Proposition 4. *(Inversion of fundamentals)*
Given data $w_i, N_i, \tilde{I}_i, \mathtt{m}_{ij}$, there exists a unique set of vectors of fundamentals, (Z_i, A_i, c_{i0}), and a unique symmetric migration cost matrix, τ_{ij}.

The proof of Proposition 4 is constructive and thus provides an algorithm to recover fundamentals. The proof extends standard static inversion arguments to our fully forward-looking dynamic setting. We can only recover symmetric migration costs because we invert them non-parametrically.[18]

5.3 Migration and investment elasticities

Our inversion argument relies on knowledge of the migration and investment elasticities ν and ζ. We estimate those internally using our reduced-form estimates of the impact of extreme events on economic

[18] Without symmetry, they are not separately identified from local amenities. If we imposed instead that migration costs depend on some distance metric, we could, of course, estimate this dependence flexibly.

activity. Thus, we nest our inversion procedure in an outer loop in which we search over candidate values for ν and ζ.

Consistently with our reduced-form results, we assume that storms only generate a capital depreciation shock in coastal counties. We denote its scalar magnitude by $\Gamma^{\text{cap dep}}$. Heat waves generate a productivity shock together with an amenity shock in warm counties. We denote by Γ^{prod} the scalar value of the productivity shock, and by $\eta \times \Gamma^{\text{prod}}$ the magnitude of the amenity shock.[19]

We leverage a key property of the FAME to estimate the migration and investment elasticities without having to specify the magnitude of shocks. The response of the economy to shocks is linear in the magnitude of the shock by construction. Hence, relative impulse responses are independent from the magnitude of a common shock. For instance, in the FAME, the impulse response of employment relative to the response of income per capita following a productivity shock is independent from the magnitude of this productivity shock. If we target relative impulse responses, we can thus use a shock of an arbitrary magnitude. This property allows us to estimate ν, ζ, and η independently of the magnitude of the underlying shocks $\Gamma^{\text{cap dep}}, \Gamma^{\text{prod}}$.

We then proceed by indirect inference. Our approach is similar to a standard grid search, although the details of our implementation differ for efficiency. In a first step, we populate our parameter space using parameter vectors $\theta \equiv (\nu, \eta, \zeta)$ from a Sobol sequence. This approach covers the multivariate space more efficiently than with a standard tensor product grid. We chose the range of this parameter space to be wide enough to include a broad range of possible values and of course to include our point estimates.

In a second step, we invert fundamentals as in Section 5.2 and solve for the steady-state following Section 2.7 and Appendix B. Next, we solve the steady-state and the FAME of our economy. We further simulate the dynamic response of the entire economy to a 1% transitory productivity shock, together with a η% amenity shock. We also simulate the dynamic response of the entire economy to a 1% capital depreciation shock. It suffices to consider a 1% shock for our purposes because of the the FAME is linear and we consider relative responses to estimate elasticities, a point to which we return below. From these counterfactual responses, we construct model analogs of the event study estimates from Section 4. We account for the empirical spatial correlation of storms and heat waves by treating each location proportionally to the empirical number of extreme events from Figure 4. We then use these model-based event study estimates to construct target moments that inform (ν, η, ζ).

In a third step, we find the parameter vector (ν, η, ζ) among our set that best matches the data. Then, starting from this parameter vector, we use a standard minimum distance solver to adjust the parameters (ν, η, ζ) and close any remaining discrepancy relative to the data.

Specifically, we denote by $\text{irf}_{v,s,\theta}$ the model impulse response function corresponding to the event study estimates for outcome variable v, shock s, and parameters θ. The outcome v denotes either income per

[19] We set the persistence of the productivity shock ψ^{prod} to match a half-life of 5 years. As we show below, this persistence aligns with the mean-reversion patterns in the data.

capita, employment, or investment.[20] The shock s denotes either a joint productivity-amenity shock or a capital depreciation shock. We denote by $\text{IRF}_{v,s}$ its counterpart in the data. We also denote by $\text{cir}_{v,s,\theta}$ and $\text{CIR}_{v,s}$ the model and data cumulative impulse responses. That is, for any impulse response irf and horizon h, we define $\text{cir}_h = \sum_{h'=0}^{h} \text{irf}_{h'}$.

What moments are best fit for our purposes? Our strategy estimates the three parameters $\theta = (\nu, \eta, \zeta)$ jointly, but we discuss how we select each moment to provide intuition for identification. We provide numerical confirmation that these parameters determine the relevant moments below.

The gravity structure of migration indicates that the migration elasticity ν is related to the response of local employment relative to the response of income per capita, holding amenities fixed. Thus, we use the response of employment relative to income per capita following a capital depreciation shock, which leaves amenity unchanged.

Specifically, we use the cumulative impulse response of local employment relative to the cumulative impulse response of income per capita at 10 years after a productivity shock, $\frac{\text{cir}_{10,\text{emp,cap dep},\theta}}{\text{cir}_{10,\text{ipc,cap dep},\theta}}$, to inform the migration elasticity ν. We target the corresponding moment in the data following a storm in coastal counties. Intuitively, if employment responds strongly relative to income per capita without any change in amenities, the migration elasticity must be large.[21] We use cumulative impulse responses—or, equivalently, average impulse responses—rather than plain impulse responses because they are less sensitive to short-term, slow adjustment mechanisms that we do not model (e.g. sticky wages).

To inform the amenity-productivity ratio η, we use the cumulative impulse response of employment relative to the cumulative impulse response of income per capita at 10 years after a productivity-amenity shock, $\frac{\text{cir}_{10,\text{emp,prod-am},\theta}}{\text{cir}_{10,\text{ipc,prod-am},\theta}}$. We target the corresponding moment in the data following a heat wave in warm counties. Intuitively, if employment responds strongly relative to income per capita holding the migration elasticity ν fixed, amenities must be a large component of the effect of heat waves.

The cumulative impulse response of investment relative to employment 10 years after a capital depreciation shock, $\frac{\text{cir}_{10,\text{inv,cap dep},\theta}}{\text{cir}_{10,\text{emp,cap dep},\theta}}$ informs the investment elasticity ζ. Intuitively, the size of the employment response encapsulates the overall magnitude of the shock. If investment responds strongly relative to employment, the investment elasticity ζ must be large. We target its counterpart in the data following storms in coastal counties.

We invert fundamentals, solve for the steady-state of the model, the FAME, and impulse responses for 2,000 triplets $\theta = (\nu, \eta, \zeta)$. We construct our target moments and contrast them with their data counterparts in Figure 7. Once we identify the triplet among the 2,000 that provides the closest fit, we use a standard Newton search to close the remaining gap between model and data moments. The figure

[20] We use income per capita as the data counterpart of wages in the model to capture self-employment and business income that is not explicitly modeled. The model does not feature non-employment so, in principle, we could use either employment or population in the data as a counterpart of employment in the model. We use employment in the data as it is the most natural counterpart of employment in the model and is measured at the annual frequency in the data.

[21] In the model, employment is related to the own migration share. Hence, our approach also resembles a gravity equation regression in which we instrument for the origin income per capita with storm.

Figure 7: Identification of migration and investment elasticities and amenity-productivity ratio.

(a) Storms and capital depreciation shocks: employment CIR relative to income per capita

(b) Heat waves and prod.-amenity shocks: employment CIR relative to income per capita

(c) Storms and capital depreciation shocks: investment CIR relative to employment CIR

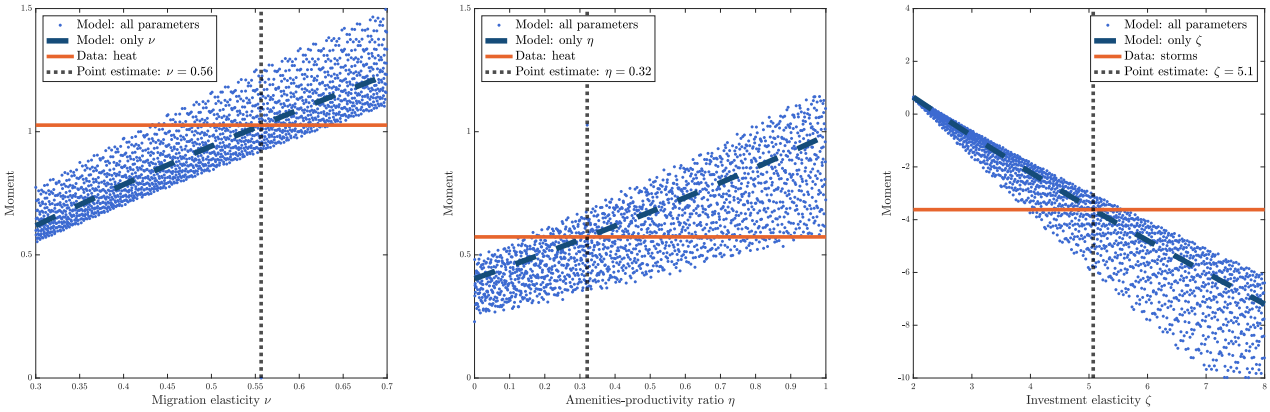

Note: Blue dots: 2,000 model simulations sequencing parameter vectors $\theta = (\nu, \eta, \zeta)$ using a Sobol sequence in the cube $[0.3, 0.7] \times [0, 1] \times [2, 8]$. Dashed dark blue line: moment in the model when only the parameter on the x-axis varies, holding other parameters at their point estimate. Horizontal solid orange line: moment in the data. Vertical dashed black line: parameter estimate.

confirms our global identification argument numerically.[22]

Panel 7(a) displays the cumulative response of employment relative to investment following a productivity-amenity shock. Each blue dot is the relative cumulative response in the model, for a given triplet of parameter values (ν, η, ζ). We order results by the migration elasticity ν on the x-axis to highlight our identification argument in a multivariate and univariate sense. The impact of ν on the relative cumulative response on the y-axis manifests clearly in the upward-sloping relationship visible in the scatterplot: on average, across all possible values (η, ζ), a higher value of ν increases the response of employment relative to income per capita (multivariate identification). The impact of the migration elasticity ν on the relative cumulative response is also visible in the upward-sloping relationship between the moment and the migration elasticity ν when we hold the other parameters (η, ζ) fixed at their point estimate (univariate identification). Panel 7(a) also reports the relative cumulative response in the data for storms in coastal counties.

Panel 7(b) depicts the cumulative response of employment relative to income per capita following a productivity-amenity shock on the y-axis. The x-axis represents the productivity-amenity ratio η. This ratio emerges visually as a key determinant of the response of income per capita relative to employment. We contrast the results from the model with the data following heat waves in warm counties.

Panel 7(c) depicts the cumulative response of investment relative to employment following a capital depreciation shock on the y-axis. The x-axis represents the investment elasticity ζ. The investment

[22] In order to be able to cover the parameter space efficiently, we aggregate counties into 100 clusters for this exercise. We choose these clusters with a k-means algorithm to group clusters based on latitude, longitude, population, income, and coastal status. Our results vary only slightly when we increase the number of clusters.

elasticity emerges visually as a key determinant of the response of investment relative to employment. We contrast the results from the model with the data following storms in coastal counties.

We estimate the migration elasticity to be $\nu = 0.56$. Consistently with our county-level specification, our value is somewhat above the value of 0.2 in the state-level specification in Caliendo et al. (2019). We estimate that amenities respond $\eta = 0.32$ times as much as productivity following heat waves. This relative response is somewhat larger than the average one in Cruz and Rossi-Hansberg (2023) for the entire world. The larger relative role of amenities in the context of the U.S. is consistent with production being better shielded from extreme heat through adaptation, such as air conditioning, than in developing nations. Our estimate of the investment elasticity $\zeta = 5.10$ implies adjustment costs that are less convex than quadratic, a common benchmark in the literature.

5.4 Damage functions

With the migration and investment elasticities in hand, we turn to estimating the damage functions for productivity, amenities, and capital depreciation χ_i, a_i, δ_i. We do so in two steps. In the first step, we estimate common economic damages from a given realization of storms $\Gamma^{\text{cap dep}}$ and heat waves Γ^{prod} using the cumulative impulse responses from Section 4.4. In the second step, we interact these damages from single events with local changes in the probability that these events occur as global mean temperatures rise, as shown in Figure 2.

In the first step, we estimate economic damages from a given realization of storms $\Gamma^{\text{cap dep}}$ and heat waves Γ^{prod} by matching the magnitude of the cumulative impulse responses. As in Section 4, we leverage the linearity of the FAME. It implies that the size of the shock is equal to $\Gamma^s = \frac{\text{CIR}_{10,v,s}}{\text{cir}_{10,v,s,\hat{\theta}}}$, where $\text{cir}_{10,v,s,\hat{\theta}}$ denotes the 10-year cumulative impulse response of variable v to a 1% shock to s (productivity-amenity or capital depreciation) for the estimates of the triplet $\hat{\theta}$ we obtained above.

For heat waves in warm counties, we target the income per capita response. Given that we match exactly the responses of employment relative to income per capita in Figure 7, we match exactly the cumulative response of employment and income per capita 10 years out. We estimate storm damages in coastal counties by targeting the cumulative impact of storms on employment 10 years out. Given that we match exactly the investment response relative to employment in Figure 7, we match exactly the cumulative investment response 10 years out.

In addition to matching exactly the cumulative response 10 years out, we ask whether the estimated model provides a plausible account of the time path of the impulse response function of targeted moments. Of course, our framework cannot be expected to match exactly the precise time path of income per capita, employment, and investment responses jointly for each extreme event. Nevertheless, Figure 8 displays impulse responses in the model and in the data for heat waves in warm counties.

Figure 8 displays the investment, employment, and income per capita impulse responses in the data (circles and dotted line) and in the model (solid line) following heat waves in warm counties. Because

Figure 8: Heat waves: impulse responses in model and in data.

(a) Income per capita (b) Employment (c) Investment

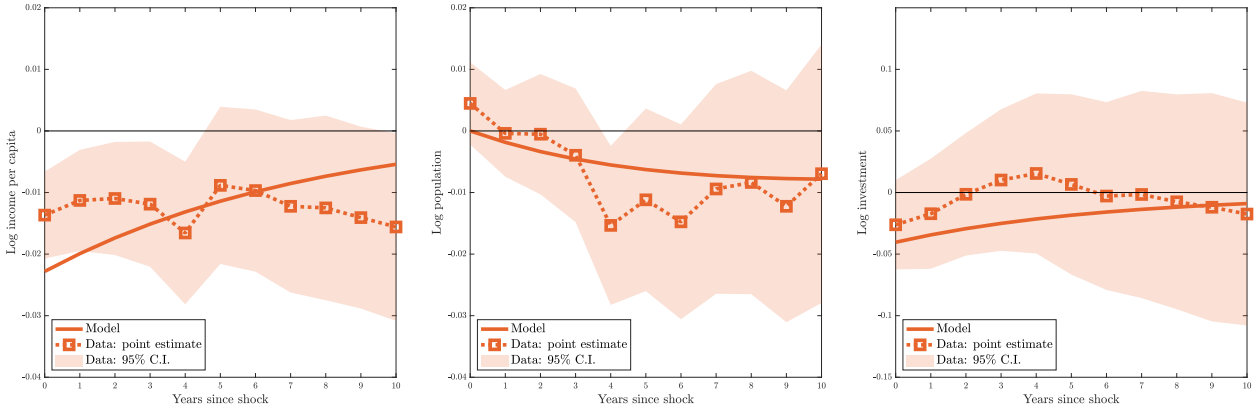

Note: Impulse responses for income per capita (a), employment (b), and investment (c) after a 1-in-20-years heat wave in a warm county. For (a) we use the response of wages, w_{it}, in the model and income per capita in the data. Solid line: model. Dashed line with circle markers: data point estimate. Shaded area: data 95% confidence band. The 10-year cumulative impulse responses for income per capita (a) and employment (b) are targeted. The impulse response for investment (c) is untargeted.

we match the 10-year cumulative response, the areas under the impulse response in the model and in the data match exactly. Figure 8 reveals that the model provides a reasonable account of the full time path of the response of income per capita, employment, and wages to heat waves. The untargeted response of investment is close to the data, too. For all three outcomes, the responses in the model lie within the 95% confidence interval around the empirical point estimates for nearly all horizons.

Our impulse response-matching exercise implies that a 1-in-20-years heat wave causes a $\Gamma^{\text{prod}} = 2\%$ negative productivity shock to a warm county, accompanied by a $\eta\Gamma^{\text{prod}} = 0.6\%$ reduction in local amenities. This impact is non-trivial. Yet, it is lower than the local effects estimated for locations in the entire world, including developing countries. For instance, Cruz and Rossi-Hansberg (2023) find that the productivity effect in the warmest locations of a 1°C increase in winter temperatures can exceed 15%.

Figure 9 displays the income per capita, employment, and investment impulse responses in the data (circles and dotted line) and in the model (solid line) following storms in coastal counties. Figure 8 reveals that the model provides a fairly good account of the full time path for employment and investment (within the 95% confidence interval for most horizons). The fit is less good for income per capita, where the model response is too quick relative to the data.[23]

Our impulse response-matching exercise implies that a 1-in-50-years storm causes a $\Gamma^{\text{cap dep}} = 30\%$ negative capital depreciation shock to a coastal county. This impact is substantial—it represents 4 years worth of baseline capital depreciation—and, to the best of our knowledge, is a new estimate to the literature at the county level. Our estimate is nearly identical to the one in Fried (2022) inferred from the

[23] As is common in macro models, matching the dynamics of impulse response functions is hard without adding ad-hoc adjustment costs that slow down income and investment responses (Christiano et al., 2018).

Figure 9: Storms: impulse responses model and in data.

(a) Income per capita (b) Employment (c) Investment

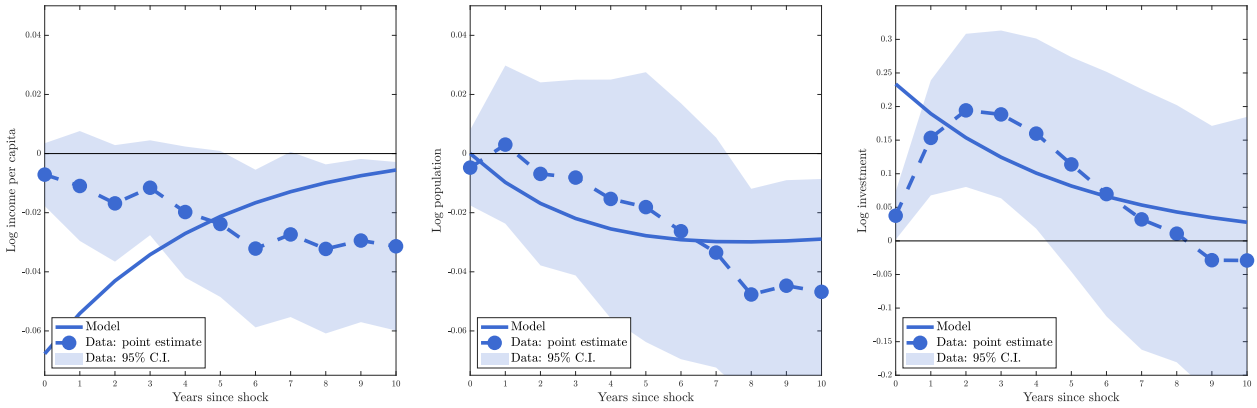

Note: Impulse responses for income per capita (a), employment (b), and investment (c) after a 1-in-50-years storm in a coastal county. For (c) we use the response of wages, w_{it}, in the model and income per capita in the data. Solid line: model. Dotted line with square markers: data point estimate. Shaded area: data 95% confidence band. The 10-year cumulative impulse response for income per capita (a), employment (b), and investment (c) are targeted.

amount of federal aid triggered by hurricanes, and comparable to the country-level estimates in Hsiang and Jina (2014) and Bakkensen and Barrage (2025).

We now turn to the second step of our estimation strategy. To construct damage functions that depend on global mean temperatures, we interact our estimates of shocks $(\Gamma^{\text{cap dep}}, \Gamma^{\text{prod}}, \eta\Gamma^{\text{prod}})$ with secular changes in the probability of the corresponding events. These changes are similar to those in Figure 2, but we construct trends location by location.

To estimate secular changes in the probability of extreme events for each location, we leverage our long-run historical data starting in 1901. We regress the change in the probability of an event $e \in \{\text{storm, heat}\}$, p^e_{it}, for each location i on changes in global mean temperatures T_t over years 1901-2019:

$$dp^e_{it} = \text{cst} + q^e_i \; dT_t + \varepsilon_{it}. \tag{15}$$

Equation (15) delivers a statistical downscaling, a well-established procedure in the climate science and economics literature (Cruz and Rossi-Hansberg, 2023) that projects the probability of local climatic events onto global mean temperature. We use the historical record to estimate this relationship in our main specification because of well-known limitations of global circulation models.[24] Nevertheless, we examine the robustness of our counterfactuals when we instead use multiple global circulation models to estimate the downscaling in (15).

[24]Climate models have difficulty producing empirically accurate distributions of extreme rain and wind, as these are outcomes that result from physical processes that occur at a much finer resolution than 0.5°×0.5° rasters used in leading global circulation models. For instance, Kim et al. (2020) shows that CMIP6 model ensembles predict extreme temperatures with over 5°C biases on the entire US East coast, the Pacific Northwest and in the US Midwest, in excess of +5°C. Similarly, Kim et al. (2020) show that CMIP6 ensembles exhibit extreme precipitation biases up to 50mm on the US East coast. Shen et al. (2022) highlights similar limitations for windspeed.

Figure 10: Damage functions from heat and storms in the United States.

(a) Change in log productivity

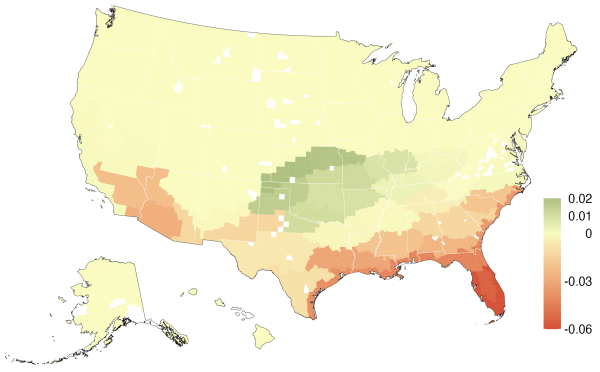

(b) Change in annual capital depreciation

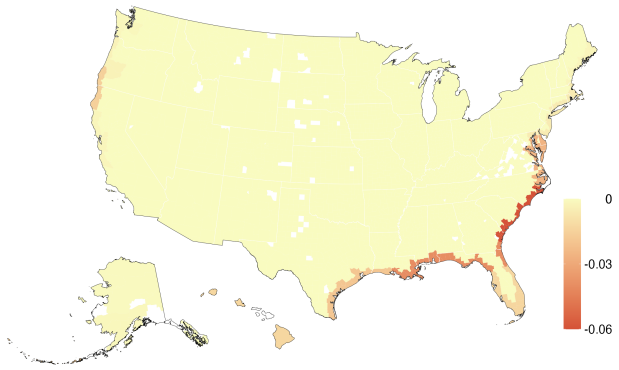

Note: Effect of a 1°C increase in global temperature on productivity and annual capital depreciation rates across counties in the U.S. Constructed according to equation (16). Panel (a): coefficients χ_i such that $d \log Z_{it} = \chi_i dT_t$. Panel (b): negative of coefficients δ_i such that $d\Delta_{it} = \delta_i dT_t$.

Finally, we construct damage functions according to:

$$\delta_i = \mathbb{1}\{i \text{ coastal}\} q_i^{\text{storm}} \Gamma^{\text{cap dep}}, \qquad \chi_i = \mathbb{1}\{i \text{ warm}\} q_i^{\text{heat}} \frac{\Gamma^{\text{prod}}}{\psi^{\text{prod}}}, \qquad a_i = \mathbb{1}\{i \text{ warm}\} q_i^{\text{heat}} \frac{\eta \Gamma^{\text{prod}}}{\psi^{\text{prod}}}, \tag{16}$$

where ψ^{prod} denotes the mean-reversion coefficient of productivity following heat-waves.[25]

Figure 10 maps our estimated damage functions, and Figure 23 in Appendix F.7 displays the underlying slopes p_i^e. Panel 10(a) shows the impact of a 1°C increase in global mean temperatures on productivity for every county in the U.S. The impact is highly heterogeneous across space. We find that southern Florida will experience productivity reductions in excess of 5% due to the rapidly rising occurrence of heat waves. For a 3°C warming scenario, this reduction compounds to more than a 15% reduction in productivity. Productivity losses of comparable magnitude are pervasive throughout the South of the U.S. Northern Texas and Oklahoma gain moderately, as our historical data shows that they experience a reduction in the frequency of heat waves. By construction, the change in amenities is proportional to the change in productivity and thus we omit the corresponding map.

Panel 10(b) shows the impact of a 1°C increase in global mean temperatures on capital depreciation for every county in the U.S. The impact is highly heterogeneous across space and only imperfectly correlated with the one for heat waves. Storms increase capital depreciation rates substantially in the South-Eastern Atlantic coast. In Louisiana and North and South Carolina, a 1°C increase in global temperature increases the capital depreciation rate by more than 4 p.p. This effect amounts to more than a 12 p.p. increase for a warming scenario of 3°C, more than doubling the baseline capital depreciation rate. These

[25] We divide by ψ^{prod} to cumulate lagged effects of heat waves and convert our estimate into the effect of a permanent rise in extreme heat exposure. In addition, to have sufficient statistical precision in practice, we construct 100 clusters of contiguous counties based on coastal status, annual mean temperature, population, and income, and estimate the slopes q_i^e at the cluster level.

capital depreciation effects are substantial, but affect a much smaller fraction of counties than heat waves. Through the lens of our structural model, we can compare their relative importance.

6 The impact of climate change in the U.S.

We start the economy in steady-state. We use 2025 as the year in which individuals learn the path of warming T_t^D and start reacting to it. We use a warming scenario T_t^D that increases temperatures by 3°C gradualy by 2100 and keep them constant afterwards.[26]

6.1 Aggregate damages from climate change

We uncover substantial effects of climate change on welfare. Figure 11(a) reports the impact of climate change on workers and capitalists in 2025 and 2100. In 2025, workers lose 2.8% in consumption-equivalent welfare on average. This impact represents an annual loss of consumption of more than $1,500 to the average resident of the U.S.[27] For comparison, estimates from the gains from trade for the U.S.—i.e. the benefits from moving from autarky to 2024 trade relations—are typically less than 3%.[28]

Crucially, these losses arise because of anticipations of future climate change. In our evaluation in 2025, climate change is just starting. Workers anticipate that climate conditions will worsen in the future, lowering productivity and amenities, depreciating capital, and ultimately affecting future real wages and the present value of future consumption streams, which are discounted at 2% annually. By 2100, climate change has largely materialized and is not discounted any longer. Thus, welfare losses to workers grow to 4.2% in consumption equivalent terms, or more than $2,500 out of current consumption expenditures.

Capitalists are, on average, initially less exposed to climate change. In 2025, their welfare loss is just above 1%. This average effect masks a considerable amount of heterogeneity, with large offsetting gains and losses across locations. In 2025, valuation effects in locations that expect to benefit from a future inflow of workers occur immediately, boosting capitalist welfare there. However, capitalist losses in locations at risk are largely driven by the depreciation of capital that occurs only in the distant future. This asymmetry implies that capitalist gains and losses closely balance in our quantification despite worsening capital depreciation rates in the coastal U.S. By 2100, welfare losses for capitalists grow to 4.9% in the aggregate as capital has had time to depreciate in the Southeast Atlantic coast by then. Welfare losses for capitalists grows more over time than welfare losses for workers because the stock of capital is immobile, while workers are mobile. Capitalists can adapt less.

The structure of the FAME allows us to efficiently construct confidence intervals around our baseline welfare results as described in Section 3.4. To construct these confidence intervals, we incorporate

[26] This path is consistent with the business-as-usual scenario of the IPCC and the slope of warming reported in Figure 2. Given the warming of 1°C in 2025 relative to pre-industrial temperatures, this warming scenario corresponds to 4°C warming relative to pre-industrial temperatures by 2100.

[27] The Bureau of Labor Statistics reports average annual expenditures of $61,334 in 2020.

[28] See for example Costinot and Rodríguez-Clare (2014).

Figure 11: Welfare impact of 3°C additional warming by 2100.

(a) Aggregates.

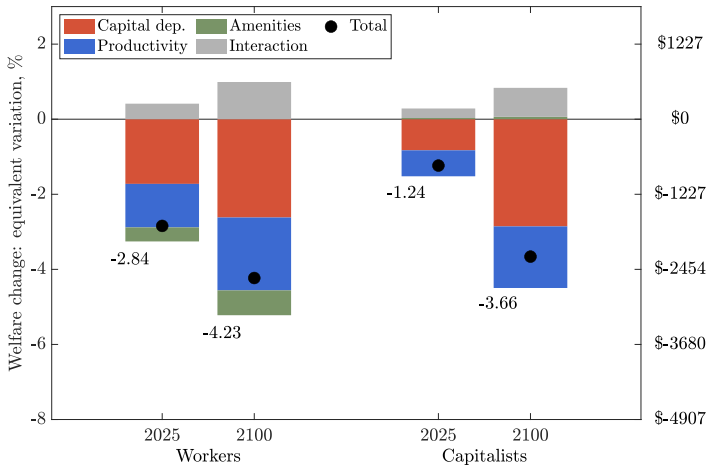

(b) 95% confidence intervals.

	Workers		Capitalists	
	2025	2100	2025	2100
Impact				
Total	-(4.2, 1.5)	-(5.6, 2.9)	(-5.7, 3.2)	-(3.9, 3.4)
Transition	-(2.8, 2.8)	-(4.2, 4.2)	(-5.9, 3.4)	-(4.2, 3.2)
Frequency				
Total	-(3.7, 2.0)	-(5.1, 3.4)	(-18.8, 16.3)	-(5.1, 2.2)
Transition	-(2.8, 2.8)	-(4.2, 4.2)	(-18.7, 16.2)	-(4.1, 3.2)
Both				
Total	-(4.6, 1.1)	-(6.0, 2.5)	(-21.3, 18.8)	-(5.5, 1.9)
Transition	-(2.8, 2.8)	-(4.2, 4.2)	(-21.2, 18.7)	-(4.4, 2.9)

Note: Panel (a): Aggregate welfare impact of a 3°C warming scenario between 2025 and 2100, with constant temperature after 2100. Welfare evaluated in 2025 and in 2100 separately for workers and capitalists. Left axis: equivalent variation per year, %. Right axis: 2025 dollars per year. Total: contribution of capital depreciation (orange), productivity (blue), amenities (green) and interaction (grey). Panel (b): 95% confidence intervals based on the Delta-method as described in Section 3.4. Impact: uncertainty associated with damage estimates $\Gamma^{\text{cap dep}}, \Gamma^{\text{prod}}$. Frequency: uncertainty associated with relationship between extreme event frequency and global mean temperature $q_i^{\text{storm}}, q_i^{\text{heat}}$. Transition: uncertainty associated with transition between initial and final steady-state. Total: additionally including uncertainty associated with final steady-state.

uncertainty around our estimated event study coefficients in Section 4, namely, $(\Gamma^{\text{cap dep}}, \Gamma^{\text{prod}})$, as well as uncertainty in the local changes in the frequency of extreme events with global mean temperatures $(p_i^{\text{storm}}, p_i^{\text{heat}})$.[29] Figure 11(b) indicates that our main conclusions for workers are robust to accounting for standard errors around the estimated damage functions (χ_i, a_i, and δ_i). The 95% confidence interval around aggregate worker welfare losses in 2025 excludes any losses smaller than 1%, and is almost entirely driven by uncertainty around the final steady-state around which we expand the FAME. For capitalists, we obtained more nuanced results. Because of offsetting gains in inland locations and losses in coastal locations, capitalist welfare in 2025 is more sensitive to the speed of the transition which varies with damage functions. The resulting confidence interval ranges from -5.7% to 3.2% when we incorporate uncertainty due to the impact of extreme events. When we additionally incorporate uncertainty due to the estimated relationship between extreme event frequency and global mean temperature, the confidence interval widens considerably. This large uncertainty is natural since it includes variance around the increase in the frequency of storms in each group of counties. By 2100, however, this uncertainty largely resolves and capitalist welfare losses are more precisely estimated.

6.2 The spatial distribution of climate damages

How unequally distributed are the welfare losses from climate change? Figure 12 depicts the spatial distribution of the impact of climate change on welfare and allocations, and Table 1, Appendix G, reports

[29] For simplicity, we hold the elasticities ν, ζ, and η fixed at their point estimates.

the corresponding summary statistics. Panel 12(a) displays 2025 welfare losses to workers in each county. Counties in red are counties that are lose, and counties in green are counties that gain.

We find that workers in almost all counties lose from climate change in 2025. Workers in the South-East of the U.S. are particularly exposed. The combination of more frequent heat waves and destructive storms on the coast implies that residents of coastal Louisiana lose up to 9% ($5,490 annually) because of climate change in 2025. Losses above 3% in 2025 ($1,830 annually) occur in Texas, Florida, and North and South Carolina. By 2100, the spatial distribution of welfare losses from climate change is similar to the one in 2025, as evidenced by Figure 12(c). The overall magnitude, however, is larger. Residents of coastal counties in Louisiana and North and South Carolina are 9% worse off in 2100.

Capitalists experience much more unequal impacts from climate change than workers, as shown in panel 12(b). Owners of capital in coastal Louisiana, Georgia, and North and South Carolina experience welfare losses between 24% and 49% in consumption-equivalent welfare in 2025 because of climate change, while capitalists gain in most inland counties. By 2100, capitalists in coastal areas can lose between 46% and 93% in consumption-equivalent welfare, while capitalists in inland counties can gain more than 50%. The standard deviation of welfare losses for capitalists in 2100 (25 p.p.) is much larger than for workers (1 p.p.), as shown in Table 1, Appendix G.

Welfare losses to capitalists are more unequally distributed than those for workers because capital cannot move, while workers can. Migration provides an important adaptation strategy that spreads losses from climate change more equally across workers. Owners of an immobile capital stock do not have that option. As a group, capitalists can only let the capital stock depreciate in locations that experience adverse climate change, and invest anew in the places where climate change is more benign.

We find that migration responds substantially to climate change. Panel 12(e) reveals that Southeastern states that are heavily exposed to extreme heat and storms in the South-East can lose more than half of their population by 2100. These workers move to Midwestern and Northern counties that are shielded from these adverse effects, some of which grow by over 25%. These population movements reflect the relative effects of climate change across space. As workers reallocate, the rental rate of capital adjusts accordingly, imposing additional losses to capitalists in locations that lose employment. Over time, changes in the local stock of capital are highly correlated with population movements, as shown in panel 12(f). Capital is no longer profitable once workers have left, and capitalists in Northern locations invest heavily to accommodate higher demand for capital and housing.

Our results highlight that climate damages—and the ensuing reallocation of economic activity—are substantial. Critically, we find large economic damages because we constrain the model to match our empirical event study results using a standard rate of time preference of 2%. We analyze how discounting affects climate damages in the 'Discount rate' section of Table 1, Appendix G. Consistent with the climate change literature,[30] we find that lower discount rates increase welfare losses from climate change

[30] See, for example, Heal (2017) for a discussion of discount rates in the climate change literature.

Figure 12: Impact of 3°C additional warming by 2100.

(a) Worker welfare in 2025

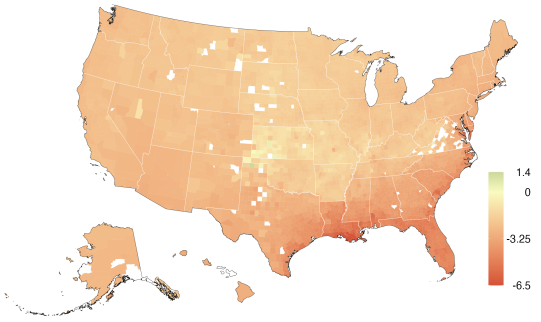

(b) Capitalist welfare in 2025

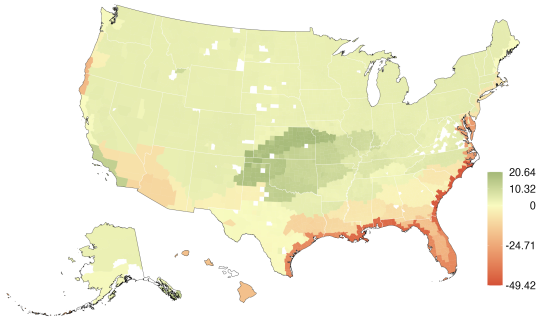

(c) Worker welfare in 2100

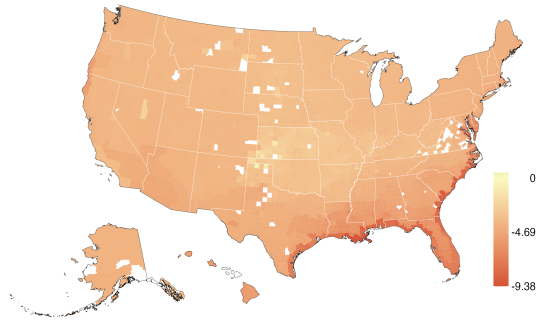

(d) Capitalist welfare in 2100

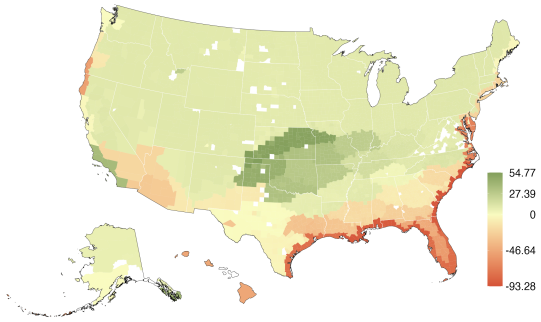

(e) Population change in 2100

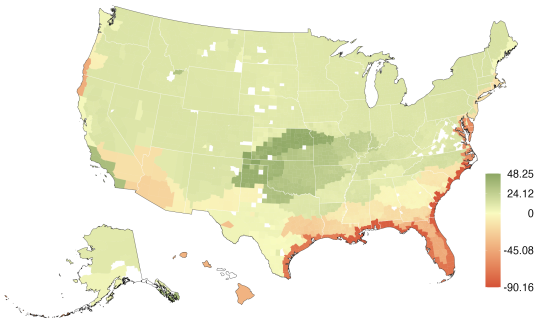

(f) Capital stock change in 2100

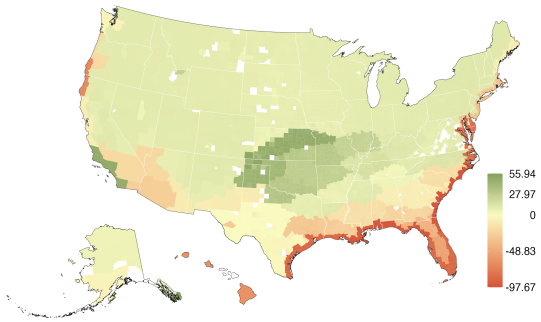

Note: Panel (a): worker welfare impact of a 3°C warming scenario, by county in 2025. Panel (b): capitalist welfare by county in 2025. Panel (c): worker welfare in 2100 by county. Panel (d): capitalist welfare in 2100 by county. Panel (e): 2025-2100 population change in percent. Panel (f): 2025-2100 capital stock change in percent.

for workers and capitalists in 2025 since climate damages remain back-loaded then.[31]

Having established the magnitude of climate damages, we now study the role of anticipation and adaptation using three distinct counterfactual exercises.

6.3 Capital depreciation and temperature

Our first exercise highlights the role of anticipation in forward-looking capital investment decisions. Introducing anticipation through the FAME lets us study the role of climate change on capital depreciation. How large is this novel role of anticipation and capital depreciation relative to the role of heat waves? We answer this question with a welfare decomposition.

Figure 11(a) and Table 1, Appendix G, reveal that the impact of capital depreciation is substantial. Despite affecting only a small subset of locations, repeated capital destruction due to rising storm activity in coastal counties accounts for 61% of aggregate welfare losses to workers. Temperature and its interaction with capital depreciation accounts for the remaining 39%.

The capital depreciation channel also accounts for 84% of the reduction of the capital stock due to climate change in the U.S. This effect reflects both the direct depreciation effect as well as reduced incentives to invest in counties that have high capital depreciation rates. Temperature and its interaction with capital depreciation is responsible for the remaining 16% of the reduction in the capital stock. As productivity drops because of extreme heat, capital becomes less valuable and investment falls. The effects of heat waves can be further split into productivity and amenity effects. Figure 11(a) and Table 1 indicate that productivity losses are nearly three times more important than amenity losses for worker welfare in 2025 and 2100.

In Table 1, Appendix G, and Appendix F.6, we assess whether the role of capital depreciation and temperature depends on our estimation procedure. The 'With cold waves' section shows that incorporating the effects of extreme cold does not affect our results meaningfully. The 'Climate models' section highlights that forecasting temperature trends using a suite of global circulation models leads to similar conclusions to our baseline. We also re-estimate our model using empirical impulse response functions from non-residualized extreme events in the 'Raw events' section. Our results become starker in that case: worker welfare losses are similar to our baseline with residualized extreme events, but they are almost entirely accounted for by capital depreciation due to coastal storms.

6.4 Anticipation

In a second exercise, we shut down climate change anticipation by either workers or capitalists. In this counterfactual, workers or capitalists experience the effect of the current and past changes in temperatures

[31] By 2100, climate change has mostly already occurred in the simulation and the discount rate does not affect worker welfare that much anymore. For capitalists, the lower cost of funding implied by a lower discount rate yields smaller losses, and even gains, from climate change by 2100.

but they believe that future temperatures will remain the same for an extended period of time.

We shut down two types of anticipatory behavior. The first one consists in adjusting behavior today to the increase in temperature from today onward We call this short-run anticipation, and shut it down by setting to zero the partial time derivative in the FAME. The second one consists in adjusting behavior today to expectations of permanent changes. We call this long-run anticipation, and capture it by using the FAME around the initial steady-state rather than the final steady-state. Households then adjust behavior as if experienced temperature changes were temporary.

We find that anticipation leads to substantial mobility. When individuals fail to anticipate future climate change, mobility falls. Figure 13(a) reveals that the gap with the baseline scenario is largest close to 2040. By 2050, the standard deviation of population changes is 5 p.p. lower when neither workers nor capitalists anticipate long-run climate change and, as a result, exhibit only limited behavioral adjustment.

Anticipation increases mobility because climate change builds up slowly over time. Individuals who anticipate future climate internalize that their location will become worse than it is today. As a result, they move out more rapidly. Crucially, the anticipation of workers and capitalists reinforce each other: when capitalists do not anticipate future climate change, they keep investing in locations that will deteriorate in the future. This excess investment further keeps workers in place through a larger capital stock, higher nominal wages, and lower housing prices.

Since the future climate is correlated with the current climate, the locations in which anticipation leads to the largest mobility gaps are also those where climate change has the largest effect in the baseline scenario. Panel 13(c) highlights that the South-East of the U.S. loses less population when workers and capitalists fail to anticipate future climate. In Louisiana, Florida, and coastal counties in North and South Carolina, these effects are large and can offset as much as one quarter of the baseline decline in 2050.

Without anticipation, worker welfare is more unequally distributed than with anticipation. Individuals in locations that suffer most from climate change experience larger losses without anticipation because they fail to pre-emptively out-migrate or divest and are continuously surprised by a worsening climate. Panel 13(d) shows that workers in in Texas, Louisiana and Florida who do not anticipate climate lose between an additional 1.5 p.p. and 3 p.p. of welfare by 2050. Across the U.S., the standard deviation of worker welfare is 0.3 p.p. higher without anticipations, 23% above the baseline warming scenario. Because capital stocks cannot move and workers move less without anticipation, capitalist tend to lose less from climate change in the most affected locations without anticipation. However, despite these changes in the dispersion of losses, aggregate welfare of workers and capitalists are largely unchanged by the lack of anticipation. For workers, the additional losses in exposed locations are offset by relative gains in non-exposed counties. For capitalists, the opposite is true. We summarize these results in the 'No Anticipation' section of Table 1, Appendix G.

Figure 13: The impact of shutting down anticipations on mobility and welfare.

(a) Population change dispersion relative to baseline.

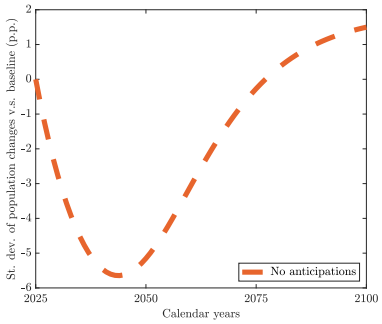

(b) Capital change dispersion relative to baseline.

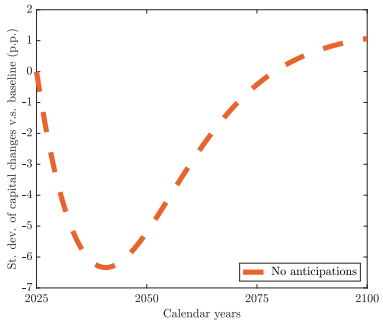

(c) Relative population change in 2050 (p.p.).

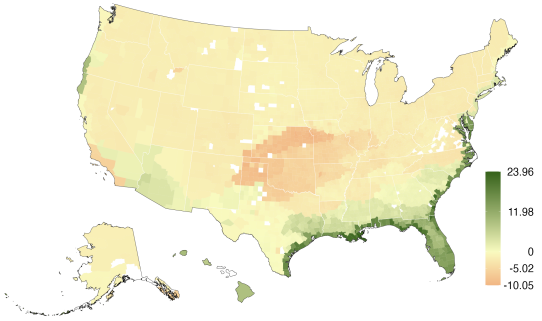

(d) Relative worker welfare change in 2050 (p.p.).

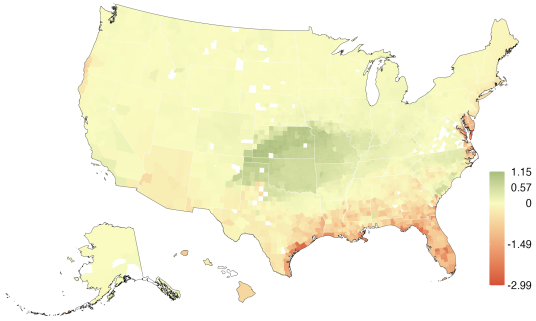

(e) Relative capital change in 2050 (p.p.).

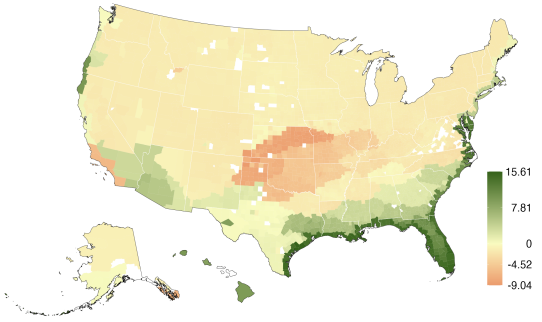

(f) Relative capitalist welfare change in 2050 (p.p.).

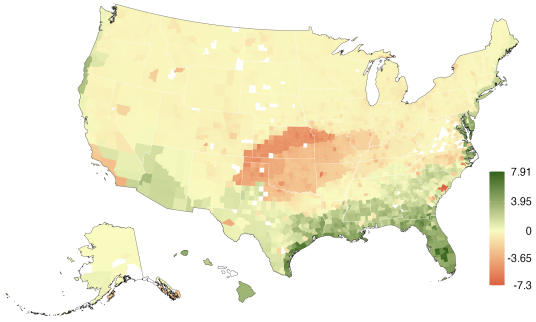

Note: Panel (a): dispersion of population changes relative to baseline. Panel (b): dispersion of capital stocks relative to baseline. Panel (c): change in population in 2050 by county relative to baseline. Panel (d): change in worker welfare in 2050 by county relative to baseline. Panel (e): change in capital sock in 2050 by county relative to baseline. Panel (f): change in capitalist welfare in 2050 by county relative to baseline.

6.5 Adaptation

The third exercise highlights the role of adaptation through migration. We evaluate the impact of global warming when we shut down migration completely, i.e. $\mu = 0$.[32] We present our main results graphically in the main text, and summarize its conclusion in the 'No adaptation' section of Table 1, Appendix G.

[32] We do not consider a counterfactual with fixed capital because we would have to assume away damages to the capital stock, which are important both quantitatively and in determining the geography of losses from climate change.

Figure 14: The impact of shutting down migration.

(a) Relative worker welfare change in 2025 (p.p.)

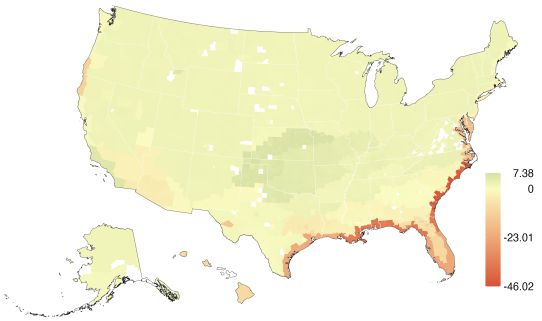

(b) Relative capitalist welfare change in 2025 (p.p.)

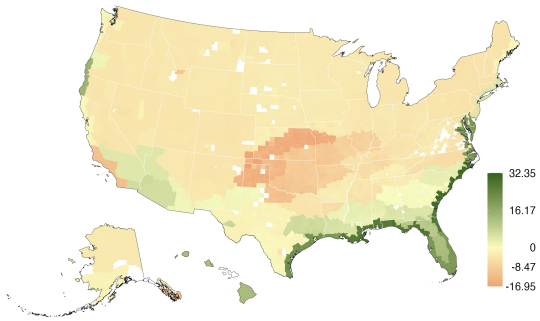

(c) Aggregate worker welfare over time

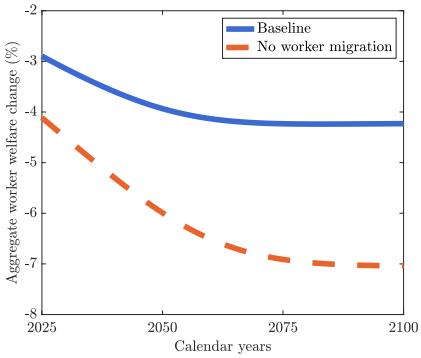

(d) Aggregate capitalist welfare over time

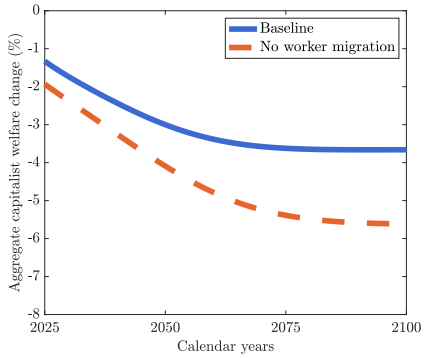

Note: Panels (a) and (b): worker (a) and capitalist (b) welfare change without migration relative to welfare change with migration. Panels (c) and (d): aggregate worker (c) and capitalist (d) welfare over time, with migration (solid blue line) and without migration (dashed orange line).

Aggregate welfare losses for workers rise to 4% in 2025 without migration. Local losses become more spatially concentrated. Figure 14(a) reveals that workers in coastal counties in the South-East lose an additional 23 p.p. to 46 p.p. in welfare terms in 2025 when they cannot move. Welfare losses in these areas in 2025 range from 25% to 50% ($30,669 per year) without migration. Across the U.S., the standard deviation of welfare losses of workers rises to 9.4 p.p. from 0.8 p.p. in 2025.

Capitalists benefit when workers remain in place. Abundant labor raises the return to capital. Panel 14(b) shows that relative capitalists gains in 2025 are the mirror image of worker losses. Overall, the dispersion of capitalist welfare losses drops from 10.1 p.p. to 3.1 p.p. when migration is shut down.

Using the final steady-state as a point of expansion implies that we capture the private benefits from migration. By contrast, a standard envelope argument implies that the private benefits from migration drop out when using the initial steady-state as a point of expansion.[33] As a result, Panel 14(c) shows that the ability to migrate offsets over one quarter of the aggregate welfare losses of workers in 2025, and

[33]In both cases, general equilibrium adjustments and reallocation of workers across locations can lead to additional aggregate welfare effects of migration depending on the specific geographic exposure of the economy to shocks. For instance, if climate change pushes workers out of locations that are less desirable to begin with, then migration can offset some of the aggregate welfare losses of climate change.

over 40% in 2100. While coastal gains and inland losses of capitalists nearly offset initially, Panel 14(d) indicates that the lack of worker migration is ultimately detrimental to capitalists in the aggregate. The lack of migration traps workers in locations where it is expensive to maintain a high capital stock due to the frequent storms.

7 Conclusion

We have proposed a quantitative dynamic spatial assessment model of the U.S. economy. The model features forward-looking migration and capital investment decisions and can be quantified at the county level, namely, for the 3,143 counties in the U.S. economy. Importantly, because of the methodological advances we employ to solve for the dynamic equilibrium of the model, a numerical solution can be computed efficiently. We leverage this feature to structurally estimate the migration and investment elasticities, two key parameters that determine adaptation responses in the model. To quantify the damage functions that map global temperature increases with increases in local capital depreciation rates, amenities, and productivity, we use an extensive dataset of daily precipitation, windspeed, and temperatures since 1900 at the county level. This data, together with economic information at the county level, allowed us to estimate reduced-form reaction functions on several economic outcomes. We choose migration and investment elasticities, as well as damage functions, that make the model match this reduced form evidence. The resulting quantified model yields damages from a 3°C increase in average world surface temperatures that are more than twice as large as what alternative models without an effect on capital depreciation yield for the U.S. (e.g. Cruz and Rossi-Hansberg, 2023).

Using this framework we reach three distinct conclusions. First, accounting for the effect of temperature on capital depreciation, through the impact of more frequent storms, is essential to obtain more accurate estimates of the welfare losses of climate change. Second, anticipation has small average effects on welfare but leads to large increases in migration flows, and large changes in the geography of investment, as workers and capitalists correctly anticipate the persistence of climate damages in particular regions. Finally, in the U.S., adaptation through migration reduces the losses from climate change for workers by more than a quarter. It leads to substantial reductions in the dispersion of worker losses, but to large increases in the dispersion of the losses for capitalists; worker movements increase the losses in the value of capital at locations harmed by climate change.

Inevitably, our analysis abstracts from a number of potentially important mechanisms. One of them is costly trade in goods and heterogeneous climate effects by sector. Another is the differential effect temperature increases can have on people with heterogeneous skills, incomes, or assets. Finally, it is essential to incorporate risk and account for the uncertainty in climate predictions. To do so, we need to rely on second rather than first-order approximations of the "Master Equation". This methodology has also been developed by Bilal (2023) and we plan to use it to study the importance and implications of

climate risk in subsequent work.

References

Bakkensen, Laura A and Barrage, Lint (June 2025). "Climate Shocks, Cyclones and Economic Growth: Bridging the Micro-Macro Gap". *The Economic Journal*, ueaf050.

Balboni, Clare (2021). "In Harm's Way? Infrastructure Investments and the Persistence of Coastal Cities". *Working Paper*.

Bilal, Adrien (2023). "Solving Heterogeneous Agent Models with the Master Equation". *NBER Working Paper 31103*.

Blanchard, Olivier Jean and Kahn, Charles M. (1980). "The Solution of Linear Difference Models under Rational Expectations". *Econometrica* 48.5, pp. 1305–1311. (Visited on 08/15/2025).

Caliendo, Lorenzo, Dvorkin, Maximiliano, and Parro, Fernando (2019). "Trade and Labor Market Dynamics: General Equilibrium Analysis of the China Trade Shock". *Econometrica* 87.3, pp. 741–835.

Cardaliaguet, Pierre, Delarue, Francois, Lasry, Jean-Michel, and Lions, Pierre-Louis (2019). *The Master Equation and the Convergence Problem in Mean Field Games*. ISBN: 9780691190709.

Christiano, Lawrence J., Eichenbaum, Martin S., and Trabandt, Mathias (2018). "On DSGE Models". *Journal of Economic Perspectives* 32.3, 113–40.

Conte, Bruno, Desmet, Klaus, and Rossi-Hansberg, Esteban (2022). *On the Geographic Implications of Carbon Taxes*. Working Paper 30678. National Bureau of Economic Research.

Costinot, Arnaud, Donaldson, Dave, and Smith, Cory (2016). "Evolving Comparative Advantage and the Impact of Climate Change in Agricultural Markets: Evidence from 1.7 Million Fields around the World". *Journal of Political Economy* 124.1, pp. 205–248.

Costinot, Arnaud and Rodríguez-Clare, Andrés (2014). "Chapter 4 - Trade Theory with Numbers: Quantifying the Consequences of Globalization". In: *Handbook of International Economics*. Ed. by Gita Gopinath, Elhanan Helpman, and Kenneth Rogoff. Vol. 4. Handbook of International Economics. Elsevier, pp. 197–261.

Courtier, P., Thépaut, J.-N., and Hollingsworth, A. (July 1994). "A Strategy for Operational Implementation of 4D-Var, Using an Incremental Approach". *Quarterly Journal of the Royal Meteorological Society* 120.519, pp. 1367–1387.

Cram, et al. (July 2015). "The International Surface Pressure Databank Version 2". *Geoscience Data Journal* 2.1, pp. 31–46.

Cruz, José-Luis and Rossi-Hansberg, Esteban (2023). "The Economic Geography of Global Warming". *Review of Economic Studies*, forthcoming.

Cruz, José-Luis (2021). "Global Warming and Labor Market Reallocation". *Working Paper*.

Cucchi, et al. (Sept. 8, 2020). "WFDE5: Bias-Adjusted ERA5 Reanalysis Data for Impact Studies". *Earth System Science Data* 12.3, pp. 2097–2120.

Davis, Morris A., Larson, William D., Oliner, Stephen D., and Shui, Jessica (2021). "The price of residential land for counties, ZIP codes, and census tracts in the United States". *Journal of Monetary Economics* 118, pp. 413–431.

Davis, Morris A. and Ortalo-Magné, François (2011). "Household expenditures, wages, rents". *Review of Economic Dynamics* 14.2, pp. 248–261.

Dell, Melissa, Jones, Benjamin F., and Olken, Benjamin A. (2012). "Temperature Shocks and Economic Growth: Evidence from the Last Half Century". *American Economic Journal: Macroeconomics* 4.3, pp. 66–95.

— (2014). "What Do We Learn from the Weather? The New Climate–Economy Literature". *Journal of Economic Literature* 52.3, pp. 740–798.

Deryugina, Tatyana (2013). "The Role of Transfer Payments in Mitigating Shocks: Evidence from the Impact of Hurricanes". *SSRN Working Paper*.

Deschênes, Olivier and Greenstone, Michael (2011). "Climate Change, Mortality, and Adaptation: Evidence from Annual Fluctuations in Weather in the US". *American Economic Journal: Applied Economics* 3.4, pp. 152–85.

Desmet, Klaus, Kopp, Robert E., Kulp, Scott A., Nagy, Dávid Krisztián, Oppenheimer, Michael, Rossi-Hansberg, Esteban, and Strauss, Benjamin H. (2021). "Evaluating the Economic Cost of Coastal Flooding". *American Economic Journal: Macroeconomics* 13.2, pp. 444–86.

Desmet, Klaus, Nagy, Dávid Krisztián, and Rossi-Hansberg, Esteban (2018). "The Geography of Development". *Journal of Political Economy* 126.3, pp. 903–983.

Desmet, Klaus and Rossi-Hansberg, Esteban (2015). "On the Spatial Economic Impact of Global Warming". *Journal of Urban Economics* 88, pp. 16 –37.

Fried, Stephie (2022). "Seawalls and stilts: A quantitative macro study of climate adaptation". *The Review of Economic Studies* 89.6, pp. 3303–3344.

Haan, Wouter J. Den and Marcet, Albert (1994). "Accuracy in Simulations". *The Review of Economic Studies* 61.1, pp. 3–17. (Visited on 10/15/2025).

Harris, et al. (Mar. 15, 2014). "Updated High-Resolution Grids of Monthly Climatic Observations - the CRU TS3.10 Dataset: Updated High-Resolution Grids of Monthly Climatic Observations". *International Journal of Climatology* 34.3, pp. 623–642.

— (Apr. 3, 2020). "Version 4 of the CRU TS Monthly High-Resolution Gridded Multivariate Climate Dataset". *Scientific Data* 7.1, p. 109.

Heal, Geoffrey (2017). "The Economics of the Climate". *Journal of Economic Literature* 55.3, pp. 1046–63.

Hersbach, et al. (July 2020). "The ERA5 Global Reanalysis". *Quarterly Journal of the Royal Meteorological Society* 146.730, pp. 1999–2049.

Hsiang, Solomon M and Jina, Amir S (2014). "The Causal Effect of Environmental Catastrophe on Long-Run Economic Growth: Evidence From 6,700 Cyclones". *National Bureau of Economic Research Working Paper 20352*.

IPCC (2022). "Climate Change 2022: Impacts, Adaptation and Vulnerability". *Cambridge University Press*, pp. 37–118.

Kim, Hyungjun (June 1, 2017). *Global Soil Wetness Project Phase 3 Atmospheric Boundary Conditions (Experiment 1)*.

Kim, Yeon-Hee, Min, Seung-Ki, Zhang, Xuebin, Sillmann, Jana, and Sandstad, Marit (2020). "Evaluation of the CMIP6 multi-model ensemble for climate extreme indices". *Weather and Climate Extremes* 29, p. 100269.

Kleinman, Benny, Liu, Ernest, and Redding, Stephen J. (2023). "Dynamic Spatial General Equilibrium". *Econometrica* 91.2, pp. 385 –424.

Klink, Katherine (1999). "Trends in mean monthly maximum and minimum surface wind speeds in the coterminous United States, 1961-1990". *Climate Research* 13.3, pp. 193–205.

Krusell, Per and Smith Anthony A, Jr. (2022). *Climate Change Around the World*. Working Paper 30338. National Bureau of Economic Research.

Lange, et al. (May 5, 2021a). *WFDE5 over Land Merged with ERA5 over the Ocean (W5E5 v2.0)*. Version 2.0.

Lange, Stefan (July 17, 2019). "Trend-Preserving Bias Adjustment and Statistical Downscaling with ISIMIP3BASD (v1.0)". *Geoscientific Model Development* 12.7, pp. 3055–3070.

— (Apr. 14, 2021b). *ISIMIP3BASD*. Version 2.5.0. Zenodo.

Leduc, Sylvain and Wilson, Daniel J. (2023). "Climate Change and the Geography of the U.S. Economy". *Working Paper*.

Mengel, Matthias, Treu, Simon, Lange, Stefan, and Frieler, Katja (Aug. 20, 2021). "ATTRICI v1.1 – Counterfactual Climate for Impact Attribution". *Geoscientific Model Development* 14.8, pp. 5269–5284.

Nath, Ishan (2022). "Climate Change, The Food Problem, and the Challenge of Adaptation through Sectoral Reallocation". *Working Paper*.

New, M, Lister, D, Hulme, M, and Makin, I (2002). "A High-Resolution Data Set of Surface Climate over Global Land Areas". *Climate Research* 21, pp. 1–25.

Phan, Toan and Schwartzman, Felipe (2023). "Climate Defaults and Financial Adaptation". *FRBR Working Paper*.

Rayner, N. A. (2003). "Global Analyses of Sea Surface Temperature, Sea Ice, and Night Marine Air Temperature since the Late Nineteenth Century". *Journal of Geophysical Research* 108.D14, p. 4407.

Reiter, Michael (2009). "Solving heterogeneous-agent models by projection and perturbation". *Journal of Economic Dynamics and Control* 33.3, pp. 649–665.

Rennert, Kevin, Errickson, Frank, Prest, Brian C., Rennels, Lisa, Newell, Richard G., Pizer, William, Kingdon, Cora, Wingenroth, Jordan, Cooke, Roger, Parthum, Bryan, et al. (2022). "Comprehensive evidence implies a higher social cost of CO2". *Nature* 610.7933, pp. 687–692.

Roth Tran, Brigitte and Wilson, Daniel (2023). "The Local Economic Impact of Natural Disasters". *FRBSF Working Paper*.

Rudik, Ivan, Lyn, Gary, Tan, Weiliang, and Ortiz-Bobea, Ariel (2022). "The Economic Effects of Climate Change in Dynamic Spatial Equilibrium".

Santos, Manuel S. (2000). "Accuracy of Numerical Solutions Using the Euler Equation Residuals". *Econometrica* 68.6, pp. 1377–1402. (Visited on 10/15/2025).

Schneider, et al. (Jan. 2014). "GPCC's New Land Surface Precipitation Climatology Based on Quality-Controlled in Situ Data and Its Role in Quantifying the Global Water Cycle". *Theoretical and Applied Climatology* 115.1-2, pp. 15–40.

— (2018). *GPCC Full Data Monthly Version 2018.0 at 0.5°: Monthly Land-Surface Precipitation from Rain-Gauges Built on GTS-based and Historic Data: Gridded Monthly Totals*. gzip compressed NetCDF. Version 2018.

Shen, Cheng, Zha, Jinlin, Li, Zhibo, Azorin-Molina, Cesar, Deng, Kaiqiang, Minola, Lorenzo, and Chen, Deliang (2022). "Evaluation of global terrestrial near-surface wind speed simulated by CMIP6 models and their future projections". *Annals of the New York Academy of Sciences* 1518.1, pp. 249–263.

Yoshimura, Kei and Kanamitsu, Masao (Aug. 1, 2008). "Dynamical Global Downscaling of Global Reanalysis". *Monthly Weather Review* 136.8, pp. 2983–2998.

Online Appendix

A Setup

A.1 Static equilibrium

We solve for equilibrium prices and quantities as functions of the local capital stock K_{it} and local number of workers N_{it}. Combining labor demand in final good and building production, we obtain $\varpi\alpha\frac{B_{it}}{N_{it}^B} = (1-\alpha)\frac{S_{it}}{N_{it}^P}$. Housing demand rewrites $\beta(1-\alpha)N_{it}\frac{S_{it}}{N_{it}^P} = \alpha H_{it}$.

We look for shares x, y such that

$$N_{it}^P = xN_{it} \quad , \quad H_{it} = yB_{it} \tag{17}$$

and so $N_{it}^B = (1-x)N_{it}$ and $S_{it} = (1-y)B_{it}$. Substituting into the previous equations, we obtain $\frac{\varpi\alpha}{1-\alpha} = \frac{(1-y)(1-x)}{x}$ and $\frac{\beta(1-\alpha)}{\alpha} = \frac{xy}{1-y}$. These two equations imply[34]

$$x = \frac{(1-\alpha)(1-\varpi\beta)}{\alpha\varpi + (1-\alpha)} \quad , \quad y = \beta\frac{(1-\alpha)+\alpha\varpi}{\alpha+(1-\alpha)\beta} \quad , \quad 1-y = \alpha\frac{1-\beta\varpi}{\alpha+(1-\alpha)\beta}. \tag{18}$$

Using these shares, we express the wage and the rental rate as

$$w_{it} = (1-\alpha)\alpha^{\alpha}\Xi^{-\alpha}Z_{it}(B_{it}/N_{it})^{\alpha} \quad , \quad r_{it} = \alpha^{\alpha}\Xi^{1-\alpha}Z_{it}(B_{it}/N_{it})^{-(1-\alpha)}, \tag{19}$$

where $\Xi = (1-\alpha)\frac{\alpha+(1-\alpha)\beta}{\alpha\varpi+(1-\alpha)}$. Before proceeding, it is useful to substitute out buildings and express prices in terms of capital:

$$w_{it} = w_{i0}Z_{it}L_i^{\omega\alpha}(K_{it}^{1-\omega-\varpi}N_{it}^{\varpi-1})^{\alpha} \quad , \quad r_{it} = r_{i0}Z_{it}L_i^{-\omega(1-\alpha)}(K_{it}^{1-\omega-\varpi}N_{it}^{\varpi-1})^{-(1-\alpha)},$$

where $w_{i0} = (1-\alpha)\alpha^{\alpha}\Xi^{-\alpha}(1-x)^{\varpi\alpha}$, $r_{i0} = \alpha^{\alpha}\Xi^{1-\alpha}(1-x)^{-(1-\alpha)\varpi}$.

We now solve for the rental rate of capital:

$$\begin{aligned}
R_{K,it} &= (1-\omega-\varpi)(1-x)^{\varpi}K_{it}^{-(\omega+\varpi)}L_i^{\omega}N_{it}^{\varpi}r_{it} \\
&= (1-\omega-\varpi)\alpha^{\alpha}\Xi^{1-\alpha}(1-x)^{\alpha\varpi}Z_{it}L_i^{\omega\alpha}K_{it}^{-\phi}N_{it}^{1-\alpha+\alpha\varpi} \\
&= \underbrace{(1-\omega-\varpi)\alpha^{\alpha}\Xi^{1-\alpha}(1-x)^{\alpha\varpi}Z_iL_i^{\omega\alpha}}_{\equiv R_{0i}}e^{\chi_{it}}K_{it}^{-\phi}N_{it}^{\psi} \\
&= R_{0i}e^{\chi_{it}}K_{it}^{-\phi}N_{it}^{\psi} \\
&\equiv R_i(\chi_{it}, K_{it}, N_{it}),
\end{aligned}$$

[34] Multiplying both equations leads to $y(1-x) = \varpi\beta$ which can then be substituted into either of the equations.

where $\phi = \omega + \varpi + (1-\omega-\varpi)(1-\alpha)$ and $\psi = 1-\alpha+\alpha\varpi$. Turning to worker consumption (the real wage) in location i, we obtain:

$$\begin{aligned}
C_{it} &= \frac{w_{it}}{r_{it}^{\beta}} \\
&= \frac{(1-\alpha)\alpha^{\alpha}\Xi^{-\alpha}(1-x)^{\varpi\alpha}Z_{it}L_i^{\omega\alpha}(K_{it}^{1-\omega-\varpi}N_{it}^{\varpi-1})^{\alpha}}{\left[\alpha^{\alpha}\Xi^{1-\alpha}(1-x)^{-(1-\alpha)\varpi}Z_{it}L_i^{-\omega(1-\alpha)}(K_{it}^{1-\omega-\varpi}N_{it}^{\varpi-1})^{-(1-\alpha)}\right]^{\beta}} \\
&= (1-\alpha)\alpha^{\alpha(1-\beta)}\Xi^{-\xi}(1-x)^{\varpi\xi}Z_{it}^{1-\beta}L_i^{\omega\xi}K_{it}^{(1-\omega-\varpi)\xi}N_{it}^{-\xi(1-\varpi)} \\
&= \underbrace{(1-\alpha)\alpha^{\alpha(1-\beta)}\Xi^{-\xi}(1-x)^{\varpi\xi}Z_i^{1-\beta}L_i^{\omega\xi}}_{\equiv C_{0i}} \cdot e^{(1-\beta)\chi_{it}}\left(\frac{K_{it}^{1-\omega-\varpi}}{N_{it}^{1-\varpi}}\right)^{\xi} \\
&\equiv C_{0i}e^{(1-\beta)\chi_{it}}\left(\frac{K_{it}^{1-\omega-\varpi}}{N_{it}^{1-\varpi}}\right)^{\xi}
\end{aligned}$$

where $\xi = \alpha + \beta(1-\alpha)$. With consumption at hand, we express the flow utility in location i at time t:

$$A_{it} + u\left(\frac{w_{it}}{r_{it}^{\beta}}\right) = A_i + a_{it} + u\left(C_{0i}e^{(1-\beta)\chi_{it}}\left(\frac{K_{it}^{1-\omega-\varpi}}{N_{it}^{1-\varpi}}\right)^{\xi}\right) \equiv U_i(a_{it}, \chi_{it}, K_{it}, N_{it}).$$

A.2 Capitalists

We denote by $Y_{it}(I,K) = R_{K,it}K - c_i(I/K)K$ the net income of a capitalist with capital stock K investing I. We first guess and verify that $\mathcal{P}_{it}(K,b) = \mathcal{Q}_{it}(K) + b + \Pi_{it}$, where $\mathcal{Q}_{it}(K)$ reflects the permanent income of capitalists from capital returns, and Π_{it} reflects the present discounted value of transfers from the national mutual fund. Substituting our guess into the capitalist problem (5), we obtain

$$\rho\mathcal{Q}_{it}(K) = \max_I Y_{it}(I,K) + (I-\delta_{it}K)\frac{\partial\mathcal{Q}_{it}}{\partial K}(K) + \frac{\mathbb{E}_t[d_t\mathcal{Q}_{it}]}{dt} \quad , \quad \rho = \overline{R}_t \quad , \quad \rho\Pi_{it} = \pi_{it} + \frac{\mathbb{E}_t[d_t\Pi_{it}]}{dt}. \tag{20}$$

Thus, investment decisions are independent from bond holdings b and from transfers. We further guess and verify that $\mathcal{P}_{it}(K) = Q_{it}K$. Substituting this guess in (20), the investment policy becomes $c_i'(I/K) = Q_{it}$ and so $I = (c_i')^{-1}(Q_{it})K$.

Using our guess, the investment policy and the functional form of the investment cost in (20), we obtain

$$(\rho+\delta_{it})Q_{it} = R_{K,it} + \frac{c_{i0}Q_{it}^{1+\zeta}}{1+\zeta} + \frac{\mathbb{E}_t[d_tQ_{it}]}{dt}, \quad I^*(K,Q_{it}) = c_{i0}Q_{it}^{\zeta}K.$$

B Steady-state computation

We solve for steady-state using the following algorithm:

1. Start by using (9) to solve for: $Q_i^{ss} = (\Delta_i/c_{i0})^{1/\zeta}$, and then (8) to obtain: $R_i^{ss} = \rho Q_i^{ss} + \frac{\zeta c_{i0}(Q_i^{ss})^{1+\zeta}}{1+\zeta}$.

2. Given R_i^{ss}, then use (8) to solve for the equilibrium capital as a function of population:

$$K_i^{ss} = R_{0i}^{1/\phi}(R_i^{ss})^{-1/\phi}(N_i^{ss})^{\psi/\phi} \equiv \mathcal{K}_i(N_i^{ss}) \tag{21}$$

3. Substitute (21) into (8) to obtain

$$\rho V_i^{ss} \quad = \quad U_i(\mathcal{K}_i(N_i^{ss}), N_i^{ss}) + \mathcal{M}_i[V^{ss}] \tag{22}$$

4. Iterate alternatively on (22) and (9) to jointly solve equilibrium values V_i^{ss} and population N_i^{ss}:

   (a) Start from a uniform guess for N_i^{ss} (or any other guess)

   (b) Solve (22) for V_i^{ss}

   (c) Update N_i^{ss} by solving (9) given V_i^{ss}

   (d) Keep iterating on (b-c) until both N_i^{ss} and V_i^{ss} have converged.

C FAME

For exposition, we state the full version of Proposition 2 and Proposition 3 before proving them.

Proposition 5. *(Deterministic FAME, full)*
The matrices v^N, v^K, q^N, q^K satisfy the generalized Sylvester matrix equation in $\mathrm{v}^d = \left(\begin{smallmatrix} v^N & v^K \\ q^N & q^K \end{smallmatrix}\right)$:

$$\rho \mathrm{v}^d = \mathrm{D}^d + \mathrm{M}\mathrm{v}^d + \mathrm{v}^d\mathrm{M}^* + \mathrm{v}^d\mathrm{P}\mathrm{v}^d,$$

where M denotes the steady-state matrix $M(V^{ss})$, and we defined the following $2\mathcal{I} \times 2\mathcal{I}$ matrices:

$$\mathrm{D}^d = \begin{pmatrix} D_{UN} & D_{UK} \\ D_{RN} & D_{RK} \end{pmatrix}, \quad \mathrm{M} = \begin{pmatrix} M & 0 \\ 0 & 0 \end{pmatrix}, \quad \mathrm{P} = \begin{pmatrix} G & 0 \\ 0 & D_{IQ} \end{pmatrix},$$

and where $D_{UN} = -\xi(1-\varpi)\mathbf{diag}\Big(u'(C_i^{ss})C_i^{ss}/N_i^{ss}\Big)$, $D_{UK} = \xi(1-\omega-\varpi)\mathbf{diag}\Big(u'(C_i^{ss})C_i^{ss}/K_i^{ss}\Big)$, $D_{RK} = -\phi\mathbf{diag}\Big(R_i^{ss}/K_i^{ss}\Big)$, $D_{RN} = \psi\mathbf{diag}\Big(R_i^{ss}/N_i^{ss}\Big)$, $G = \mu\nu\Big(\mathbf{diag}(N^{ss}) - m^*\mathbf{diag}(N^{ss})m\Big)$, $D_{IQ} = \zeta\mathbf{diag}\left(K_i^{ss}c_{i0}(Q_i^{ss})^{\zeta-1}\right)$.

Proposition 6. *(Trend FAME, full)*
The matrices v_t^T, q_t^T satisfy the Ordinary Differential Equation system:

$$\rho \mathrm{v}_t^T = D_t^T + \mathrm{M}\mathrm{v}_t^T + \frac{\partial \mathrm{v}_t^T}{\partial t} + \mathrm{v}^d\mathrm{P}\mathrm{v}_t^T, \qquad \mathrm{v}_t^T \equiv \begin{pmatrix} v_t^T \\ q_t^T \end{pmatrix}, \qquad D_t^T \equiv T_t^D \begin{pmatrix} D_{UT} - v^K D_{\Delta T} \\ D_{QT} - q^K D_{\Delta T} \end{pmatrix},$$

and where: $D_{UT} = \mathbf{vec}\Big(a_{i1} + u'(C_i^{ss})C_i^{ss}(1-\beta)\chi_{i1}\Big)$, $D_{\Delta T} = \mathbf{vec}\Big(K_i^{ss}\delta_{i1}\Big)$, $D_{QT} = \mathbf{vec}\Big(R_i^{ss}\chi_{i1} - \delta_{i1}Q_i^{ss}\Big)$.

Proposition 7. *(Transitional dynamics, full)*
Given initial conditions n_0, k_0*, the transitional dynamics in response to a sequence of shocks* $\{z_t\}_t$ *and* $\{T_t^D\}_t$ *are given by paths* $\{n_t, k_t\}_t$ *such that:*

$$\frac{d}{dt}\begin{pmatrix} n_t \\ k_t \end{pmatrix} = D_t^p + (\mathrm{M}^* + \mathrm{Pv}^d)\begin{pmatrix} n_t \\ k_t \end{pmatrix} + \mathrm{P}(\mathrm{v}_t^T + z_t\mathrm{v}^Z), \tag{23}$$

where: $D_t^p = -(T_t^D + z_t)\begin{pmatrix} 0 \\ D_{\Delta T} \end{pmatrix}$.

Proposition 8. *(Confidence intervals)*
When $z_t = 0$*,* $\mathcal{V}_t$ *and* $\mathcal{P}_t$ *satisfy the Ordinary Differential Equation system:*

$$\rho\mathcal{V}_t = \mathcal{D}_t + \mathrm{M}\mathcal{V}_t + \frac{\partial \mathcal{V}_t}{\partial t} + \mathrm{v}^d\mathrm{P}\mathcal{V}_t, \qquad\qquad \frac{d\mathcal{P}_t}{dt} = \mathcal{D}_t^p + (\mathrm{M}^* + \mathrm{Pv}^d)\mathcal{P}_t + \mathrm{P}\mathcal{V}_t,$$

where: $\mathcal{D}_t = T_t^D\big(\mathcal{D}_{UT} - v^K\mathcal{D}_{\Delta T},\ \mathcal{D}_{QT} - q^K\mathcal{D}_{\Delta T}\big)$, $\mathcal{D}_{UT} = \big(\mathbf{diag}((1-\beta)u'(C_i^{ss})C_i^{ss}),\ I_{\mathcal{I}},\ 0_{\mathcal{I}}\big)$, $\mathcal{D}_t^p = -T_t^D(0, \mathcal{D}_{\Delta T})^*$, $\mathcal{D}_{\Delta T} = \big(0_{\mathcal{I}},\ 0_{\mathcal{I}},\ \mathbf{diag}(K_i^{ss})\big)$*, and* $\mathcal{D}_{QT} = \big(0_{\mathcal{I}},\ \mathbf{diag}(R_i^{ss},\ -\mathbf{diag}(Q_i^{ss})\big)$.

We now prove Propositions 5, 6 and 7. Proposition 8 then follows immediately.

C.1 Flow payoffs

C.1.1 Workers

The flow payoffs become, to first order,

$$\frac{U_{it} - U_i^{ss}}{\epsilon} = a_{i1}\big(z + T_t^D\big) + u'(C_i^{ss})C_i^{ss}\cdot\left((1-\beta)\chi_{i1}\big(z + T_t^D\big) + \xi(1-\omega-\varpi)\frac{k_i}{K_i^{ss}} - \xi(1-\omega)\frac{n_i}{N_i^{ss}}\right),$$

with $u'(C) = C^{-\gamma}$. In vector notation,

$$\begin{aligned}\epsilon^{-1}(U_t - U^{ss}) &= \mathbf{vec}\Big(a_{i1}\Big)\big(z + T_t^D\big) + \mathbf{diag}\Big(u'(C_i^{ss})C_i^{ss}\Big)\Bigg[(1-\beta)\mathbf{vec}(\chi_{i1})\big(z + T_t^D\big) \\ &\qquad + \xi(1-\omega-\varpi)\mathbf{diag}\Big(1/K_i^{ss}\Big)k - \xi(1-\omega)\mathbf{diag}\Big(1/N_i^{ss}\Big)n\Bigg] \\ &\equiv \mathrm{D}_{UZ}z + \mathrm{D}_{UT}T_t + \mathrm{D}_{UK}k + \mathrm{D}_{UN}n,\end{aligned}$$

where we have defined

$$\begin{aligned}\mathrm{D}_{UT} = D_{UZ} &= \mathbf{vec}\Big(a_{i1} + u'(C_i^{ss})C_i^{ss}(1-\beta)\chi_{i1}\Big)\\ \mathrm{D}_{UK} &= \xi(1-\omega-\varpi)\mathbf{diag}\Big(u'(C_i^{ss})C_i^{ss}/K_i^{ss}\Big)\\ \mathrm{D}_{UN} &= -\xi(1-\varpi)\mathbf{diag}\Big(u'(C_i^{ss})C_i^{ss}/N_i^{ss}\Big).\end{aligned}$$

C.1.2 Capitalists

Similarly, to first order and in vector notation,

$$\begin{aligned}&\epsilon^{-1}\left[\left(R_{K,it} + \frac{c_{i0}Q_{it}^{1+\zeta}}{1+\zeta} - \Delta_{it}Q_{it}\right) - \left(R_{K,i}^{ss} + \frac{c_{i0}(Q_i^{ss})^{1+\zeta}}{1+\zeta} - \Delta_i Q_i^{ss}\right)\right]_{i=1}^{\mathcal{I}}\\ =\ &\mathrm{D}_{RK}k + \mathrm{D}_{RN}n + \mathrm{D}_{CQ}\big[q^N n + q^K k + q^Z z + q^T\big] + \mathrm{D}_{QT}T_t^D + \mathrm{D}_{QZ}z,\end{aligned}$$

where

$$\begin{aligned}\mathrm{D}_{RK} &= -\phi\mathbf{diag}\Big(R_i^{ss}/K_i^{ss}\Big) & \mathrm{D}_{RN} &= \psi\mathbf{diag}\Big(R_i^{ss}/N_i^{ss}\Big)\\ \mathrm{D}_{CQ} &= \mathbf{diag}\Big(c_{i0}(Q_i^{ss})^{\zeta} - \Delta_i\Big) = 0 & \mathrm{D}_{QT} &= \mathrm{D}_{QZ} = \mathbf{vec}\Big(R_i^{ss}\chi_{i1} - \delta_{i1}Q_i^{ss}\Big),\end{aligned}$$

where $\mathrm{D}_{CQ} = 0$ from the steady-state investment equation of capitalists.

C.2 Continuation value from migration

Denote by M the steady-state matrix $M(V^{ss})$. The continuation value from migration becomes, to leading order,

$$\frac{\mathcal{M}[V] - \mathcal{M}[V^{ss}]}{\epsilon} = Mv^N n + Mv^K k + Mv^Z z + Mv_t^T.$$

C.3 Continuation value from changes in population distribution

To linearize the law of motion of population, first note that

$$\frac{\partial m_{ji}}{\partial V_k} = \begin{cases} -\nu m_{ji}m_{jk} & \text{if} \quad i \neq k\\ \nu m_{ji}(1-m_{ji}) & \text{if} \quad i = k\end{cases}$$

and so

$$M_{ij}^*(V+dV) \;=\; M_{ij}^*(V) + \mu\sum_k \frac{\partial m_{ji}}{\partial V_k}dV_k = M_{ij}^*(V) + \mu\nu m_{ji}\Big\{dV_i - \big[m\cdot dV\big]_j\Big\}.$$

Then to leading order,

$$\begin{aligned} M_i^*(V+dV)[N^{ss}] &= M_i^*(V)[N^{ss}] + \mu\nu \sum_j m_{ji}\Big\{dV_i - \big[m\cdot dV\big]_j\Big\}N_j^{ss} \\ &= M_i^*(V)[N^{ss}] + \nu\mu\Big[\Big(\mathbf{diag}(m^*N^{ss}) - m^*\mathbf{diag}(N^{ss})m\Big)\cdot dV\Big]_i \\ &\equiv M_i^*(V)[N^{ss}] + (G\cdot dV)_i \end{aligned}$$

where $G = \nu\mu\Big(\mathbf{diag}(m^*N^{ss}) - m^*\mathbf{diag}(N^{ss})m\Big)$. In vector notation, to leading order,

$$\epsilon^{-1}\left(\sum_j \frac{\partial V_i}{\partial N_j}(M^*(V)N)_j\right)_{i=1}^{I} = v^N M^* n + v^N G\big(v^N n + v^K k + v^Z z + v_t^T\big)$$

Similarly,

$$\epsilon^{-1}\left(\sum_j \frac{\partial Q_i}{\partial N_j}(M^*(V)N)_j\right)_{i=1}^{I} = q^N M^* n + q^N G\big(v^N n + v^K k + v^Z z + v_t^T\big)$$

C.4 Continuation value from changes in capital distribution

We obtain, to leading order,

$$\begin{aligned} \epsilon^{-1}\sum_j \frac{\partial V_i}{\partial K_j}K_j\big(c_{j0}Q_j^{\zeta} - \Delta_{jt}\big) &= \sum_j v_{ij}^K K_j^{ss}\left\{\epsilon^{-1}dI_j^* - \delta_{1j}\big(z + T_t^D\big)\right\} \\ &= \sum_j v_{ij}^K K_j^{ss}\left\{\zeta c_{j0}(Q_j^{ss})^{\zeta-1}\left[\sum_j q_{j\ell}^N n_\ell + \sum_\ell q_{j\ell}^K k_\ell + q_j^Z z + q_{tj}^T\right] - \delta_{j1}\big(z + T_t^D\big)\right\} \\ &= v^K\Big\{\mathrm{D}_{IQ}\left[q^N n + q^K k + q^Z z + q_t^T\right] - \big(z + T_t^D\big)\mathrm{D}_{\Delta T}\Big\} \end{aligned}$$

where

$$\mathrm{D}_{IQ} = \zeta\mathbf{diag}\Big(K_j^{ss}c_{j0}(Q_j^{ss})^{\zeta-1}\Big) \qquad\qquad \mathrm{D}_{\Delta T} = \mathbf{vec}\Big(K_j^{ss}\delta_{j1}\Big)$$

Similarly, to leading order,

$$\left(\epsilon^{-1}\sum_j \frac{\partial Q_i}{\partial K_j}K_j\big(c_{j0}Q_j^{\zeta} - \Delta_{jt}\big)\right)_i = q^K\Big\{\mathrm{D}_{IQ}\left[q^N n + q^K k + q^Z z + q_t^T\right] - \big(z + T_t^D\big)\mathrm{D}_{\Delta T}\Big\}$$

C.5 FAME in vector notation

C.5.1 Workers

Thus, the linearized master equation for the worker value becomes, in vector notation,

$$\begin{aligned}
&\rho\big(v^N n + v^K k + v^Z z + v^T\big) - \frac{\partial v^T}{\partial t} \\
= \; & \overbrace{\mathrm{D}_{UZ} z + \mathrm{D}_{UT} T_t^D + \mathrm{D}_{UK} k - \mathrm{D}_{UN} n}^{\text{flow payoff}} + \overbrace{M\big(v^N n + v^K k + v^Z z + v^T\big)}^{\text{continuation value from migration}} + \overbrace{\mathcal{A}(z)[v^Z z]}^{\text{c.v. from climate shocks}} \\
+ \; & \underbrace{v^N M^* n + v^N G\big(v^N n + v^K k + v^Z z + v^T\big)}_{\text{continuation value from changes in the population distribution}} + \underbrace{v^K\Big\{\mathrm{D}_{IQ}\left[q^N n + q^K k + q^Z z + q^T\right] - (z + T_t^D)\mathrm{D}_{\Delta T}\Big\}}_{\text{continuation value from changes in the capital distribution}}
\end{aligned}$$

We impose that z_t follows an AR(1) process: $\mathcal{A}(z)[V] = -\theta z V'(z) + \frac{z^2}{2} V''(z)$. Identifying coefficients, and with unknowns in bold notation,

$$\begin{aligned}
\rho \boldsymbol{v^N} &= \mathrm{D}_{UN} + M\boldsymbol{v^N} + \boldsymbol{v^N} M^* + \boldsymbol{v^N} G \boldsymbol{v^N} + \boldsymbol{v^K} \mathrm{D}_{IQ} \boldsymbol{q^N} \\
\rho \boldsymbol{v^K} &= \mathrm{D}_{UK} + M\boldsymbol{v^K} + \boldsymbol{v^N} G \boldsymbol{v^K} + \boldsymbol{v^K} \mathrm{D}_{IQ} \boldsymbol{q^K} \\
\rho \boldsymbol{v^Z} &= \mathrm{D}_{UZ} + M\boldsymbol{v^Z} - \theta \boldsymbol{v^Z} + \boldsymbol{v^N} G \boldsymbol{v^Z} + \boldsymbol{v^K} \mathrm{D}_{IQ} \boldsymbol{q^Z} - \boldsymbol{v^K} \mathrm{D}_{\Delta T} \\
\rho \boldsymbol{v^T} - \frac{\partial \boldsymbol{v^T}}{\partial t} &= \mathrm{D}_{UT} T_t^D + M\boldsymbol{v^T} + \boldsymbol{v^N} G \boldsymbol{v^T} + \boldsymbol{v^K} \mathrm{D}_{IQ} \boldsymbol{q^T} - \boldsymbol{v^K} \mathrm{D}_{\Delta T} T_t^D.
\end{aligned}$$

C.5.2 Capitalists

Similarly, the linearized master equation for capitalists becomes, in vector notation,

$$\begin{aligned}
&\rho\big(q^N n + q^K k + q^Z z + q^T\big) - \frac{\partial q^T}{\partial t} \\
= \; & \overbrace{\mathrm{D}_{RK} k + \mathrm{D}_{RN} n + \mathrm{D}_{CQ}\left[q^N n + q^K k + q^Z z + q^T\right] + \mathrm{D}_{QT} T_t^D + \mathrm{D}_{QZ} z}^{\text{flow payoff}} + \overbrace{\mathcal{A}(z)[q^Z z]}^{\text{c.v. from climate shocks}} \\
+ \; & \underbrace{q^N M^* n + q^N G\big(v^N n + v^K k + v^Z z + v^T\big)}_{\text{continuation value from changes in the population distribution}} \\
+ \; & \underbrace{q^K\Big\{\mathrm{D}_{IQ}\left[q^N n + q^K k + q^Z z + q^T\right] - (z + T_t^D)\mathrm{D}_{\Delta T}\Big\}}_{\text{continuation value from changes in the capital distribution}}
\end{aligned}$$

Identifying coefficients, and with unknowns in bold notation,

$$\begin{aligned}
\rho \boldsymbol{q^N} &= \mathrm{D}_{RN} + \mathrm{D}_{CQ} \boldsymbol{q^N} + \boldsymbol{q^N} M^* + \boldsymbol{q^N} G \boldsymbol{v^N} + \boldsymbol{q^K} \mathrm{D}_{IQ} \boldsymbol{q^N} \\
\rho \boldsymbol{q^K} &= \mathrm{D}_{RK} + \mathrm{D}_{CQ} \boldsymbol{q^K} + \boldsymbol{q^N} G \boldsymbol{v^K} + \boldsymbol{q^K} \mathrm{D}_{IQ} \boldsymbol{q^K} \\
\rho \boldsymbol{q^Z} &= \mathrm{D}_{QZ} + \mathrm{D}_{CQ} \boldsymbol{q^Z} - \theta \boldsymbol{q^Z} + \boldsymbol{q^N} G \boldsymbol{v^Z} + \boldsymbol{q^K} \mathrm{D}_{IQ} \boldsymbol{q^Z} - \boldsymbol{q^K} \mathrm{D}_{\Delta T} \\
\rho \boldsymbol{q^T} - \frac{\partial \boldsymbol{q^T}}{\partial t} &= \mathrm{D}_{QT} T_t^D + \mathrm{D}_{CQ} \boldsymbol{q^T} + \boldsymbol{q^N} G \boldsymbol{v^T} + \boldsymbol{q^K} \mathrm{D}_{IQ} \boldsymbol{q^T} - \boldsymbol{q^K} \mathrm{D}_{\Delta T} T^D(t)
\end{aligned}$$

Collecting terms for $\boldsymbol{v^N}, \boldsymbol{v^K}, \boldsymbol{q^N}, \boldsymbol{q^K}$, Proposition 2 obtains. Collecting terms for $\boldsymbol{v^T}, \boldsymbol{q^T}$, Proposition 2 obtains. The stochastic FAME writes

$$(\rho+\theta)\begin{pmatrix}\boldsymbol{v^Z}\\ \boldsymbol{q^Z}\end{pmatrix} = \begin{pmatrix}\mathrm{D}_{UZ}-v^K\mathrm{D}_{\Delta T}\\ \mathrm{D}_{QZ}-q^K\mathrm{D}_{\Delta T}\end{pmatrix}+\begin{pmatrix}M+v^NG & v^K\mathrm{D}_{IQ}\\ q^NG & \mathrm{D}_{CQ}+q^K\mathrm{D}_{IQ}\end{pmatrix}\begin{pmatrix}\boldsymbol{v^Z}\\ \boldsymbol{q^Z}\end{pmatrix}. \tag{24}$$

This is now a standard matrix equation.

C.6 Computation

Two methods are available to solve the nonlinear Sylvester matrix equation: $0 = \mathrm{D}_d + (\mathrm{M}-\rho\mathrm{Id})\mathrm{v}^d + \mathrm{v}^d\mathrm{M}^* + \mathrm{v}^d\mathrm{P}\mathrm{v}^d$. The first one is a simple iterative algorithm that leverages standard numerical packages solving standard Sylvester equations of the form: $AX + XB + C = 0$. We need to iterate to include the quadratic term $\mathrm{v}^d\mathrm{P}\mathrm{v}^d$. We use an efficient iteration scheme that mirrors the structure of a Newton updating step.

The second method is to recast this nonlinear Sylvester equation as a larger $4\mathcal{I}\times 4\mathcal{I}$ linear rational expectation system (Blanchard and Kahn, 1980; Reiter, 2009) and use standard rational expectations solution methods. Both methods exhibit comparable performance in our setting. We provide more details below.

Iterative method. We start with the iterative method to solve for v^d. Given a guess v^d_n at step n, we solve for v^d_{n+1} as follows:

$$\begin{aligned}0 &= \mathrm{D}_d + \Big(\mathrm{M}-\rho\mathrm{Id}+f(\mathrm{v}^d_n)\Big)\mathrm{v}^d_{n+1} + \mathrm{v}^d_{n+1}\Big(\mathrm{M}^*+g(\mathrm{v}^d_n)\Big)\\ \implies \mathrm{v}^d_{n+1} &= h(\mathrm{v}^d_n) + \texttt{sylvester}\Big(\mathrm{M}-\rho\mathrm{Id}+f(\mathrm{v}^d_n),\ \mathrm{M}^*+g(\mathrm{v}^d_n),\ \mathrm{D}_d-k(\mathrm{v}^d_n)\Big),\end{aligned}$$

where $\texttt{sylvester}(A,B,C)$ denotes the solution X of the Sylvester equation $AX+XB+C=0$, and f,g,h,k denote in this section arbitrary functions to be chosen. Given v^d_n, standard numerical packages solve efficiently for v^d_{n+1} as the root of a standard Sylvester equation. For instance, Matlab has a built-in `sylvester.m` function.

The standard Picard iteration sets $f=g=h=0$ and will usually achieve linear convergence rates. It is not difficult to construct a more efficient Newton iteration scheme that achieves quadratic convergence. After constructing the derivatives of the nonlinear Sylvester equation with respect to the entries of v^d, we show that a Newton iteration scheme sets $h(v)=v$, $f(v)=v\mathrm{P}$, $g(v)=\mathrm{P}v$, $k(v)=\mathrm{M}v+v\mathrm{M}^*+v\mathrm{P}v$. With an heuristic initial guess that leverages the near block-separately of the Sylvester equation however, the Picard and Newton schemes tend to converge after a similar number of iterations in our case. Without an informed initial guess, the difference can be more meaningful.

Linear rational expectation method. Another, more traditional method is to recast the nonlinear Sylvester equation as a linear rational expectation system Bilal (2023). In that case, the solution method mirrors Blanchard and Kahn (1980).

Transitional dynamics. Once we have solved for the deterministic impulse value v^d, we solve for the trend impulse value leveraging Proposition 2 in two steps. In the first step, we solve for the long-run trend impulse value. When time t is large enough, temperatures do not change anymore. The economy has then reached the new steady-state, and $\frac{\partial \mathrm{v}^T}{\partial t} = 0$. Hence, we specify a large enough time $t = \bar{t}$ where the time derivative is zero, and where we use Proposition 2 to solve for $\mathrm{v}^T_{\bar{t}}$. Specifically, $\mathrm{v}^T_{\bar{t}} = (\rho \mathrm{Id} - (\mathrm{M} + \mathrm{v}^d \mathrm{P}))^{-1} \mathrm{D}^T_{\bar{t}}$. The solution $\mathrm{v}^T_{\bar{t}}$ is our terminal condition.

In the second step, we iterate backward in time from the terminal condition $\mathrm{v}^T_{\bar{t}}$. We construct the $2\mathcal{I} \times 1$ vector D^T for each time t. Given a time step dt, we construct a solution v^T_t to the ODE system in Proposition 2 given $\mathrm{v}^T_{t+\mathrm{dt}}$ by iterating backward in time: $\mathrm{v}^T_t = \big(\mathrm{Id} + \mathrm{dt}(\rho \mathrm{Id} - (\mathrm{M} + \mathrm{v}^d \mathrm{P}))\big)^{-1} \big(\mathrm{dt}\, \mathrm{D}^T_t + \mathrm{v}^T_{t+\mathrm{dt}}\big)$. Once we have solved for the deterministic and trend impulse values, we compute any impulse response to a shock or initial conditions with a simple forward iteration using Proposition 2. In practice, we solve for capitalist welfare nonlinearly to improve accuracy given their linear preferences.

C.6.1 Accuracy

Figure 15 displays additional statistics using different specifications for the perturbation.

Figure 15: Accuracy of perturbation.

(a) St. dev. 2050 worker welfare. (b) St. dev. 2050 local population. (c) St. dev. 2050 local capital.

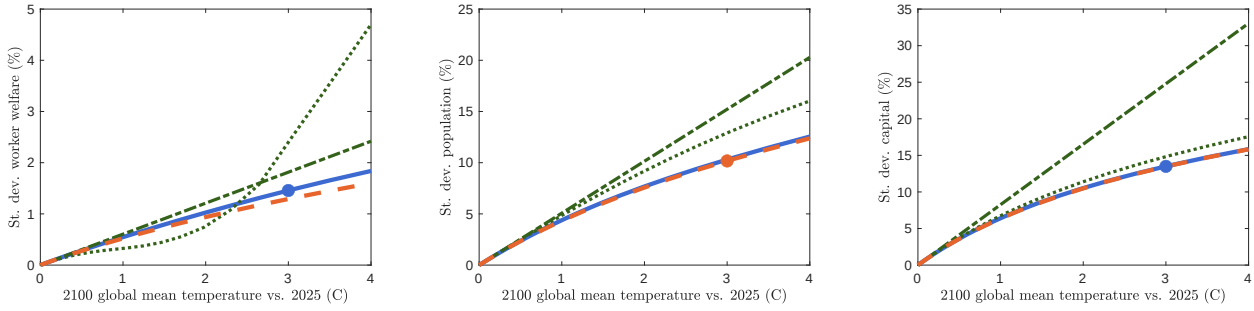

Note: Panel (a): initial population-weighted standard deviation of worker welfare across locations in 2050. Panel (b): initial population-weighted standard deviation of percent population changes relative to date 0 across locations in 2050. Panel (c): initial capital-weighted standard deviation of percent capital changes relative to date 0 across locations in 2050. All panels shown as a function of global mean temperature in 2100 relative to global mean temperature in 2025 in degrees Celsius. Green dash-dot line: using the FAME expanded around the initial steady-state, with capital and population in level deviations. Green dotted line: using the FAME expanded around the initial steady-state, with capital and population in log deviations. Solid blue line: using the FAME expanded around the final steady-state, with capital and population in log deviations Dashed orange line: using the nonlinear value function (in panel a) or the nonlinear law of motion (in panel b) given allocations (in panel a) or decisions (in panel b) from the FAME.

C.7 Welfare

C.7.1 Consumption equivalent welfare

For any period τ, we compute consumption equivalent welfare change between the steady-state ss and any counterfactual as $\omega_{i\tau}$, such that

$$\mathbb{E}_\tau \int_\tau^\infty e^{-\rho(t-\tau)} \Big\{ A^{ss}_{i(t)} + \varepsilon_{i(t)t} + u((1+\omega_{i\tau})C^{ss}_{i(t)}) \Big\} dt = \mathbb{E}_\tau \int_\tau^\infty e^{-\rho(t-\tau)} \Big\{ A_{i(t),t} + u(C_{i(t),t}) \Big\} dt$$

where ε_{it} denotes the preference shock for the current (chosen) location.

Worker welfare: lump-sum preference shocks We start with the definition of welfare when preference shocks are 'lump-sum', that is, when they are realized upon moving. In that case, preference shocks are not included in the welfare metric, which simply becomes V_{it} in location i at time t.

Log utility. Under log utility $\gamma = 1$, we obtain

$$V^{ss}_i + \rho^{-1} \log(1 + d\omega_{i\tau}) = V_{i\tau} \iff d\omega_{i\tau} = e^{\rho(V_{i\tau} - V^{ss}_i)} - 1.$$

When shocks are small $\epsilon \to 0$, to a first order,

$$d\omega_{i\tau} = \rho \; dV_{i\tau} \tag{25}$$

CRRA utility. With CRRA utility when $\gamma \neq 1$, $u(C) = \frac{C^{1-\gamma}-1}{1-\gamma}$,

$$V^{A,ss}_i + (1 + d\omega_{i\tau})^{1-\gamma} V^{C,ss}_{i\tau} - \frac{1}{\rho(1-\gamma)} = V_{i\tau},$$

where

$$V^{A,ss}_i = \mathbb{E}_0 \int_0^\infty e^{-\rho t} \Big\{ A^{ss}_{i(t)} \Big\} dt \implies (\rho + \mu) V^{A,ss}_i = A^{ss}_i + \mu \sum_j m_{ij} V^{A,ss}_j$$

$$V^{C,ss}_i = \mathbb{E}_0 \int_0^\infty e^{-\rho t} \frac{(C^{ss}_{i(t)})^{1-\gamma}}{1-\gamma} dt \implies (\rho + \mu) V^{C,ss}_i = \frac{(C^{ss}_i)^{1-\gamma}}{1-\gamma} + \mu \sum_j m_{ij} V^{C,ss}_j.$$

Then

$$(1 + d\omega_{i\tau})^{1-\gamma} V^{C,ss}_{i\tau} - V^{C,ss}_i = V_{i\tau} - V^{ss}_i \iff d\omega_{i\tau} = \left(1 + \frac{V_{i\tau} - V^{ss}_i}{V^{C,ss}_i} \right)^{\frac{1}{1-\gamma}} - 1$$

When shocks are small $\epsilon \to 0$, to a first order,

$$d\omega_{i\tau} = \frac{1}{1-\gamma}\frac{dV_{i\tau}^{IRF}}{V_i^{C,ss}} = \frac{\rho\ dV_{i\tau}^{IRF}}{\widetilde{V}_i}, \tag{26}$$

where

$$\widetilde{V}_i = \rho\mathbb{E}_0\int_0^\infty e^{-\rho t}(C_{i(t)}^{ss})^{1-\gamma}dt \quad\Longrightarrow\quad (\rho+\mu)\widetilde{V}_i = \rho(C_i^{ss})^{1-\gamma} + \mu\sum_j m_{ij}\widetilde{V}_j.$$

Aggregate welfare Aggregate welfare is defined as

$$\overline{V}_t = \sum_i N_{it}V_{it} \quad , \quad \overline{Q}_t = \sum_i K_{it}Q_{it}.$$

Derivations and formulas are identical to the local welfare case above after replacing local values with aggregate values.

Worker welfare: permanent preference shocks

Log utility. When preference shocks are permanent until the next moving opportunity, then local welfare is given by

$$\mathcal{W}_i[V_t] = \frac{1}{\nu}\log\left(\sum_j e^{\nu(V_{jt}-\tau_{ij})}\right).$$

In response to a change, we have

$$d\mathcal{W}_i = \sum_j m_{ij}dV_{jt} = \Big(m\cdot dV_t\Big)_i.$$

Under log utility, similar derivations as above for small ϵ lead to

$$\Big(m\cdot dV_t\Big)_i = \left(m\cdot\left(\frac{d\omega_{i\tau}}{\rho}\right)_j\right)_i = \frac{d\omega_{i\tau}}{\rho},$$

so that

$$d\omega_{i\tau} = \rho\Big(m\cdot dV_t\Big)_i.$$

CRRA utility. Similar derivations as above lead to

$$d\omega_{i\tau} = \frac{\rho\big(m\cdot dV_t\big)_i}{\big(m\cdot\tilde{V}\big)_i}.$$

Aggregate worker welfare. Aggregate welfare is defined as $\overline{\mathcal{W}}_t = \sum_i N_{it}\mathcal{W}_{it}$.

Capitalist welfare. For capitalists we must take a stand on how claims to the national mutual fund are distributed—and hence land rents rebated. For simplicity, we assume that capitalists own claims to land rents in their location. That is, land is locally owned. We define capitalist welfare in location i at time t as $\tilde{\mathcal{P}}_{it} = Q_{it}K_{it} + \Pi_{it}$, and aggregate welfare is $\overline{\mathcal{P}}_t = \sum_i \tilde{\mathcal{P}}_{it}$.

D Estimation: Proof of Proposition 4

We use the steady-state investment rate (9) to obtain an estimate of the steady-state capital stock in each location: $K_i = \tilde{I}_i/\delta$. Next, we recover an estimate of the stock of buildings B_i and housing H_i from the constant shares rule (17)-(18) and the buildings production function:

$$B_i = L_i^{\omega}\Big((1-x)N_i\Big)^{\varpi}K_i^{1-\omega-\varpi} \quad , \quad H_i = yB_i$$

The wage equation (19) then delivers an estimate of fundamental productivity in county i:

$$Z_i = \frac{w_i}{(1-\alpha)\alpha^{\alpha}\Xi^{-\alpha}\big(B_i/N_i\big)^{\alpha}}.$$

From there we construct $R_{0i} = (1-\omega-\varpi)\alpha^{\alpha}\Xi^{1-\alpha}(1-x)^{\alpha\varpi}Z_iL_i^{\omega\alpha}$. Combining equations (8) and (9) then delivers local investment costs:

$$c_{i0} = \delta\left[\frac{1}{R_{0i}K_i^{-\phi}N_i^{\psi}}\left(\rho + \frac{\zeta\delta}{1+\zeta}\right)\right]^{\zeta}$$

Next, we construct $C_{0i} = (1-\alpha)\alpha^{\alpha(1-\beta)}\Xi^{-\xi}(1-x)^{\varpi\xi}Z_i^{1-\beta}L_i^{\omega\xi}$ and so $u_{i0} = u\left(C_{0i}K_i^{(1-\omega-\varpi)\xi}N_i^{-(1-\varpi)\xi}\right)$ which implies $U_i = A_i + u_{i0}$.

To recover migration costs, we construct migration shares as $m_{ij} = \frac{\mathtt{m}_{ij}}{\sum_k \mathtt{m}_{ik}}$. The equation for migration shares (3) implies that $X_{ij} \equiv \log m_{ij} - \log m_{ii} = \nu(V_j - V_i) - \nu\tau_{ij} \equiv Y_j - Y_i + \varepsilon_{ij}$ after imposing the normalization $\tau_{ii} = 0$. We exploit that $X_{ij} + X_{ji} = \varepsilon_{ij} + \varepsilon_{ji}$. We assume symmetric migration costs $\tau_{ij} = \tau_{ji}$, which we then recover as

$$\tau_{ij} = -\frac{X_{ij} + X_{ji}}{2\nu}.$$

We are left with estimating local amenities. We proceed in two steps. The first step consists in recovering local valuations from the steady-state population distribution. Defining $X_i = e^{\nu V_i}$ and $T_{ki} =$

$e^{-\nu\tau_{ki}}$, equation (9) implies, together with a normalization of values:

$$X_i = \frac{N_i}{\sum_k \frac{N_k T_{ki}}{\sum_j T_{kj} X_j}} \quad , \quad \sum_i X_i = 1. \tag{27}$$

The system of equations (27) satisfies the gross substitutes property, and so has at most one solution. A simple iterative method delivers the solution to equation (27), and we recover $V_i = \frac{1}{\nu} \log\big(X_i\big)$.

With an estimate of local valuations V_i at hand, the second step consists in inverting the HJB (2) to recover amenities. In particular,

$$A_i = \rho V_i - \Big(u_{i0} + \mathcal{M}_i[V]\Big).$$

E Data description

E.1 Economic data

We use county-year population data from the BEA. The BEA constructs annual population data starting from the decennial Census population figures. They estimate population at intercensal dates using the Das Gupta method. Estimates are replaced with official Census intercensal figures as they are released, which are generated via the Das Gupta and location and demographic-specific adjustments.

Income per capita is measured as personal income from the BEA. It includes income of individuals, nonprofit institutions serving individuals, private noninsured welfare funds, private trust funds, transfer receipts, employer contributions to health and pensions plans, interest received, imputed incomes. Personal income excludes personal contributions for government social insurance, pension and annuity benefits from private and government employee pension plans, and income from interpersonal transfers. To measure wages, we use salary income from the BEA.

We also obtain employment from the BEA. They weight full-time and part-time jobs.

To measure investment, we use capital expenditures, which consist of total capital expenditures for the manufacturing sector from the Census of Manufacturers from 1958 to 1992, and the Economic Censuses from 1997 to 2012. The Census of Manufacturers reports are digitized via the ICPSR 2896 project. Economic Censuses are released with a lag. Presently, capital expenditures at the county level are available for 2002, 2007, and 2012. The economic census is conducted by the Census Bureau every 5 years and includes more than 4 million selected business locations to get metrics on the American economy. Because our measure of investment of available every 5 years only, we linearly interpolate between Census years prior to running our event studies.

We also collect information on local government expenditures from the Government Finance Database, which assembles and standardizes data provided by the Census of Governments. We use total government expenditures (Census codes E, F, G, L, and M) as a control in our analysis, that we linearly interpolate

in between Census years.

E.2 ISIMIP3a data

The Inter-Sectoral Impact Model Intercomparison Project (ISIMIP) models the impacts of climate change on natural and human systems. ISIMIP simulation round 3a introduced several global, high-frequency datasets quantifying several atmospheric variables across the 20th and early 21st centuries. We use the observed climate dataset, spanning 1901-2019 at a $0.5° \times 0.5°$ resolution. This dataset harmonizes two constituent datasets, Global Soil Wetness Project Phase 3 (GSWP3, 1901-1978) (Kim, 2017) and WATCH Forcing Data methodology applied to ERA5 reanalysis dataset (W5E5, 1979-2019) (Lange, 2021a), each generated through a combination of numerical weather prediction (NWP) models and station-level atmospheric observations (Mengel et al., 2021).

The foundation of the GSWP3 is the Twentieth Century Reanalysis Project dataset (20CR), covering 1871 to 2008 at a 2° resolution and 6-hour frequency. Using the NOAA's NCEP Global Forecast System to first simulate a suite of atmospheric variables, the resulting weather predictions are then disciplined using reported and derived surface and sea-level pressure observations via an Extended Kalman Filter data assimilation system (Cucchi, 2020). Lower boundary conditions used to run the NWP consist of sea surface temperature and sea-ice concentration from the UK Met Office HadIssT1.1 dataset (Rayner, 2003) interpolated from monthly mean data to a daily frequency. Pressure observations for the data assimilation step were obtained from the International Surface Pressure Databank version 2 (Cram, 2015), which collates data from numerous international meteorological organizations.

Drawing from 20CR, GSWP3 was created by dynamically downscaling and applying bias-adjustment to several selected variables. Variables were first cast from a 2° to a roughly 0.5° resolution from 1901-2010 at a 3 hour frequency using a spectral nudging technique in a Global Spectral Model (Yoshimura and Kanamitsu, 2008). The downscaled dataset was then bilinearly interpolated to a regular 0.5° grid, with model biases further corrected by variable using observational data: Global Precipitation Climatology Centre Full Data Monthly Product Version 7 (Schneider, 2014) for precipitation; Climatic Research Unit CL2.0 (New et al., 2002) dataset for windspeed; and Climatic Research Unit TS3.23 (Harris, 2014) dataset for temperature, pressure, and humidity.

Similar to the bias-adjustments applied to 20CR in order to create GSWP3, W5E5 is built on the European Centre for Medium-Range Weather Forecast's (ECMWF) reanalysis dataset version 5 (ERA5) (Hersbach, 2020). ERA5 first leverages the ECMWF's Integrated Forecasting System Cycle 41r2 for numerical weather prediction. These modeled estimates are then reconciled with station-level observations to create a high-resolution dataset using a two-part data assimilation system: 1) the incremental 4D-Variable Assimilation method (Courtier et al., 1994) for atmospheric variables and ozone, and 2) a land data assimilation system comprising optimal interpolation schemes for temperature, relative humidity, and snow and a Simplified Extended Kalman Filter for soil moisture. The ensemble data assimilation

incorporates approximately 96 billion observed data points across the complete dataset (1979-2019) from a plethora of sources, spanning conventional meteorological measurements to satellite data, around the globe. The final ERA5 dataset is at a resolution of 31km and an hourly frequency.

Following the framework for land surface models and global hydrological models set out by the EU WATCH program, time series from ERA5 were bias-corrected and aggregated to a 0.5° resolution to create the WATCH Forcing Data methodology applied to ERA5 reanalysis (WFDE5) (Cucchi, 2020) dataset. Adjustments to match observed monthly moments were applied using the Climatic Research Unit TS40.3 (Harris, 2020) dataset for surface air temperature, shortwave radiation, rainfall rate, and snowfall rate, and the Global Precipitation Climatology Centre Full Data Monthly Product Version 2018 (Schneider, 2018) for rainfall and snowfall rates. W5E5, used in the ISIMIP dataset, was created by combining WFDE5 observations over land with ERA5 observations over the ocean (Lange, 2021a).

Inconsistent availability in the data used to produce 20CR, as well as in the subsequent bias-adjustment to generate GSWP3, produced known artifacts and spurious trends. Furthermore, many more observations were used for data assimilation in ERA5, and thus WFDE5, leading the authors of ISIMIP3a to consider W5E5 the more realistic dataset. In order to temporally extend W5E5 backward to 1901, GSWP3 data from 1901-1978 were homogenized with W5E5 to smooth discontinuities between the datasets at the 1978/1979 threshold. Within the common 1979-2004 reference period, GSWP3 time series were quantile mapped (Lange, 2019; Lange, 2021b) to match the distribution of the corresponding W5E5 time series. The resulting GSWP3-W5E5 dataset preserves the trends of the GSWP3 data and is identical to the original W5E5 data from 1979 onwards, but differs from the original 1901-1978 GSWP3 data.

E.3 Extreme event indicators

Heat—The 95$^{\text{th}}$ percentile of the annual mean temperature distribution in 1901-1910 is equal to 20°C. Importantly, an annual mean temperature of 20°C or above is highly correlated with extreme heat. For instance, the 95$^{\text{th}}$ percentile of daily maximum temperature is 33°C. The correlation between annual mean temperature and annual maximum temperature is high, at 0.71.

The 95$^{\text{th}}$ percentile of days spent above the 95$^{\text{th}}$ percentile of annual mean temperature for the 1901-1910 distribution is 20% of the year spent above 20°C. Crucially, this proportion is highly correlated with a high fraction of the year spent at much higher temperatures. The 95$^{\text{th}}$ percentile of days spent above the 95$^{\text{th}}$ percentile of maximum temperature for the 1901-1910 distribution is 18% of the year spent above 33°C. The correlation between these two fractions is substantial, at 0.91.

Storms—For comparison with our residualized percentiles, the 99$^{\text{th}}$ percentile of the un-residualized distribution of daily maximum windspeed for the years 1901-1910 is 10 meters per second (m/s). The largest windspeed is 18 m/s. Recall that these measures are daily averages, and thus allow for much faster gusts in small time windows. Similarly, the 99$^{\text{th}}$ percentile of the un-residualized distribution of daily maximum precipitation for the years 1901-1910 is 100 millimeters per day (mm/d). The maximum

is above 220 mm/d.

F Reduced-form evidence

F.1 Natural disaster counts

Figure 16: Natural disasters across counties, non-residual definition.

(a) Storm counts since 1990 (winsorized)

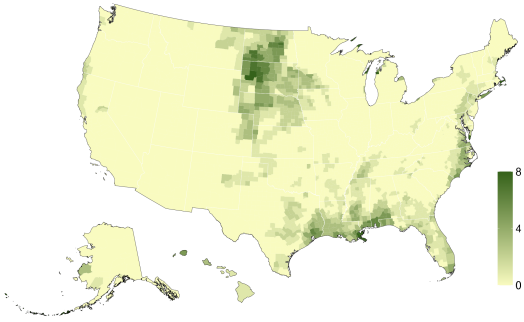

(b) Heat wave counts since 1990

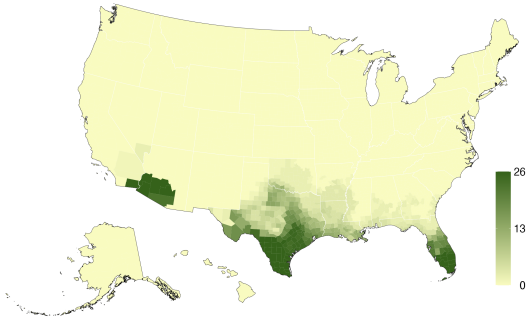

Note: Panel (a): total count of 1-in-50-years storms summed over 1990-2015 for each county in the U.S. Winsorized at 8 storms for comparability. Maximum number of storms per county in raw data: 25. Panel (b): total count of 1-in-20-years heat waves summed over 1990-2015 for each county in the U.S. White: missing data. Natural disasters based on definition without residualizing.

F.2 Investment manufacturing adjustment

Figure 17 displays the response of investment after adjustment by the manufacturing employment share for every year in every county. Figure 18 shows the response of interpolated and raw investment, aggregated into 5-year intervals.

Figure 17: The response of investment adjusted for the manufacturing employment share.

(a) 1-in-50-years storms

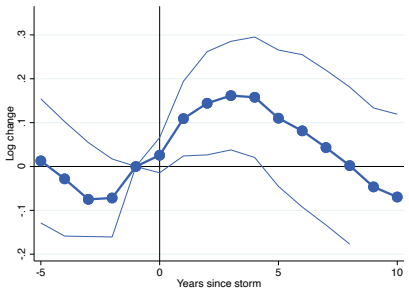

(b) 1-in-20-years heat waves

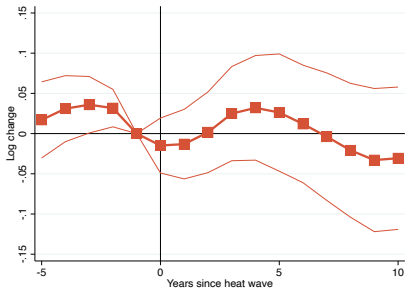

Note: Point estimates of coefficients γ_h from distributed lag regressions (14) for 1-in-50-years storms and 1-in-20-years heat waves, and 95% confidence bands clustered by county. Storms: coastal counties only. Heat wages: warm (above-median annual average temperature) counties only. Panel (a,b): log investment. Years 1990-2015. Controls: county and year fixed effects; nonparametric trends by state, local annual mean temperature decile, population and income per capita decile; 5-year lag of local government expenditures. Additional controls: panel (a): local maximum daily windspeed and maximum precipitation deciles; panel (b): deciles of fraction of hot days. Weighted by average county population in 1960-1980. Standard errors clustered by county.

Figure 18: The response of investment: interpolated and raw, aggregated at 5-year intervals.

(a) 1-in-50-years storms

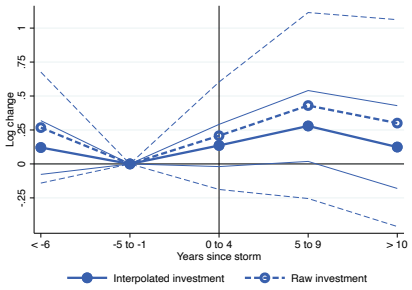

(b) 1-in-20-years heat waves

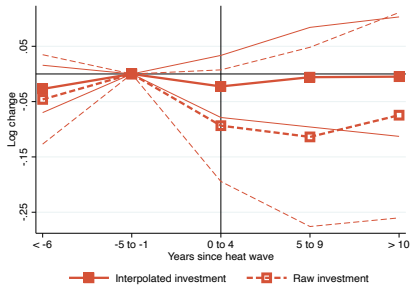

Note: Point estimates of coefficients γ_h from distributed lag regressions (14) aggregated at 5-year intervals, for 1-in-50-years storms and 1-in-20-years heat waves, and 95% confidence bands clustered by county. Storms: coastal counties only. Heat wages: warm (above-median annual average temperature) counties only. Panel (a,b): log investment. Years 1990-2015. Controls: county and year fixed effects; nonparametric trends by state, local annual mean temperature decile, population and income per capita decile; 5-year lag of local government expenditures. Additional controls: panel (a): local maximum daily windspeed and maximum precipitation deciles; panel (b): deciles of fraction of hot days. Weighted by average county population in 1960-1980. Standard errors clustered by county.

F.3 The impact of storms: alternative definition and inland counties

Figure 19: The impact of 1-in-50-years-storms: unresidualized definition, and inland counties.

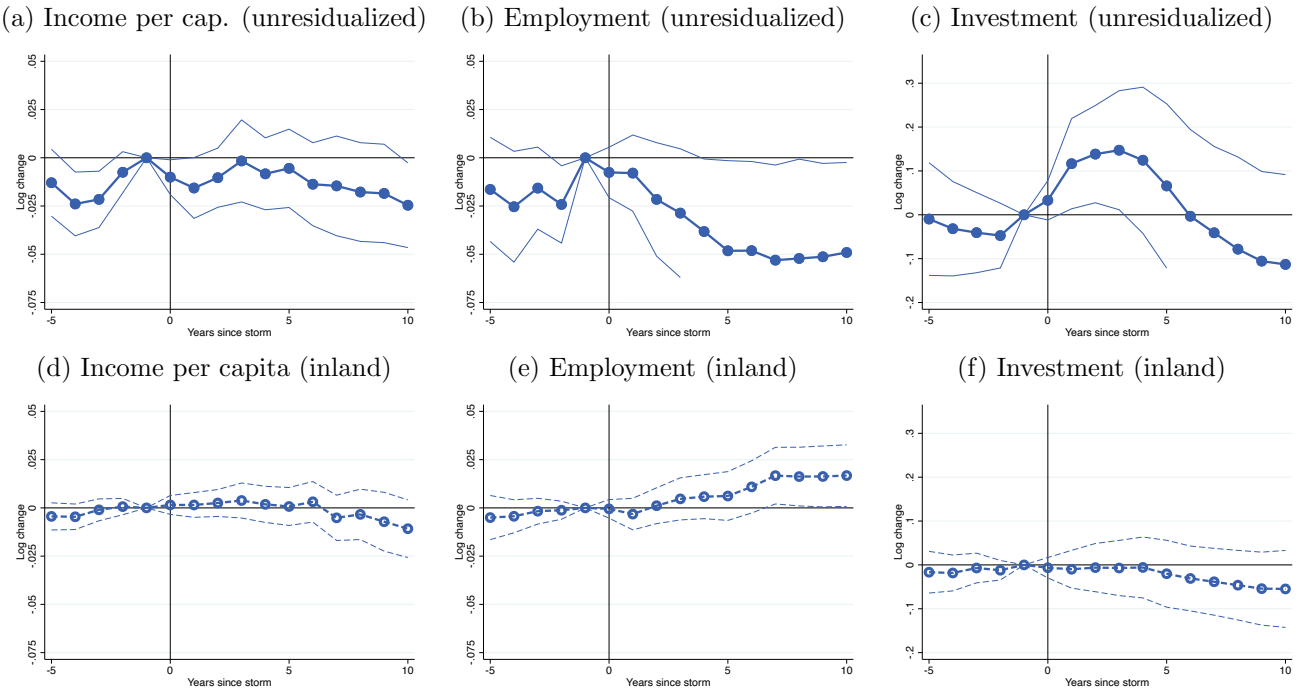

Note: Point estimates of coefficients γ_h from distributed lag regressions (14) for 1-in-50-years storms, and 95% confidence bands clustered by county. Panels (a-c): coastal counties only, using unresidualized weather to define storms. Panels (d-f): inland counties only, using residualized weather to define storms. Panels (a,d): log income per capita. Panel (b,e): log employment. Panel (c,f): log investment. Years 1990-2015. Controls: county and year fixed effects; nonparametric trends by state, local annual mean temperature decile, local maximum daily windspeed and maximum precipitation deciles, population decile, and income per capita decile; 5-year lag of local government expenditures. Weighted by average county population in 1960-1980. Standard errors clustered by county.

F.4 The impact of heat waves: alternative definition and cold counties

Figure 20: The impact of 1-in-20-years heat waves: unresidualized definition, and cold counties.

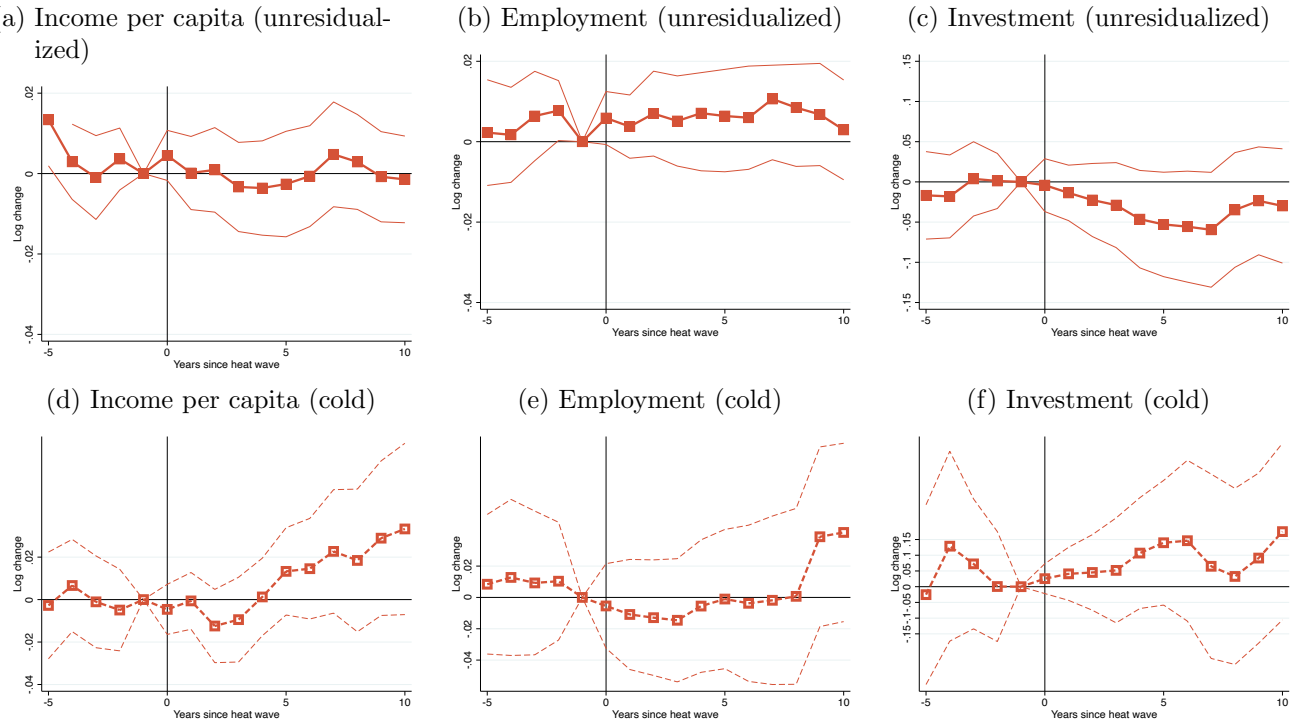

Note: Point estimates of coefficients γ_h from distributed lag regressions (14) for 1-in-20-years heat waves, and 95% confidence bands clustered by county. Panels (a-c): warm (above-median average annual temperature) counties, using unresidualized weather to define heat waves. Panels (d-f): cold (below-median average annual temperature) counties, using residualized weather to define heat waves. Panels (a,d): log income per capita. Panel (b,e): log employment. Panel (c,f): log investment. Years 1990-2015. Controls: county and year fixed effects; nonparametric trends by state, local annual mean temperature decile, local quantile of fraction of hot days, population decile, and income per capita decile; 5-year lag of local government expenditures. Weighted by average county population in 1960-1980.

F.5 Trends in cold waves

F.6 The impact of cold waves

Figure 21: 1-in-20-years cold waves and global mean temperature.

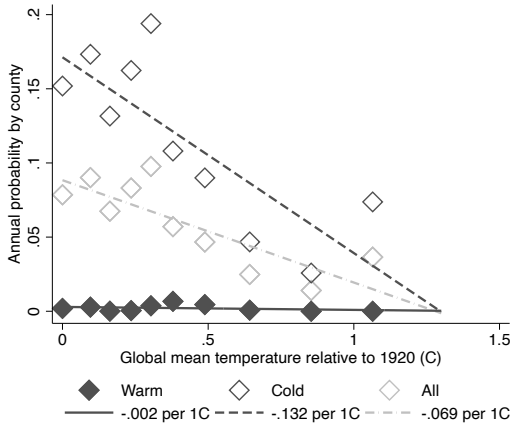

Figure 22: The impact of 1-in-20-years cold waves

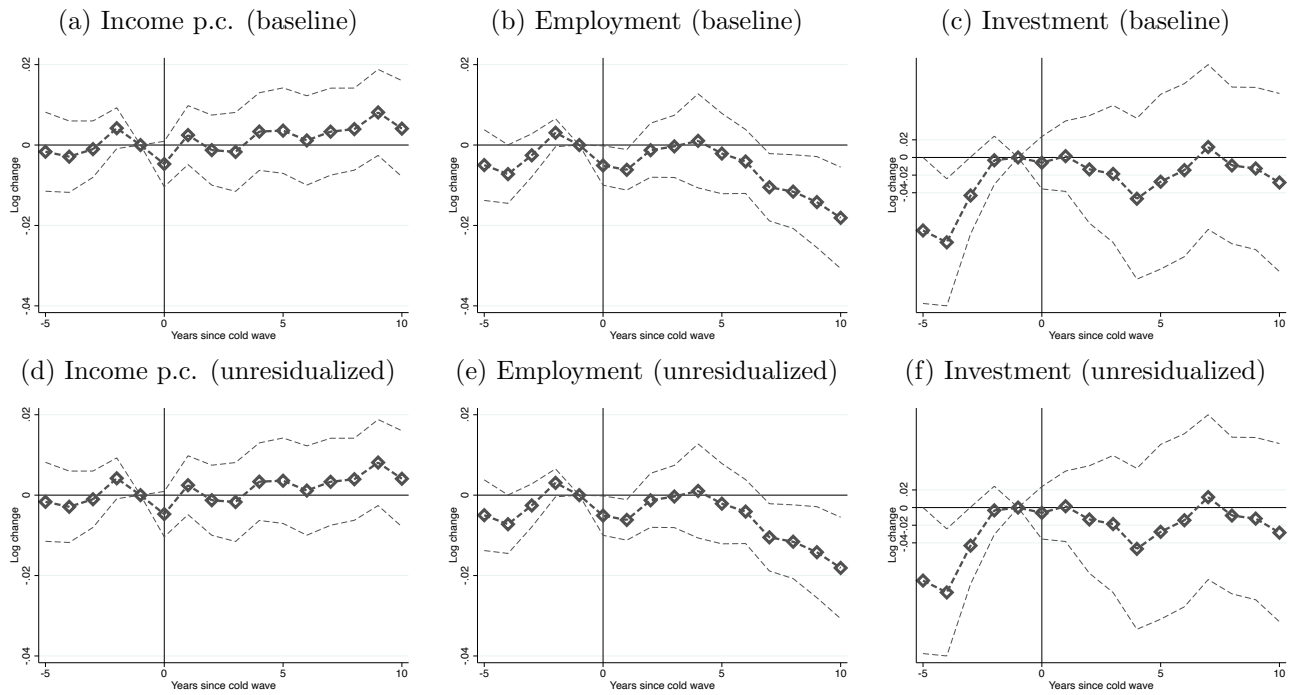

Note: Point estimates of coefficients γ_h from distributed lag regressions (14) for 1-in-20-years cold waves, and 95% confidence bands clustered by county. Panels (a-c): cold (below-median average annual temperature) counties, using residualized weather to define heat waves as the baseline. Panels (d-f): cold (below-median average annual temperature) counties, using residualized weather to define heat waves. Panels (a,d,g): log income per capita. Panel (b,e,h): log employment. Panel (c,f,i): log investment. Years 1990-2015. Controls: county and year fixed effects; nonparametric trends by state, local annual mean temperature decile, local quantile of fraction of hot days, population decile, and income per capita decile; 5-year lag of local government expenditures. Weighted by average county population in 1960-1980.

F.7 Statistical downscaling slopes

Figure 23 describes how the frequency of (residualized) natural disasters change with global mean temperature.

Figure 23: Estimated slopes of statistical downscaling in historical record.

(a) Heat wave frequency with global temperature

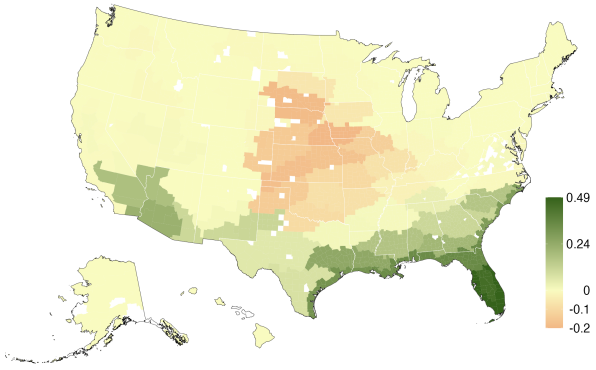

(b) Storm frequency with global temperature

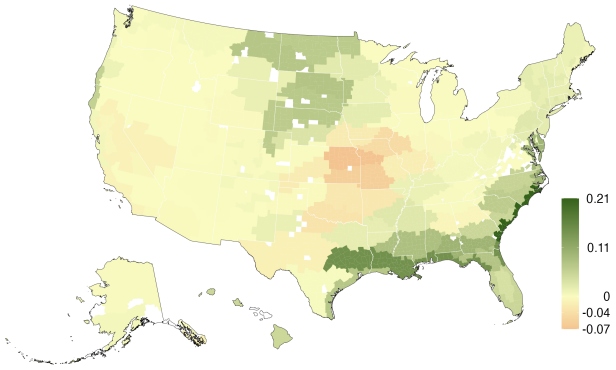

Note: The effect of a 1°C increase in global temperature on the frequency of heat waves (q_i^{heat}, panel a) and storms (q_i^{storm}, panel b) estimated from equation (15).

G Additional results

Figure 24 describes how the frequency of non-residualized natural disasters change with global mean temperature. Table 1 collects summary statistics describing our counterfactuals under alternative specifications.

Figure 24: Estimated slopes of statistical downscaling in historical record, non-residualized definition.

(a) Heat wave frequency with global temperature

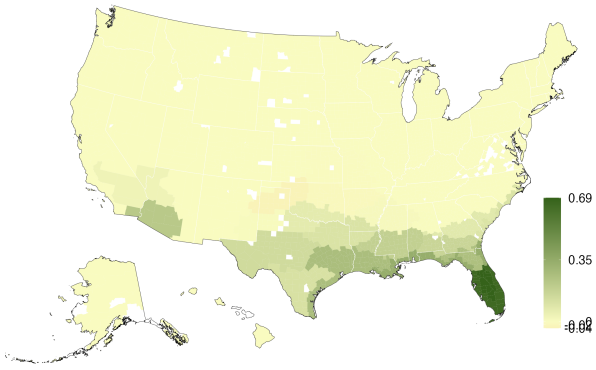

(b) Storm frequency with global temperature

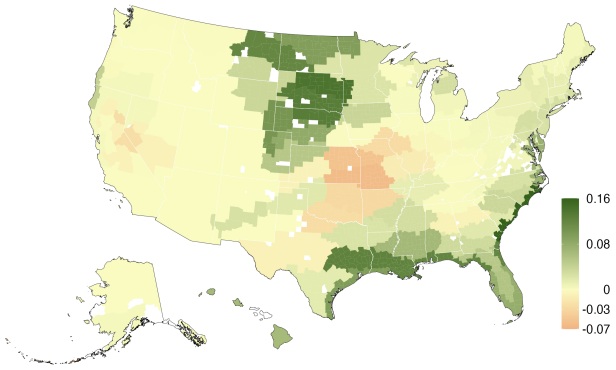

Note: The effect of a 1°C increase in global temperature on the frequency of unresidualized heat waves (q_i^{heat}, panel a) and unresidualized storms (q_i^{storm}, panel b) estimated from equation (15).

Table 1: Impact of climate change on welfare and allocations in alternative specifications.

	Welfare				Allocations	
	Workers		Capitalists		Population	Capital
	2025	2100	2025	2100	2100	2100
Baseline						
Aggregate (%)	-2.8	-4.2	-1.2	-3.7		-7.9
St. dev. (p.p.)	0.8	1.0	10.1	24.3	28.3	36.1
Discount rate: Aggregate (%)						
5%	-1.7	-4.5	-0.1	-4.8		-8.1
1%	-3.5	-4.2	-3.9	-2.1		-7.8
0.5%	-4.0	-4.2	-9.8	1.0		-7.8
By type of damages: Aggregate (%)						
Capital depreciation	-1.7	-2.6	-0.8	-2.9		-6.6
Productivity	-1.2	-1.9	-0.7	-1.6		-3.8
Amenities	-0.4	-0.7	0.0	0.1		-0.4
With cold waves						
Aggregate (%)	-3.0	-4.5	-1.3	-3.9		-8.1
St. dev. (p.p.)	0.7	1.0	10.1	24.2	28.3	36.0
No climate anticipations: Workers						
Aggregate (%)	-2.9	-4.4	-1.5	-3.4		-7.7
St. dev. (p.p.)	1.1	0.7	9.4	25.1	30.1	37.4
No climate anticipations: Capitalists						
Aggregate (%)	-2.6	-4.4	-1.7	-3.5		-7.7
St. dev. (p.p.)	0.3	0.7	11.1	25.6	30.5	37.6
No climate anticipations: Workers and capitalists						
Aggregate (%)	-2.8	-4.4	-1.7	-3.4		-7.7
St. dev. (p.p.)	1.1	0.8	9.6	25.0	29.9	37.2
No adaptation: Fixed population						
Aggregate (%)	-4.0	-7.0	-1.8	-5.6		-10.7
St. dev. (p.p.)	9.4	16.3	3.1	9.3	0	22.2
Raw events: Aggregate (%)						
Total	-2.8	-4.2	0.3	-4.0		-7.8
Capital depreciation	-2.8	-4.2	0.3	-4.0		-7.8
Productivity	0.0	0.0	0.0	0.0		0.0
Amenities	0.0	0.0	-0.0	-0.0		0.0
Climate models: Aggregate (%, heat only)						
Baseline	-1.4	-2.3	-0.6	-1.5		-4.0
GFDL-ESM-4	-1.5	-2.4	-0.5	-1.2		-0.5
EC-Earth-3	-1.3	-2.1	-0.6	-1.3		-0.9
ACCESS-CM-2	-1.1	-1.9	-0.5	-1.2		-1.8

Notes: Aggregate: percent deviation from initial steady-state. St. dev.: percentage point deviation from initial steady-state. Discount rate: effects under different rate of time preference ρ. Counterfactuals calculated using expansion around initial steady-state together with proportional rescaling to hold expansion point at constant preferences. By type of damages: decomposition into damage channels. Need not be additive because of expansion around final steady-state. No climate anticipations: Imposes that workers and/or capitalists believe that temperature stays constant at its time-t value for a long enough time, before returning to initial steady-state. No adaptation: Imposes that migration rate is zero $\mu = 0$. Raw events: uses damage coefficient and frequency slope estimates from unresidualized extreme events to construct damage functions. Climate models: uses frequency slope estimates from global circulation models to construct damage functions.